Compressive Properties of Laminates with UACS Plies and Their Applications to the Crashworthy Structure

アリフィン, アブドュラ アティック ビン

https://doi.org/10.15017/1785391

Compressive Properties of Laminates with UACS Plies and Their Applications to the Crashworthy Structure

by

ABDULLAH ATIQ BIN ARIFIN

A Dissertation Presented to

Department of Aeronautics and Astronautics
Graduate School of Engineering
Kyushu University

June 2016

ABSTRACT

In this dissertation, novel materials made of highly aligned discontinuous fibres, namely, unidirectionally arrayed chopped strands (UACS) are proposed for crashworthy structure application to improve crashworthiness properties of existing conventional continuous carbon fibre reinforced polymer (CFRP) laminate. The basic strategy to optimise crashworthiness properties is by developing a new trigger function directly in the interior of composite laminate, thus making the failure process in a controllable way and increasing energy absorption performance of structure. These concepts offer scope through shearing slit at small inclined angle of 11.3 in intra-laminar region and reducing catastrophic failure through suppression of delamination at inter-laminar region to ensure that the laminated structure is progressively collapsed in a controlled manner. Two kinds of UACS plies, namely, one with discontinuous bi-angle slit pattern and another with discontinuous staggered slit, were selected to study the effects on the crashworthiness parameters (maximum peak load, energy absorption, specific energy absorption, mean crushing load, crush efficiency) and failure mechanism.

At first, the effects of slit angle on the compressive strength and progressive crushing properties of UACS quasi-isotropic laminates with bi-angle slit configuration were determined. Test results revealed UACS laminate with ±11.3˚ degrees gives relatively high energy absorption ability, which is comparable to conventional laminate without slits. Additionally, all the specimens of ±11.3˚ bi-angle UACS laminates showed

controllable fracture during progressive crushing, which resulted in the highest of total energy absorption and specific energy absorbed among all kind UACS laminates. These results suggested that the UACS laminate with ±11.3˚ bi-angle slits may provide a new selection of composite materials for the application of energy absorbing structures with complex geometry.

Considering that crashworthy structure requires high energy absorption capability with better crush efficiency, baseline cross-ply stacking sequence with $[0/90]_{4s}$ and $[90/0]_{4s}$ and with different kinds of 0˚ plies were chosen to investigate the crashworthiness performance of laminates. UACS plies with highly aligned slits of bi-angle pattern and staggered pattern were used as 0˚ plies, respectively, instead of conventional continuous fibre 0˚ plies to study the effects of UACS 0˚ plies on the static compression and progressive crushing properties. The results showed that the $[90/0]_{4s}$ laminate with UACS 0˚ plies of bi-angle slit pattern was successfully improved by 24% of energy absorption and the $[90/0]_{4s}$ laminate with UACS 0˚ plies of staggered slit pattern improved by 29% energy absorption compared to conventional cross-ply laminate.

In order to incorporate with realistic geometries used in many vehicle structures for crashworthiness application, composite circular tubes made of cross-ply CFRP laminate with different kinds UACS 0˚ plies are fabricated and tested under quasi-static progressive compression. The tubular structure made of 0˚ UACS plies was demonstrated to achieve more stability and controllable progressive crushing through extensive fracture. Comparison of the results with conventional tube showed that tubular laminates with UACS 0˚ plies of bi-angle and staggered slits were successfully enhanced by 6.4% and 4.5% energy absorption, respectively.

CONTENTS

CHAPTER 1

Introductions

This chapter introduces the overview of composite crashworthiness and its challenges to apply composite materials to automotive structures in the automotive industry, the overview development of highly aligned discontinuous fibres, namely, unidirectionally arrayed chopped strands (UACS), and the present works in improving crashworthiness integrity of composite structure using UACS plies, as well as the main objective and outline of this study.

1.1 General background

1.1.1 Overview on composite crashworthiness performance

Composite structures made of carbon fibre reinforced polymer (CFRP) have drawn increasing attention and have rapid growth in transportation vehicle structures, particularly in aircraft, commuter, helicopters and sailplane, due to their significant advantages including low weight, high specific strength and stiffness, corrosion resistance, durability and energy transmission. As the importance of lightweight vehicle increases, composite has become more predominant in recent years. Besides being an environmentally-friendly and energy saving vehicle, the crashworthiness characteristics of CFRP attracted many researchers' attention over the past few decades, particularly in evaluating the energy absorbing performance thus improving the crashworthiness integrity of composite structure. In automotive engineering, crashworthiness is defined as the capability of a vehicle to absorb impact energy and be survivable for the occupant [1] or in other words, by increasing the vehicle's crashworthiness, it provides occupants with a greater extent of protection and chance of survival in the accident of a severe crash. Crashworthy structures should be designed to absorb energy in controlled manner, thereby bringing the passenger compartment to rest without the occupant being subjected to high decelerations that could cause serious injury or death.

Composite crashworthiness performance is based largely on absorbing energy through structural deformation or controlled failure mode that enables maintenance of gradual decay in load profile during energy absorption. In addition to their attributes of high stiffness and strength-to-weight ratios, the ability to tailor composites has made

them very attractive for crashworthiness structure application. Contrary to metal, most composites are generally characterised by a brittle rather than ductile responses to the applied load, especially under compression. CFRP absorbs lots of energy through progressive crushing modes by a combination of multi-crack, splitting, bending, delamination and friction with higher specific energy absorption (SEA) values than metallic crash box. It is well known that with proper construction and architecture of composite structure, CFRP can achieve higher energy absorption than metal alloys.

The crush behaviour of composite specimens can be generally classified as either stable or unstable. Unstable crushing is characterised by an initial load peak followed by a sudden catastrophic failure. After this failure the specimen is no longer capable of sustaining a significant compression load. In contrast, stable crushing is characterised by an increase in load until an initial failure occurs. At this point, the specimen, although locally damaged, can still support significant compression loads through further displacement. Previous investigations indicated that the energy absorption capability of composite could be affected by various factors such as raw materials (fibre material, fibre volume and polymer matrix) [2-8], stacking sequence and fibre orientation [9-15], trigger mechanism [16-19], specimen geometry [20-23], crushing speed [24], frictional effect [25] and so on. As far as I know, there is no any available standardized test method for progressive crushing test [26]. In general, crushing tests can be carried out in one of two conditions of impact and quasi-static conditions [27-29]. Impact test gives a true simulation of the actual crash condition. The impact speed is generally between 7 m/s to 12 m/s which corresponds to strain rate between 15 to 23 s^{-1}. However, impact tests require very expensive testing equipment and high speed video-camera to follow the

crushing process. In contrast, quasi-static crush tests (at strain rate around 0.1 s^{-1}) are simple and easy to control. For this reason, quasi-static crush tests are widely used to study the failure mechanism of composite structure during the crushing process although they may not give a true simulation of real crash conditions. Many testing results [28, 29] demonstrate that similar force-displacement curves are found for both impact crushing test and quasi-static crushing test. Therefore, due to the limitation of experimental equipment, quasi-static crush testing was carried in this dissertation to investigate the energy absorption capability and crashworthiness characteristics of composite materials.

A significant issue associated with composite energy absorbing structures is that the device must collapse progressively in a controlled manner. However, previous works have reported that a drawback in the utilisation of composites is that most composite structures that deformed instantly and catastrophically at the start of the crush will result in absorption with negligible energy. In addition, their anisotropic nature coupled with the interactions that develop between fracture processes makes failure prediction difficult. Unlike isotropic materials which commonly fractures to the direction of principles stress, fracture in continuous fibre composite is a combination of different interacting failure modes. Several types of possible modes that lead to catastrophic failure such as buckling/microbuckling, longitudinal splitting, plies delamination, unstable intralaminar or interlaminar crack growth, fibre kinking and shear failure of laminate have been observed and reported [3-4,30-31]. Given these drawbacks, some researchers also used various types of composite structures in the form of fibre-reinforced composite tubes, sandwich panels, and hybrid in an effort to achieve improved levels of crashworthiness.

In a transportation system, the aerospace industry has pioneered the use of high performance fibre reinforced plastic composites in structural applications. Composite based CFRP has accomplished a great achievement when it was successfully applied to the primary structures of Boeing's 787 and Airbus's A350. This can be seen from the dramatic growth of CFRP composite penetration since 1980, where as low as 5-6% up to 50% of the latest modern aircraft such as Boeing's 787 Dreamliner and Airbus A350 were being applied with CFRP on its airframe including fuselage and wing (Fig. 1-1 and Fig. 1-2) [32]. Moreover, the great advantage of using carbon fibre, as opposed to traditional metal, is that it gives designers much more freedom when trying to juggle the conflicting demands of aerodynamic efficiency, fuel savings, reducing engine noise, and damage tolerant. Therefore, the percentage users of CFRP for airplane parts are expected to progressively increase for future aircraft.

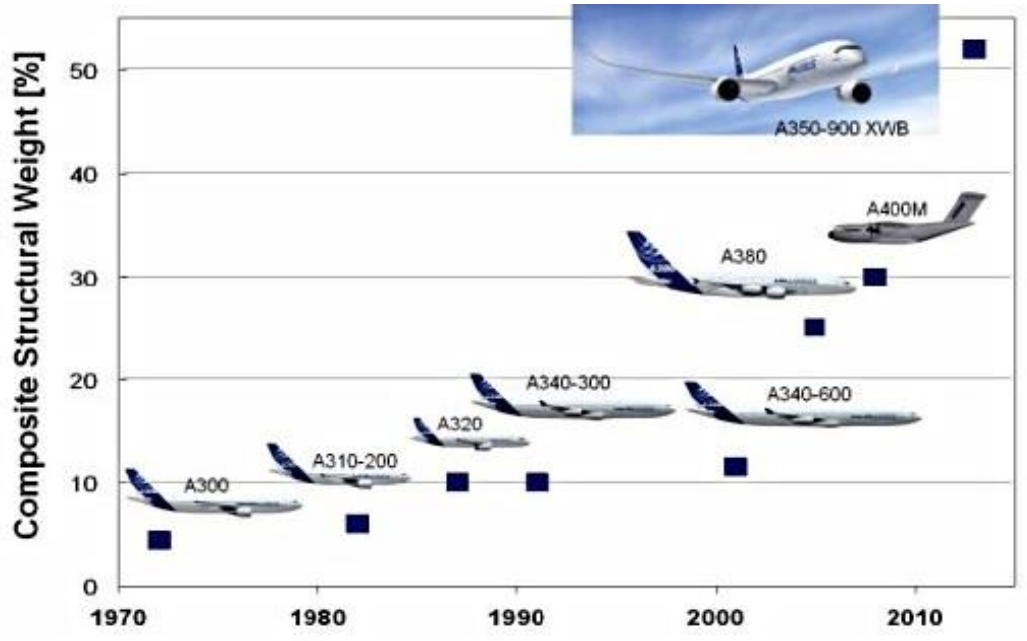

http://amazingdata.com/mediadata8/Image/amazing_fun_science_technology_2009072911532949.jpg

Figure 1-1: Overview of composite structural weight development on modern Airbus A350. Sources: Jenny body, Airbus UK R&7, 2007.

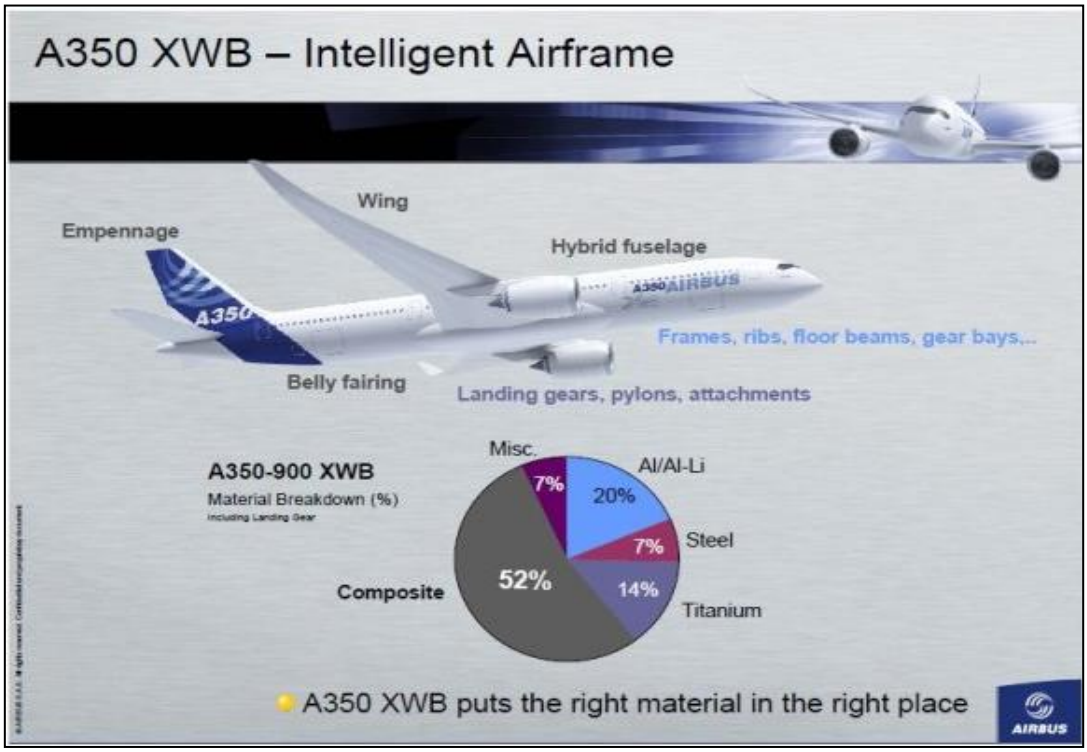

Photo: Airbus A350 XWB. Retrieved Jun, 2016, from http://scribol.com/technology/aviation/ airbus-a350-composites-on-trial-part-i/

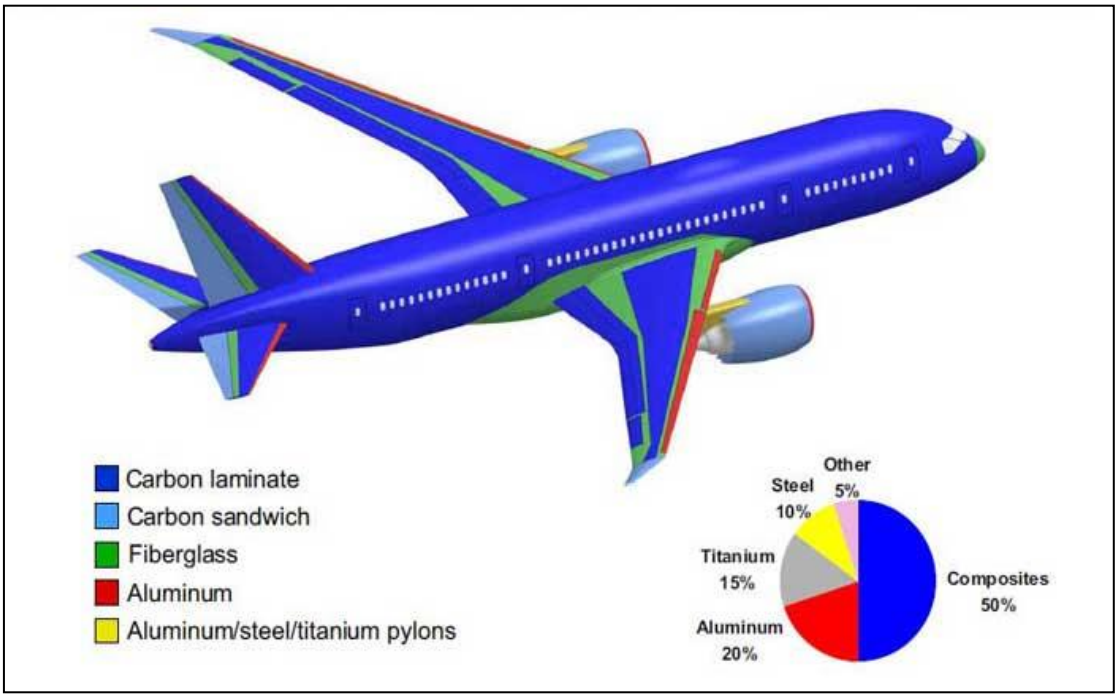

Photo: Fay Baylis. August, 2012. Retrieved Jun, 2016, from http://aviationknowledge.wikidot.com/

Figure 1-2: Overview of material application in the Airbus A350 WXB and Boeing 787.

Driven mainly by the increasing use of these materials for aircraft and aerospace structures, there have been substantial efforts by many researchers and automotive manufacturers that have devoted to investigating the crushing behaviour of composite laminate materials for the design of their energy-absorbing components. Although composite energy absorbers based CFRP have been shown to have significantly higher SEA than conventional short fiber composite and metallic absorber, automobiles must consider different requirements compared with aircraft applications because the structural components of automobiles are relatively smaller and their geometries are more complicated. Moreover, with the increasing number of vehicles over past two decades that resulted in an increasing number of collision and fatalities each year on roadways, it showed that safety is the most concerning issue that needs to be resolved before any replacement or adoption composites into mainstream structures.

1.1.2 The challenge of composite crashworthiness in automotive structure

Over the past 30 years, the use of composites in the automotive sector has significantly grown well beyond its original applications. Since 1980s, most of the Formula 1 racing car chassis, suspension, wings, and engine cover have been built with carbon fibre composites [33]. In parallel, the application of composites has also been extended to luxury and premium vehicles such as Lamborghini, Tesla, Ferrari, and others for low volume production. In recent years, the automotive composite value chain is currently undergoing a major redesign to meet customer demand and international requirements targeting reduced fuel consumption and carbon emission together with improving of passenger safety. One of the most significant methods by which fuel economy can be achieved is by reducing the weight of the vehicle. Therefore, more parts are being manufactured from composite materials replacing traditional materials in the process as represented in Fig. 1-3 [34].

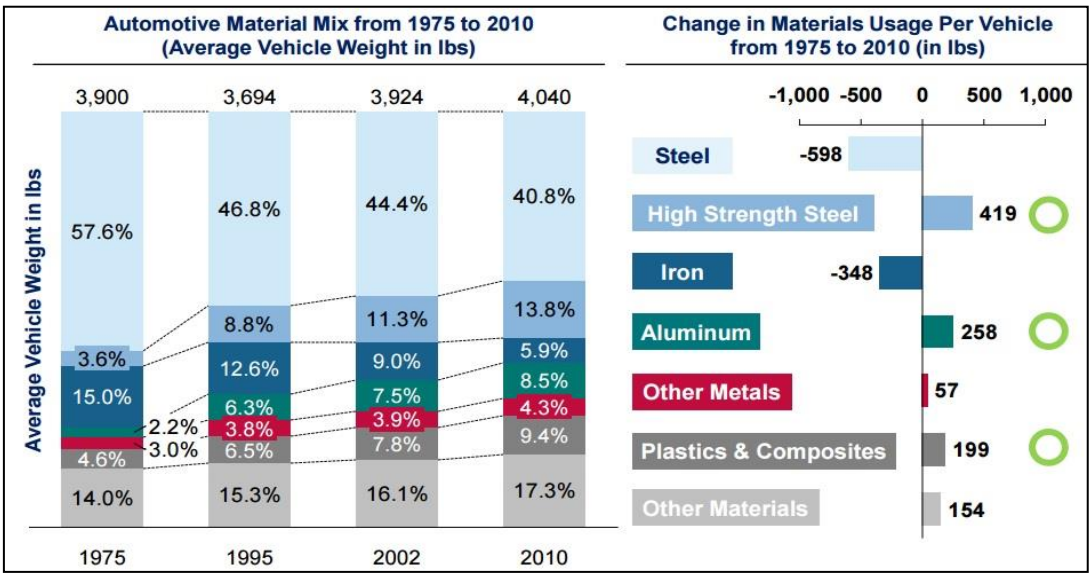

Figure 1-3: Material trends in automotive industry since 1975 to 2010 [34].

Although glass fibre composite dominates the composite materials used in automotive application, other polymer composites such as carbon fibre composites, show great promise. These alternatives are attractive because they offer weight reduction potentially twice that of the conventional glass fibre composite used today. Furthermore, carmakers are specifically targeting some car parts with more potential for development with carbon fibre composite. These include chassis, roof, tailgate, floor panel, side panel, trunk, fender and bumper. Table 1-1 represents an overview of some examples of composite applied to commercial automotive components in the past few years [35].

Table 1-1: Example of composite components applied to automotive [35].

OEM-Model	Application	Material	Year
BMW i3	Passenger cell	CFRP	2013
BMW i8	Passenger cell	CFRP	2014
Alfa Romeo 4C	Chassis	Prepreg	2013
Alfa Romeo 4C	Outer body	SMC	2013
McLaren MP-4-12C Spider	Car roof, chassis	CF monocell	2013
BMW M6 convertible	Roof, trunk lid	GFRP	2013
Daimler Smart	Wheel rims	GFRP	2012
Lexus LFA	Cabin, floor,pillar	CFRP	2012
Lamborghini Aventador	Bumper,body	CFRP	2012

CFRP with their high strength-to-weight ratio provides an excellent platform upon which to develop the next generation of lightweight vehicles. Significant successes in the aerospace sector have led to the initial integration of carbon fibre composites into passenger frame vehicles such as BMW's i3 electric car, which demonstrated the viability of composites in the ground vehicle. This viability is not only related to a successful lightweight vehicle that is more fuel efficient, but one that possesses both significant crashworthiness and high durability. Based on this success, integrating carbon fibre composites into commercial vehicles clearly showed that mass production is within reach. However, the integration of CFRP into the vehicle and many of its components require significant modifications to many of the vehicles designed and analysis practices, where new material models and design characteristics must be considered.

The major challenge in adopting composite in CFRP automotive domain is the economic constraint in mass production, both from basic material cost and fabrication viewpoint. Virtually, the usage of composite in high volume vehicle is currently restricted to decorative or semi-structural application. Sheet moulding compound (SMC) materials are the highest-performing composite in general automotive used today. However, SMC contains lower fibre volume fraction of chopped strand glass fibre compared with continuous CFRP composite which cannot really be classified as high-performance composite [36]. The randomly distributed chopped fibre of SMC contains many stress concentration areas which is currently employed only in non-loadbearing structure due to reduced properties of alignment. Therefore, demand for high strength components made from CFRP will grow significantly stronger than demand of glass fiber SMC.

The next major challenge for composites in the automotive business is extension of use into truly structural applications such as the primary body structure (Fig. 1-4). These are the areas that consist of complex geometry structure, which have to sustain all the major road load inputs and impact loads. These functional requirements must be totally satisfied for any new material to find extensive application in these structures and it is no small challenge to structural composites to meet these criteria effectively. The limitation on the usefulness of SMC type materials in truly structural application have yet to be established. Provided continuous fibre is strategically incorporated, these materials promises to be capable of providing high structural integrity and this may well prove to be the pioneering fabrication in high load bearing application. Although continuous CFRP composite with high specific energy shows great potential to replace conventional steel as main structure, the poor flowability of continuous fibre CFRP during fabrication structure with complex geometry shape and their unstable failure of laminates under impact, which led to catastrophic failures, are limiting the use of these class materials.

For this reason, in order to meet the future demand of automakers, carbon fibre precursors will need to be found from alternative sources rather than petrochemical, and for automotive needs lignin base precursors maybe more suitable, although the derived fibres currently lacks the desired properties. Material will also have a greater degree of multifunctional. The major drivers for employing discontinuous composites revolve around the ability to increase productivity by utilising forming unavailable to continuous CFRP laminate, changing design criteria to allow geometrical complexity, and increasing fibre hybridisation by intermingling a larger array of fibre types to tailor material

properties for certain requirement and reclaimed fibres in non-loadbearing cases. Thus, there has been a resurgent interest in highly aligned discontinuous fibre in recent years with a number of processing methods and investigations being reported in open literature [37-45]. Unidirectionally arrayed chopped strand (UACS) is one of the latest examples in the development of highly aligned discontinuous fibre which introduces discontinuity into virgin continuous fibre prepreg via breaking and slicing through mechanical mechanism. Although previous investigations on UACS laminate showed an excellent formability for fabrication of complex geometry structure and high tensile properties, the compressive properties and crashworthiness capabilities of UACS laminates are not yet investigated.

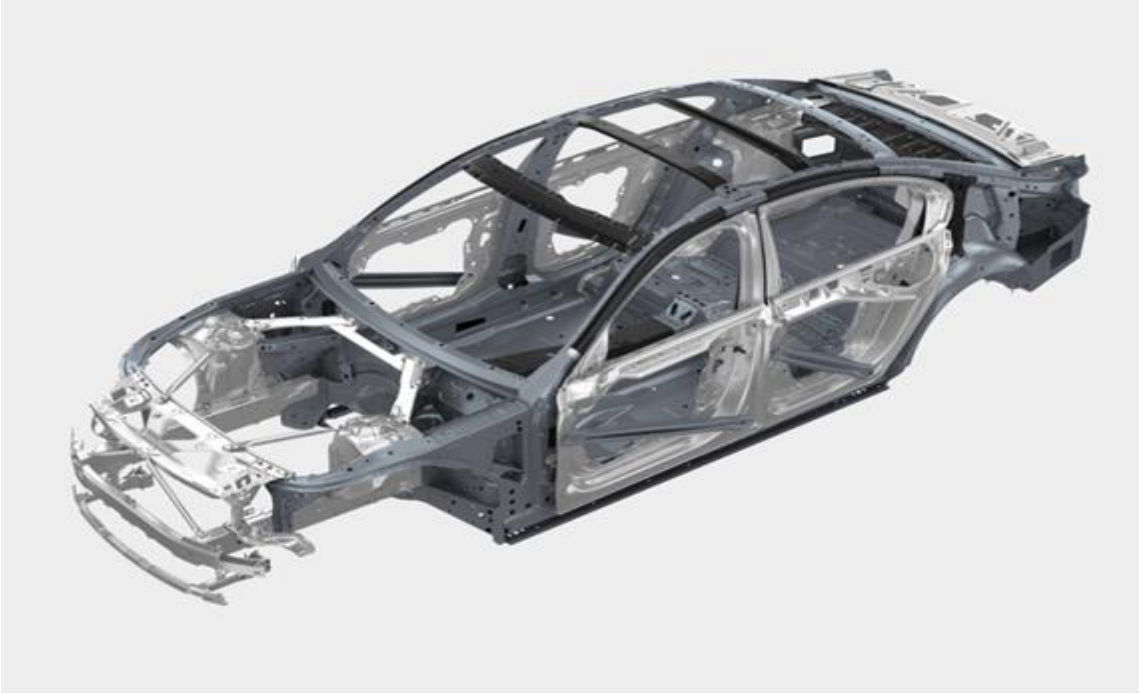

Photo: Bill Howard, July15, 2015. Retrieved from http://www.extremetech.com/extreme/209812

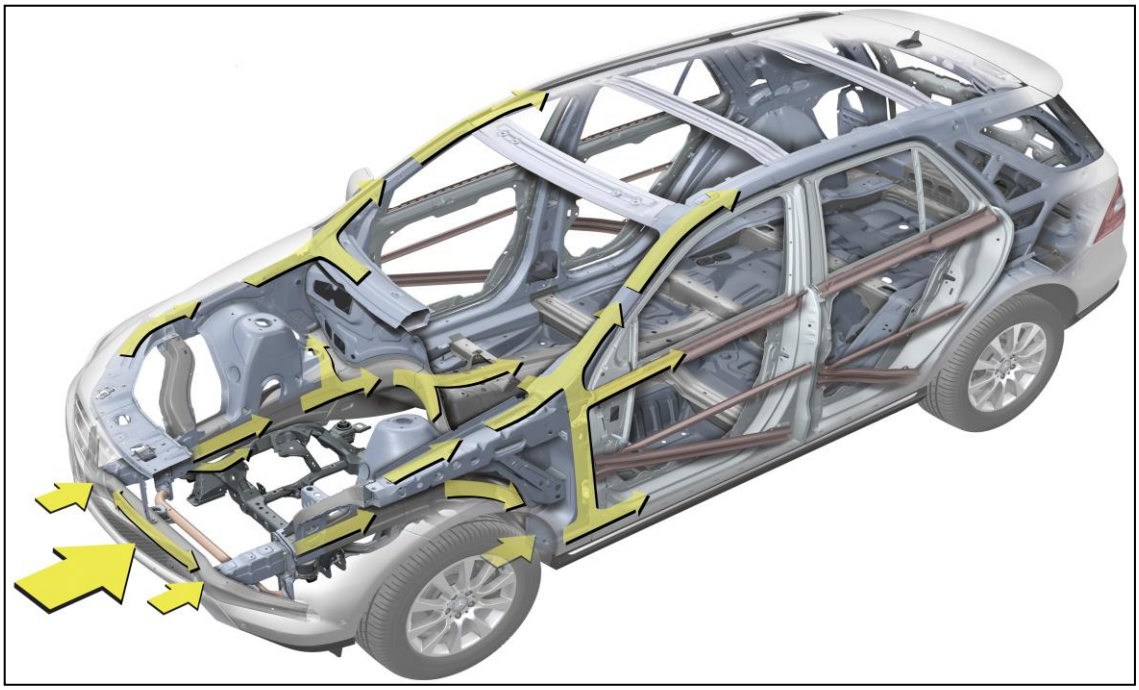

Photo: scientific Market, Jun 20, 2016. Retrieved from http://www.edadevelopment.com

Figure 1-4: Schematic of primary body structure

1.2 Overview of the development of UACS laminates

The development of early UACS laminates and their previous works progressed on enhanced UACS, which is described in this subsection. UACS was firstly developed by Taketa et al. in 2008 [37-40] by introducing slits into conventional prepregs where continuous fibre arrayed unidirectionally before curing. Fig. 1-5 showed schematic diagram of the first design and development of UACS. In this early study, discontinuous slits of 12.5 mm in length at an interval of 25 mm was introduced into the prepreg with slits being arranged perpendicular to the fibre direction. After forming the slit and stacking in laminate configuration, UACS laminate were cured using hot press at 3MPa pressure and 150 ºC for 30 minutes. It was found that UACS laminate exhibits excellent formability almost the same as that SMC and fibre orientation remained the same after its area was increased. Another important feature of UACS is that the layer structure is maintained even when complex-shaped components such as rib structures were fabricated from UACS plies (Fig. 1-6) [40]. The UACS laminates were able to be stacked by multiple UACS plies or hybridisation according to the design of the layer sequence.

In order to investigate the mechanical properties of UACS laminates, Taketa used three kinds of laminates; UACS laminate, SMC, and conventional laminate. For comparison all laminates stacked into the quasi-isotropic lamination of $[45/0/-45/90]_{2S}$ configuration. The volume fraction of both UACS and conventional laminate was about 58%. SMC was made by random distributed chopped strand (25 mm in length) into the same epoxy resin with volume fraction of about 40%. Fig. 1-7 showed experiment results of tensile strength and modulus for first designed quasi-isotropic UACS laminate.

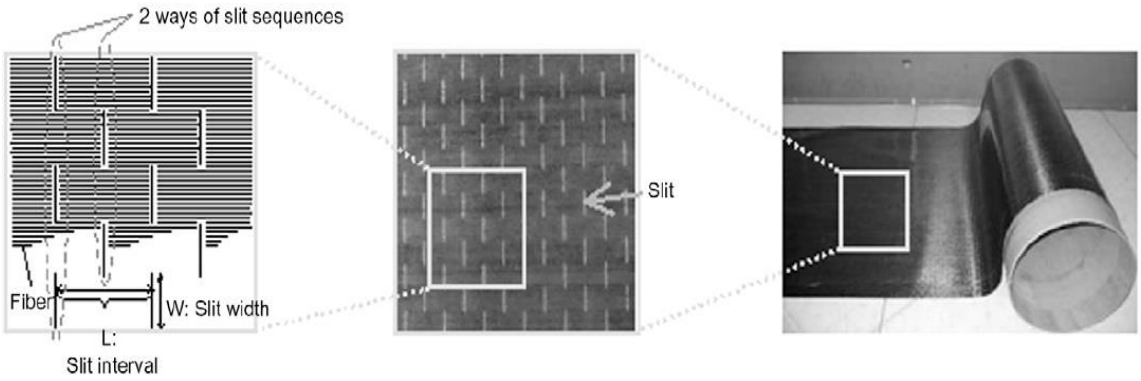

Figure 1-5: Schematic of the first designed UACS developed by Taketa by introducing aligned distribution slit into conventional prepreg [37].

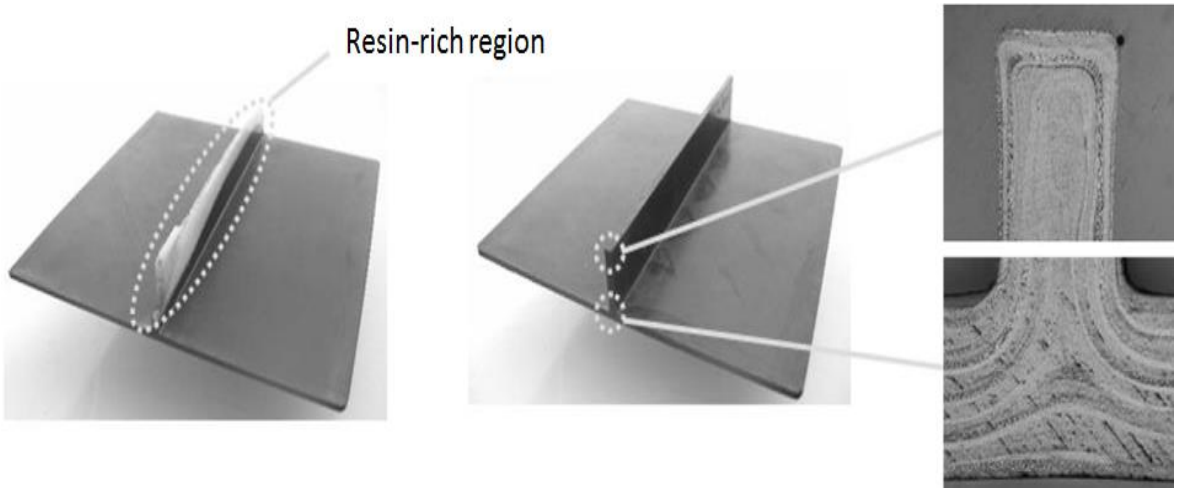

Figure 1-6: Example of rib structure moulded in quasi-isotropic stacks of conventional prepreg (left) and the first UACS prepreg (right) [40].

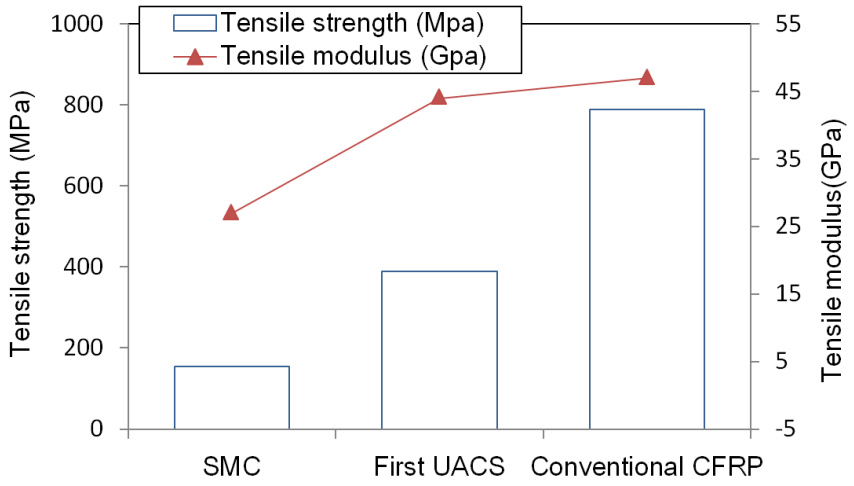

Figure 1-7: Comparison of modulus and strength between SMC, the first UACS and conventional CFRP [38].

Test result demonstrated that tensile strength of UACS laminate was twice that of SMC. In addition, the tensile modulus, which is close to that of conventional CFRP laminate, was much higher than SMC. From microstructure observation of fractured specimen, they found resin-rich regions appearing only around the slits and is the reason why UACS laminate gave high modulus. Delamination was assumed to be induced only by the shear stress concentration around the slits, without the matrix cracking effect. No fibre breakage occurred even near the slits in the UACS laminate. It concluded that the final failure of the UACS was dominated by interlaminar delamination.

In the second stage of development, Taketa et al. carried out further investigation in improving the strength of UACS by introducing continuous slit with angle to the fibre's direction instead of using slits that was perpendicular to the fibres. Based from problem of high stress concentration around the tips of slits that caused the first designed UACS to give relatively low tensile strength and large delamination, Taketa then proposed

continuous slit with an angle in their second UACS design. The main principle is to maintain the excellent flowability in the first design of UACS and reduce stress concentration around the tips of slits in the UACS laminate. Figure 1-8 represent schematic diagram of the second UACS plies design [39]. Effects of continuous slit with angle to fibre's direction were investigated experimentally. In this study, UACS laminate were stacked and cured the same as reported in their previous work. Tensile tests for the second UACS laminates design were also conducted. The relation between the tensile strength of quasi-isotropic UACS laminates and the slit angle θ are presented in Fig. 1-9. As the slit angle became less than 45°, the tensile strength dramatically increased, approaching that of conventional laminate without slits (θ = 0°). Yet, observation showed continuous angled slit still easily induced large delamination and extended along the continuous slits due to the stress concentration, which could reduce the strength of UACS laminates. Delamination between 0˚ plies and adjacent angle ply dominates the final failure and few fibre breakages were observed.

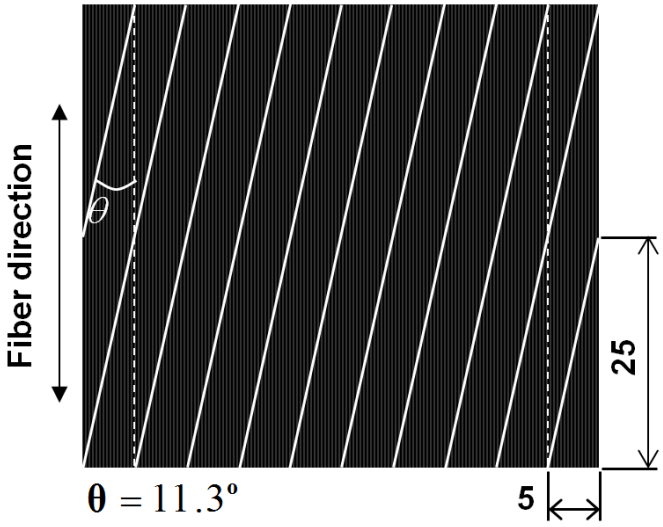

Figure 1-8: Schematic diagram of second designed UACS by introducing continuous angled slits into prepreg [39].

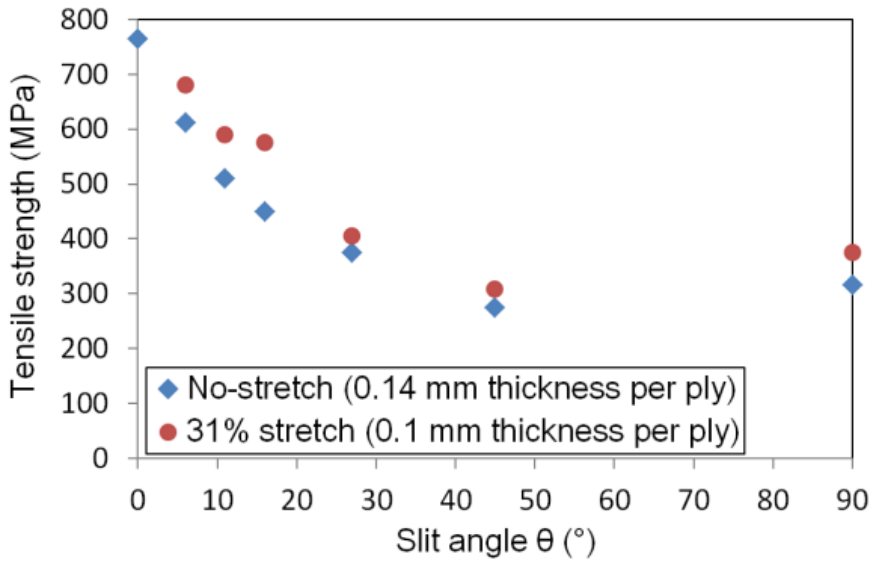

Figure 1-9: Relation between tensile strength of quasi-isotropic UACS laminates and the slit angle [35].

Continuation of work undertaken by Taketa, Li et al. [40, 41] lately was proposed two new designs of UACS to improve the strength of the early UACS laminates by introducing two distribution patterns of discontinuous angled slits into a unidirectional prepreg of conventional CFRP. Two newly designed UACS prepreg namely with discontinuous staggered angled slit and discontinuous bi-angle slits were investigated experimentally and numerically. In addition, existing continuous angled slit was also fabricated for comparison. Based on earlier works done by Taketa [39], Li et al used the slit angle between the slit and the fibre direction at 11.3˚ and fibre length of all UACS prepregs is 25 mm. Figure 1-10 represents the schematic of two designed discontinuous angled slit. Both kinds of slit patterns were designed on printed white paper before introducing on prepreg sheet using a commercial paper cutter. The UACS prepreg was then stacked in the sequence of $[45/0/-45/90]_{2S}$ as depicted in Fig. 1-11. Afterwards, the

stacked laminates were cured using an autoclave. As benchmark, conventional without slits is also fabricated to compare the influence of two newly designed discontinuous slit on mechanical properties.

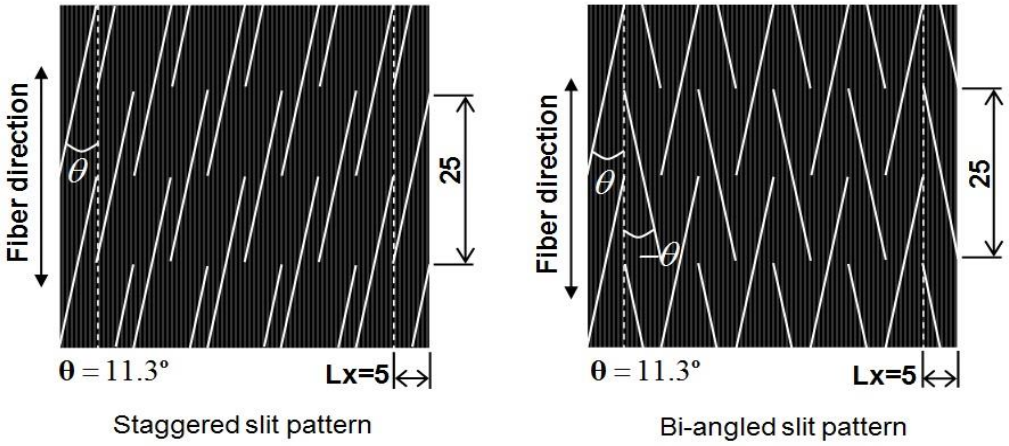

Figure 1-10: Two newly designed UACS with discontinuous angled slits by Li et al [41].

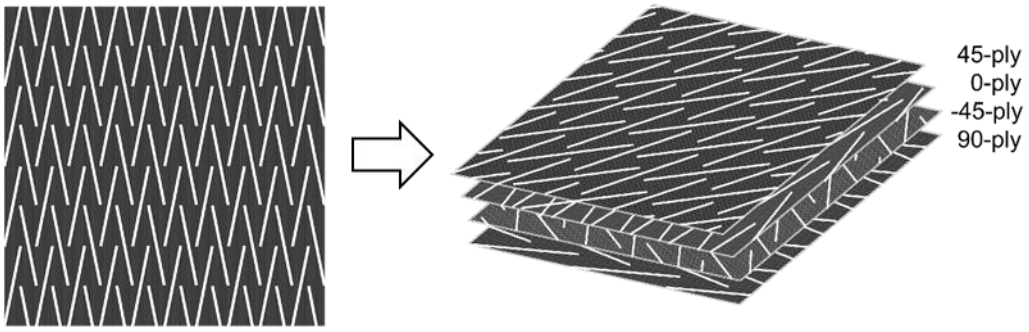

Figure 1-11: Stacking sequence of quasi-isotropic UACS laminate [41].

Results of tensile tests conducted by Li et al. are presented in Fig. 1-12. Stress-strain curves showed similar nonlinear behaviour near peak value on UACS, although stress range gave relatively smaller than that of the conventional laminate. In contrast, in the case of the existing UACS laminate with continuous slits, stress increased linearly with the increase of strain until failure. Newly designed UACS laminates with staggered discontinuous angled slits and discontinuous bi-angle slits enhanced the tensile strength by about 10% and 15% respectively, compared with the previous UACS laminate with continuous angled slit. From numerical analysis, discontinuous slit distribution in the two newly designed UACS laminates showed positive role in suppressing the delamination progression in the outside regions around the ends of discontinuous slit distribution. Tested result revealed newly designed UACS laminate with discontinuous bi-angle slit distribution gave the best material properties including stiffness, strength, and formability among the three kinds of UACS laminates.

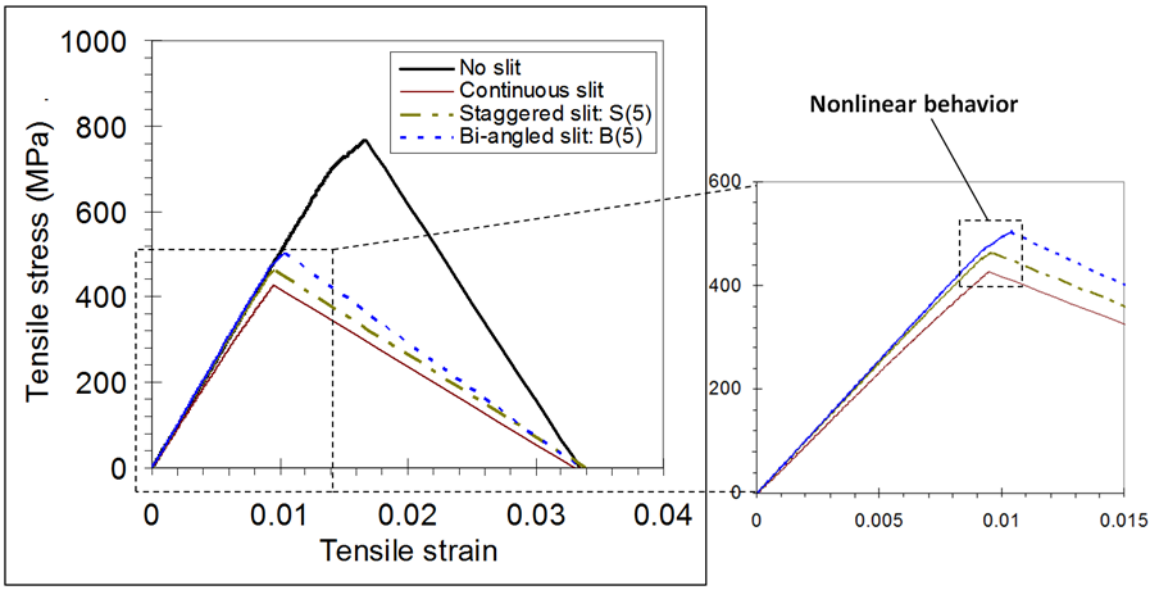

Figure 1-2: Typical stress-strain curves of cured UACS laminate with various slit patterns [41].

1.3 Objective and outline

Although the above mentioned that UACS laminates with discontinuous angled slits exhibit better tensile mechanical properties and similar flowability compared with conventional short fibre composite laminates, the compressive properties and crashworthiness capabilities of UACS laminates are not yet investigated. Is there a possibility that discontinuous slits allow UACS laminates to perform not only with excellent flowability, but also give higher specific energy absorption than conventional continuous fibre CFRP? In order to explore the answer, two discontinuous slit patterns of UACS prepregs, namely, staggered slits [37] and bi-angled slits [41], are proposed and investigated experimentally to determine their crashworthiness properties and characteristics, thus looking at the possibility to expand their application onto crashworthy structure application.

The objective of the present dissertation is to reveal the compressive properties and progressive crushing failures of UACS laminates with two different slit patterns and with different stacking configuration. Quasi-static compression and progressive crushing tests were conducted to investigate their relations between crashworthiness parameter and progressive crushing failure configurations with the purpose to optimise the crashworthiness capabilities of composite material.

The outline of this dissertation is listed as below:

Chapter 1 introduces the general background of composite crashworthiness, its challenges on automotive structural application, overview of previous research on the UACS laminates, and the motivation of the present study.

Chapter 2 describes experimental investigation on compressive and progressive crushing properties of quasi-isotropic bi-angle UACS laminates with different angles. Fabrication of bi-angle UACS laminates and experimental procedure are described in detail. The effects of three different slit angles in UACS laminates with bi-angle configuration on their compressive stiffness, strength, and energy absorber capability are clarified. For a benchmark, conventional quasi-isotropic laminate without slit was also fabricated and tested.

Chapter 3 presents a research on the compression and crush responses of cross-ply laminates with 0˚ UACS plies. Cross-ply laminates of $[0/90]_{4s}$ and $[90/0]_{4s}$ with different kinds of 0˚ UACS plies were chosen to investigate the compression and progressive crushing properties of laminates with 0˚ UACS plies. UACS plies with bi-angle slit pattern and staggered pattern were used as 0˚ ply, respectively, instead of conventional continuous fibre ply. Static compression test and progressive crushing tests were carried out to explore the feasibility of applying UACS ply to crashworthy structure to make the failure process in a controllable way and increase energy absorption performance of structure.

Chapter 4 investigates the progressive crushing behavior of composite circular tube with 0˚ UACS plies. Two kinds of 0˚UACS plies with bi-angle slit pattern and staggered pattern were used as 0˚plies in the fabrication of composite circular tubes, respectively, instead of conventional continuous fibre 0˚ plies. Prepreg based fabrication procedure of cross-ply composite circular tube and progressive crushing test procedure are described. For a benchmark, conventional cross-ply composite circular tube with continuous fibre 0˚ plies was also fabricated and tested. Furthermore, comparative progressive crushing tests

for conventional steel circular tube and continuous E-glass fiber reinforced polyester composite square tube are described. Values of specific energy absorption obtained from circular tubes made of CFRP laminates with UACS plies are compared with those of these two tubes of comparative tests.

Chapter 5 summarises the major results of the dissertation and suggests some future research topics which may concern to this study.

Bibliography

[1] Jacob GC, Feller JF, Simunovic S, Starbuck JM. Energy absorption in polymer composites for automotive crashworthiness. *Journal of Comp Materials*, 2002; 36(07): 813-849.

[2] Jane Maria FP, Mayer S, Rezende MC. Evaluation of mechanical properties of four different carbon/epoxy composites used in aeronautical field. *Material Research*, 2005; 8(1): 91-97.

[3] Tao WH, Robertson RE, Thornton PH. Effect of material properties and crush conditions on the crush energy absorption of fiber composite rods. *Composite Sciences and Technology*, 1993; 47: 405-418.

[4] Jumahat A, Soutis C, Jones FR, Hodzic A. Fracture mechanisms and failure of carbon fibre/toughned epoxy composite subjected to compressive loading. *Composite Structures*, 2010; 92:295-305.

[5] Savona SC, Hogg PJ. Investigation of plate geometry on the crushing of flat composite plates. *Composite Science and Tech*, 2006;66:1639-1650.

[6] Esnaola A, Ulacia I, Aretxabaleta L, Aurrekoetxea J, Gallego I. *Materials and Design*, 2015; 76: 18-25.

[7] Kim JS, Yoon HJ, Shin KB. A study on crushing behaviors of composite circular tubes with different reinforcing fibers. *International Journal of Impact Engineering*, 2011;38:198-207.

[8] Warrior NA, Turner TA, Robitaille F, Rudd CD. The effect of interlaminar toughening strategies on the energy absorption of composite tubes. *Composite Part A*, 2004;35:431-437.

[9] Israr HA, Rivallant S, Barrau JJ. Experimental investigation on mean crushing stress characterization of carbon-epoxy plies under compressive crushing mode. *Composite Structures*, 2013;96: 357-364.

[10] Fuller JD, Wisnom MR. Pseudo-ductility and damage suppression in thin ply CFRP angle-ply laminates. *Composite: Part A*, 2015;69: 64-71.

[11] Daniel L, Hogg PJ, Curtis PT. The crush behaviour of carbon fibre angle-ply reinforcement and the effect of interlaminar shear strength on energy absorption capability. *Composite: Part B*, 2000;31: 435-440

[12] Kawai M, Saito S. Off-axis strength differential effects in unidirectional carbon/epoxy laminates at different strain rates and predictions associated failure envelopes. *Composite: Part A*, 2009; 40: 1632-1649.

[13] Lee J, Soutis C. Thickness effect on the compressive strength of T800/924C carbon fibre-epoxy laminates. *Composite:Part A*, 2015; 36: 213-227.

[14] David-West OS, Alexander NV, Nash DH, Banks WM. Energy absorption and bending stiffness in CFRP laminates: the effect of 45˚ plies. *Thin-Walled Structures*, 2008; 46: 860-869.

[15] Mamalis AG, Manolakos DE, Ioannidis MB, Papapostolou DP. Crashworthiness characteristics of axially statically compressed thin-walled square CFRP composite tubes: experimental. *Composites Structures*, 2004; 63: 347-360.

[16] Pressurised composite tubes as variable load energy absorbers. *Composite Structures*, 2015; 120: 346-357.

[17] Palanivelu P, Paepegem WV, Degrieck J, Ackeren JV, Kakogiannis D, Hemelrijck DV, Wastiels J, Vantomme J. Experimental study on the axial crushing behavior of pultruded composite tubes. *Polymer Testing*, 2010;29:224-234.

[18] Troiani E, Donati L, Molinari G, Sante RD. Influence of plying strategies and trigger types on crashworthiness properties of carbon fiber laminates cured through autoclave processing. *Journal of Mechanical Engineering*, 2014;60:375-381.

[19] Huang J, Wang X. Numerical and experimental investigations on the axial crushing response of composite tubes. *Composites Structures*, 2009; 91: 222-228.

[20] L. Grauers, R. Olsson, R. Gutkin. Energy absorption and damage mechanisms in progressive crushing of corrugated NCF laminates: Fractographic analysis. *Composite Structures*, 2014; 110: 110-117.

[21] Mahdi E, Sebaey TA. An investigation into crushing behavior of radially stiffened GFRP composite tubes. *Thin-Walled Structures*, 2014;76: 8-13.

[22] Dayyani I, Shaw AD, Flores EIS, Friswell MI. The mechanics of composite corrugated structures: A review with application morphing aircraft. *Composite Structures*, 2015;133:358-380.

[23] Palanivelu S, Paepegem WV, Degrieck J, Ackeren JV, Kakogiannis D, Hemelrijck DV, Wastiels J, Vantomme J. Expermiental study on the axial crushing behavior of pultruded composite tubes. *Polymer Testing*, 2010; 29: 224-234.

[24] Xu J, Ma Y, Zhang Q, Sugahara T, Yang Y, Hamada H. Crashworthiness of carbon fiber hybrid composite tubes molded by filament winding. *Composites Structures*, 2016; 139: 130-140.

[25] Ghafari-Namini N, Ghasemnejad H. Effect of natural stitched composite on the crashworthiness of box structures. *Material and Design*, 2012; 39: 484-494.

[26] Wade B, Deleo F, Feraboli P. Toward the development of a test standard for characterizing the energy absorption of composite materials. Proceedings of ICCM17, Edinburgh, UK, 2009; paper No. F11:1, 1-6.

[27] Jacob GC, Fellers JF, Simunovic S, Starbuck JM. Energy Absorption in Polymer Composites for Automotive Crashworthiness Journal of Composite Materials 2002;36:813-850.

[28] Jackson A, David M, Gunnion AJ, Kelly D, Dutton S. Dynamic and quasi-static crush testing of closed carbon-fiber/epoxy elements. Proceedings of 27th International Congress of the Aeronautical Sciences, Nice, France, 2010;1-9.

[29] Chiu LNS, Falzon BG, Ruan D, Xu S, Thomson RS, Chen B, Yan W. Crush responses of composite cylinder under quasi-static and dynamic loading. Compos Structure 2015;131:90–98.

[30] Hull D. A unified approach to progressive crushing of fibre-reinforced composite tubes. *Composite Science and Tech*, 1991; 40: 377-421.

[31] Mamalis AG, Robinson M, Manolakos DE, Demonsthenous GA, Ioannidis MB, Carruthers J. Review Crashworthy capability of composite material structures. Composite Structures, 1997; 37: 109-134.

[32] Onishi M. Torays business strategy for carbon fiber composite materials. Toray Industries Inc, 21 Sept 2012.

[33] Report of Composites for Mass-Produced Vehicle: Leveraging an end-to-end solution for design,analysis and manufacturing. Dassault Systemes, 2010.

[34] Sanjay M. Opportunity and challenges in automotive composites industry. Report of Lucintel, 2013.

[35] Report of Polymer composites for automotive sustainability. SusChem, 2005.

[36] P. Beardmore and C. F Johnson. The potential for composites in structural automotive applications. *Composites Science and Technology*, 1986; 26: 251-281.

[37] Taketa I, Okabe T, Kitano A. A new compression-molding approach using unidirectionally arrayed chopped strands. *Composites Part A*, 2008; 39: 1884-1890.

[38] Taketa I, Okabe T, Kitano A. Strength improvement in unidirectional arrayed chopped strands with interlaminar toughening. *Composites Part A*, 2009; 40:1174-1178.

[39] Taketa I, Sato N, Kitano A, Nishikawa M, Okabe T. Enhancement of strength and uniformity in unidirectionally arrayed chopped strand with angled slits. *Composites Part A*, 2010; 42: 1639-1646.

[40] Taketa I, Okabe T, Matsutani H, Kitano A. Flowability of unidirectionally arrayed chopped strands in compression molding. *Composite Part B*, 2011; 42: 1764-1769.

[41] Li H, Wang WX, Takao Y, Matsubara T. New designs of unidirectionally arrayed chopped strands by introducing discontinuous angled slits into prepreg. *Composites Part A*, 2013; 45: 127-133.

[42] Li H, Wang WX, Matsubara T. Multiscale analysis of damage progression in newly designed UACS laminates. Composites Part A, 2014; 57: 108-117.

[43] Feraboli P, Cleveland T, Ciccu M, Stickler P, Deoto L. Defect and damage analysis of advanced discontinuous carbon/epoxy composite materials. *Composites Part A*, 2010; 41(7): 888-901.

[44] Gergely C, Pimenta S, Wisnom MR, Robinson P. Demonstration of pseudo-ductility in undiriectional discontinuous carbon fibre/epoxy prepreg composites. Composite Sciences and Technology, 2015; 106: 110-119.

[45] Yu H, Longana ML, Jalalvand M, Wisnom MR, Potter KD. Pseudo ductility in intermingled carbon/glass hybrid composites with highly aligned discontinuous fibers. *Composites Part A*, 2015; 73: 35-44.

CHAPTER 2

Compressive and progressive crushing properties of quasi-isotropic UACS laminate with bi-angle slit

In this chapter, further investigation on compressive strength and progressive crushing properties of laminates consisting of unidirectionally arrayed chopped strands (UACS) with distribution bi-angle slits has been carried out. Three kinds of bi-angle UACS laminates with different slit angles of ±11.3°, ±27.5°, and ±45° were fabricated and tested to investigate the effects of slit angle on the compressive and crushing properties of bi-angle UACS laminates. For a benchmark, quasi-isotropic laminates without slit were also fabricated and tested.

2.1 Introduction

In this chapter, bi-angle UACS laminates are investigated to determine compressive and progressive crushing properties. Quasi-static compression and progressive crushing tests were performed for quasi-isotropic laminates of $[45/0/-45/90]_{2s}$ and compression tests were conducted according to ASTM D3410 procedure. To my knowledge, there is no standard for progressive crushing test. In general, crushing test can be carried out in one of two conditions of impact and quasi-static conditions. Impact test requires very expensive testing equipment and high speed video-camera to follow the crushing process. Due to the limitation of experimental condition, quasi-static crushing tests are adopted in this study. Three kinds of bi-angle UACS laminates with different slit angles of ±11.3˚, ±27.5˚, and ±45˚ were fabricated and tested to investigate the effects of slit angles on the compressive and crushing properties of bi-angle UACS laminates. For a benchmark, quasi-isotropic laminates without slit are also fabricated and tested. In order to make UACS plies, a handmade technique is employed to introduce the slits into the prepreg using a commercial paper cutter. Crashworthiness properties and fracture mechanism of three different angle bi-angle UACS are investigated and compared with those of conventional laminate without slit.

2.2 Experimental procedures

2.2.1 Material

The material used in this study is unidirectional prepreg of T700SC/2592 carbon fibre/epoxy by Toray Inc. The prepreg sheet is 0.12 mm thickness with fibre volume fraction (V_f) of 67%. The tensile strength, tensile modulus, and density of carbon fibre are 4900 MPa, 230.GPa, and 1.80g/cm^2 respectively.

2.2.2 Fabrication of bi-angle UACS laminates

As mentioned above, in this work UACS was fabricated by introducing slits using paper cutter and hand-made technique, which was the same in the previous work [1]. Firstly, UACS plies were prepared by cutting sheets of 250 × 250 mm out of prepreg sheet. Rectangular prepreg sheets were cut for 0°, 45°, 90°, and -45° plies before introducing the slits as shown in Fig. 2-1(a). Then, a separate polymer sheet and a white paper with a printed slit distribution were put on the prepreg, which is shown in Fig. 2-1(b). Next, slits with bi-angle distribution were introduced into the prepreg following the slit lines printed on the white paper using a paper cutter. All the fibres were cut into 25 mm length. Fig. 2-1(c) shows the photograph of the hand-made cutting process using a paper cutter. In order to avoid prepreg becoming soft gradually during the introduction of the slit, the cutting process was carried out quickly and the room temperature was maintained below 18˚C. It is important to complete the cuttings within a short time to ensure the quality and properties of the laminas were not changed.

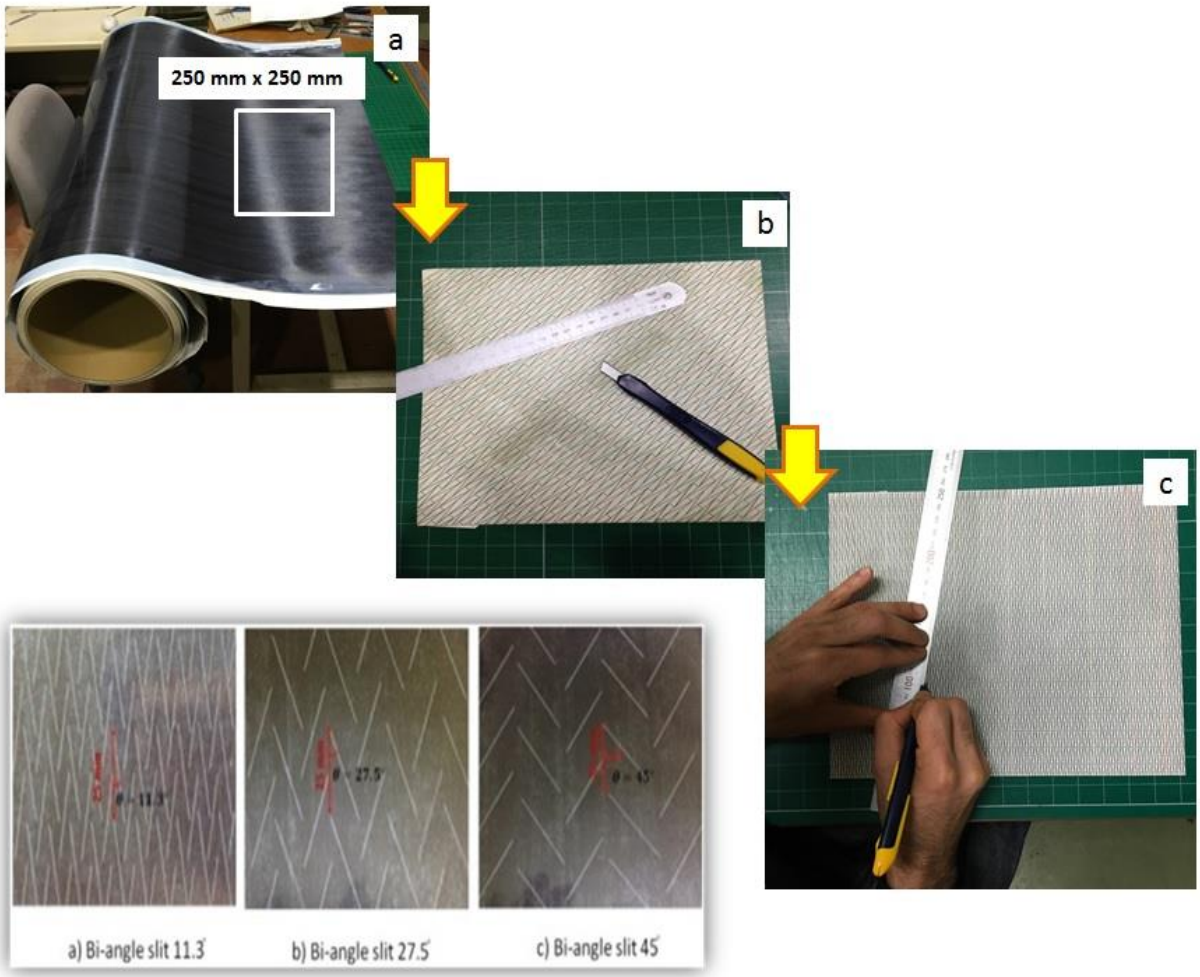

Figure 2-1: Schematic diagram of cutting procedures for fabricating UACS bi-angle plies with different discontinuous slits : (a) cut-out of prepreg sheet, (b) prepreg covered with white paper slit pattern, (c) cutting of slit using paper cutter.

In the present work, the slit angles between the slit and the fibre direction were 11.3, 27.5, and 45 degrees, as these angles showed significant effects on tensile strength properties for continuous angle slits based on previous research reported by Taketa [2]. Illustration of a UACS sheet with bi-angle slit distribution and stacking sequence of the UACS sheets are shown in Fig. 2-2. White lines denote slits. The projection of all slits on the fibre direction is 25 mm length and the projections on the line normal to the fibre direction are 5 mm, 13 mm, and 25 mm for bi-angle slits ±11.3˚, ±27.5˚ and ±45˚, respectively, as shown in Fig. 2(a). Fig. 2(b) illustrates the stacking sequence of UACS plies with different fibre orientations with bi-angle slits. Afterwards, the UACS sheets were stacked into a quasi-isotropic laminate of $[45/0/-45/90]_{2S}$ and then the laminate was cured using an autoclave.

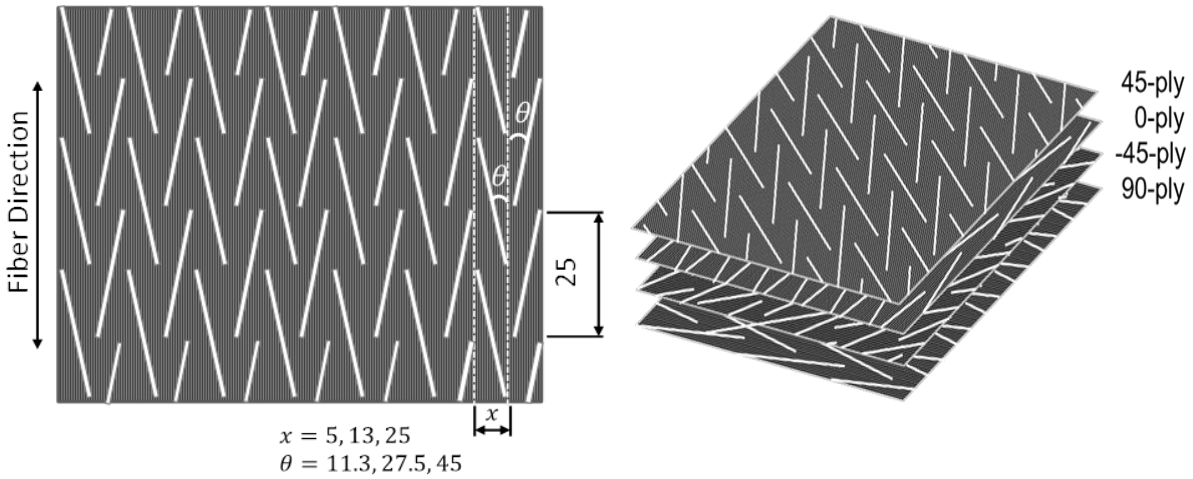

(a) UACS sheet with bi-angle slits (b) Stacking of UACS sheets

Figure 2-2: Illustrations of UACS lamina with bi-angle slit distribution and stacking of UACS laminas: (a) UACS sheet with bi-angle slits, (b) Stacking UACS laminas.

The cure temperature and pressure for autoclave are 135˚C and 0.3 MPa, respectively, following the cure cycle recommended by the manufacturer as shown in Fig. 2-3. The average thickness of the cured laminates was 2.0 mm. Typical side view images of cured UACS bi-angle laminates with three different slit angles are shown in Fig. 2-4, respectively. It is obviously seen that the slit is filled by an excess of resin in the ply. It is noted that the different dimensions of slits in different plies are mainly due to the different angle of the slits.

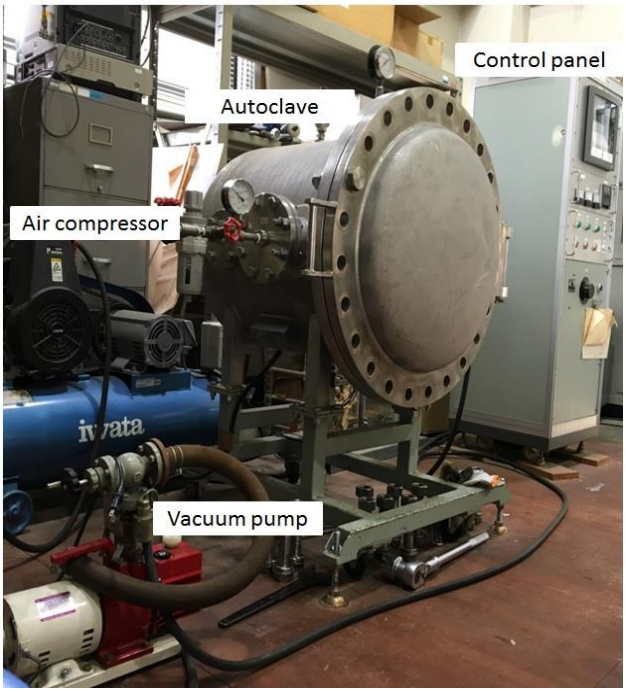

(a) Autoclave

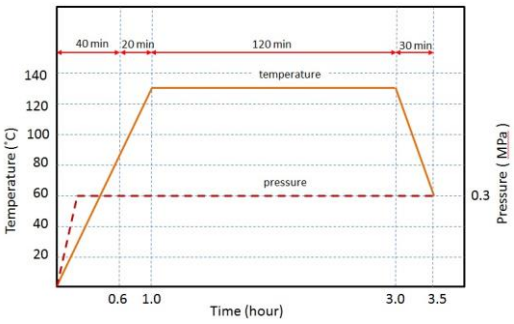

(b) Cure cycle

Figure 2-3: Curing process of UACS using autoclave: (a) Autoclave, (b) cure cycle.

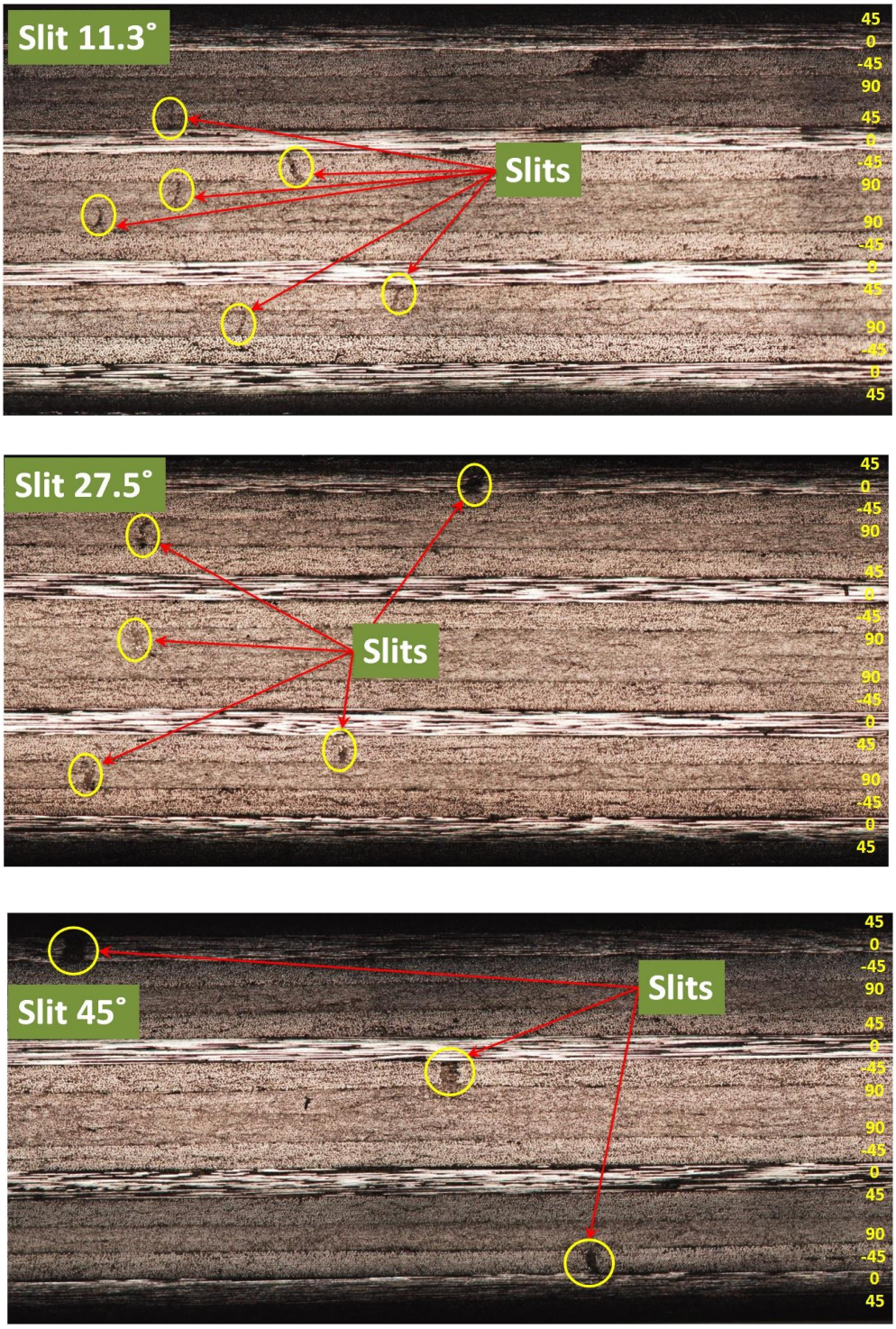

Figure 2-4: Typical side view images of slits in cured UACS bi-angle laminates with 3 different slit angles.

2.2.3 Specimen and compressive tests

Two types of compression tests were carried out in this study to investigate the compressive strength and progressive crushing properties of UACS laminates with bi-angle slits. Geometries and images of specimens for these two types of tests are presented in Fig. 2-5. All tests were carried out using a MTS-810 testing machine at constant crosshead speed. First, the static compression test was performed in accordance to ASTM D3410 to measure the compressive strength. The geometry and images of the specimen for static compressive test are presented in Fig 2-5(a). The specimen, 110 mm in length with 10 mm gauge section, was cut from the laminate using a diamond cutter. Aluminium tabs were bonded on the two ends of the specimen, and a 5 mm strain gauge bonded on the centre was used to measure the compressive strain. The crosshead speed used in this test was 1.0 mm/min. There are at least five specimens tested for each kind of bi-angle UACS laminate and the laminate without slit, respectively. In order to clarify the failure characteristics of the specimen, microscopic observation of tested specimens was also carried out using optical microscope.

The second test performed was the progressive crushing test. The geometry of the specimen is 80 mm × 10 mm × 2 mm with 30 mm gauge section, as shown in Fig 2-5(b). One end was grounded to form a 45˚ chamfering-type trigger mechanism. Another end was bonded by an aluminium tab of 50 mm in length and 1 mm in thickness. Three specimens were prepared for each kind of bi-angle UACS laminate and the laminate without slit, respectively. The specimens were crushed at displacement rates of 3 mm/min using the MTS-810 testing machine and were interrupted after 8 mm crushing

displacement, which is considered to be enough to determine the mean crushing load. In order to avoid buckling that will influence tests result, special anti-buckling jig are developed and used during the crushing of the specimen, as illustrated in Fig. 2-6.

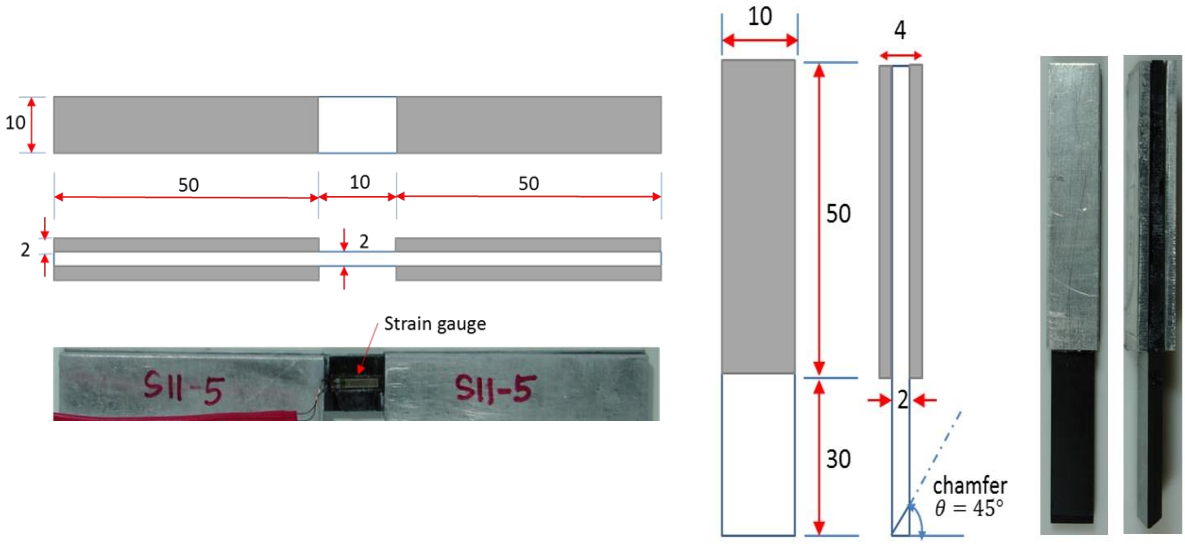

(a) Specimen for static compression test (b) Specimen for progressive crushing test

Figure 2-5: Geometries of specimens for two kinds of tests: (a) specimen for static compression test, (b) specimen for progressive crushing test.

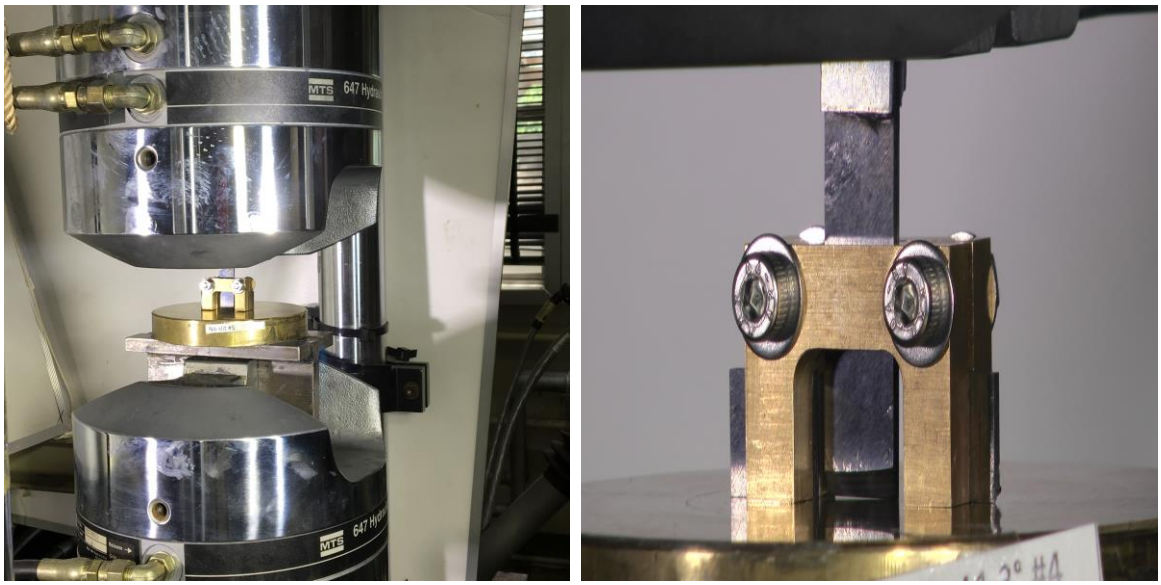

Figure 2-6: Jig attached on MTS 810 material testing system used in progressive crushing test.

In order to characterise the progressive crushing properties of the specimen, the following characteristic quantities in the next subsection 2.2.4 are defined from the force-displacement curve of each specimen.

2.2.4 Crashworthiness parameters

Generally, energy absorption (EA), specific energy absorption (SEA), mean crushing force, peak force, and crash force efficiency (CFE) are extensively used to measure the crashworthiness characteristics of materials [3-5]. Taking from the force-displacement curve, the maximum force of the first peak of the curve is defined as peak load (P_{max}). Absorbed energy (A_e)is defined by the area under force-displacement curve and was

calculated from the following Eq. (1).

$$A_e(L) = \int_0^L P(l)dl \tag{1}$$

Where P is the value of force at collapse displacement l and L is a specified displacement during the crushing test. In the present study, $L = 8$ mm was specified. The mean load of the collapse, P_{mean} is defined by the absorbed energy and crushing length during the post crush process as written in Eq. (2).

$$P_{\text{mean}} = \frac{\int_{L_p}^{L} P(l)dl}{L - L_p} \tag{2}$$

Where L_p is the crushing displacement at the peak load. Specific energy absorption (SEA) is the absorbed energy per unit of crushed specimen mass (m) and is calculated with Eq. (3).

$$\text{SEA} = \frac{A_e(L)}{m} \tag{3}$$

Another useful parameter to measure the crushing performance effectiveness of a material is crush force efficiency (CFE), which is defined by the percentage of P_{mean} to peak load (P_{max}) and is calculated with Eq. 4.

$$\text{CFE} = \frac{P_{mean}}{P_{max}} \times 100 \ \ (\%) \tag{4}$$

2.3 Results and discussion

2.3.1 Effects of slit angles on the compressive strength of bi-angle UACS laminates

Typical compressive stress-strain curves for each kind of specimen are depicted in Fig. 2-7. The bi-angle UACS laminate with large slit angle gives low stiffness. The average compressive strength of quasi-isotropic laminate without slit is 533 MPa. The UACS laminate with ±11.3˚ bi-angle slits gives the highest compressive strength (469 MPa) among the three kinds of bi-angle UACS laminates, which is 88% of the compressive strength of the original laminate without the slit. UACS laminates with ±45˚ and ±27˚ bi-angle slits give 371 MPa and 352 MPa, respectively. Variant reductions of about 12%, 30%, and 34% in compressive strength for bi-angle UACS laminates with slit angle ±11.3˚, ±45˚ and ±27.5˚, respectively, which indicates that slit angle gives significant effect on the strength of the bi-angle UACS laminate. It is interesting that UACS laminate with ±45˚ bi-angle slits gives the highest failure strain.

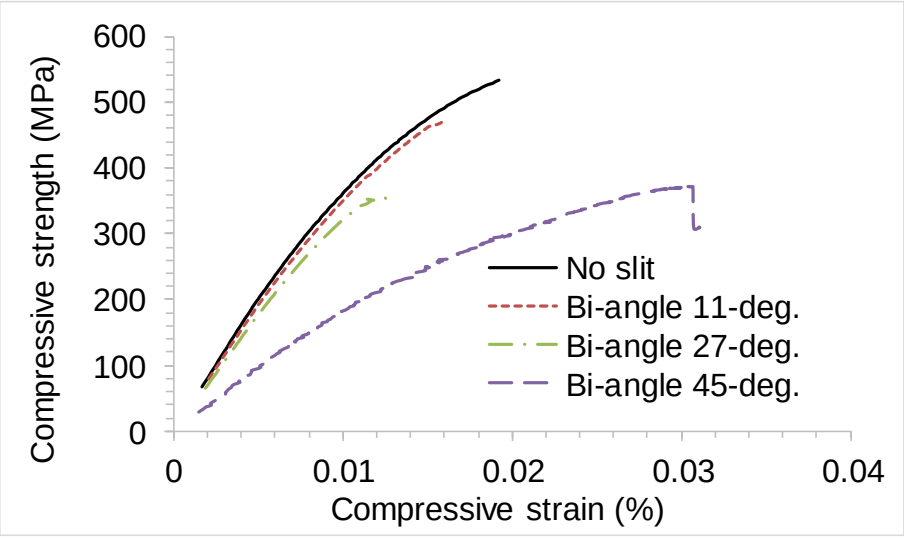

Figure 2-7: Typical compressive stress-strain responses for various kinds of specimens.

Typical images of tested specimen under optical microscopy are shown in Figure 2-8. As can be seen in Fig. 2-8(a), in laminate without slit, damaged zones mainly consist of multiple delaminations, a cluster of locally crushed fibres, and cracked laminates along a large shear band with an angle of about 37˚ to the loading axis. These damage zones lead to instability in the nearby fibre and matrix, thus initiating microbuckling and kink bands. Large delamination seems to appear at the interface of -45˚/0˚. In contrast, a little different failure behaviour is observed from the tested specimens of bi-angled UACS laminates. In the specimen of bi-angle UACS laminate with slit angle ±11.3˚ (Fig. 2-8(b)), delamination became smaller and multiple shear bands occurred at different locations due to the effect of slits. Compared with laminate without slits, slits in bi-angle UACS laminates are resin-rich. Weakening zones with high-stress concentration play a role of a trigger to originate and localise, thus suppressing large delamination [6,7]. We can see more debris and broken fibres from shear and kink bands at slit zones.

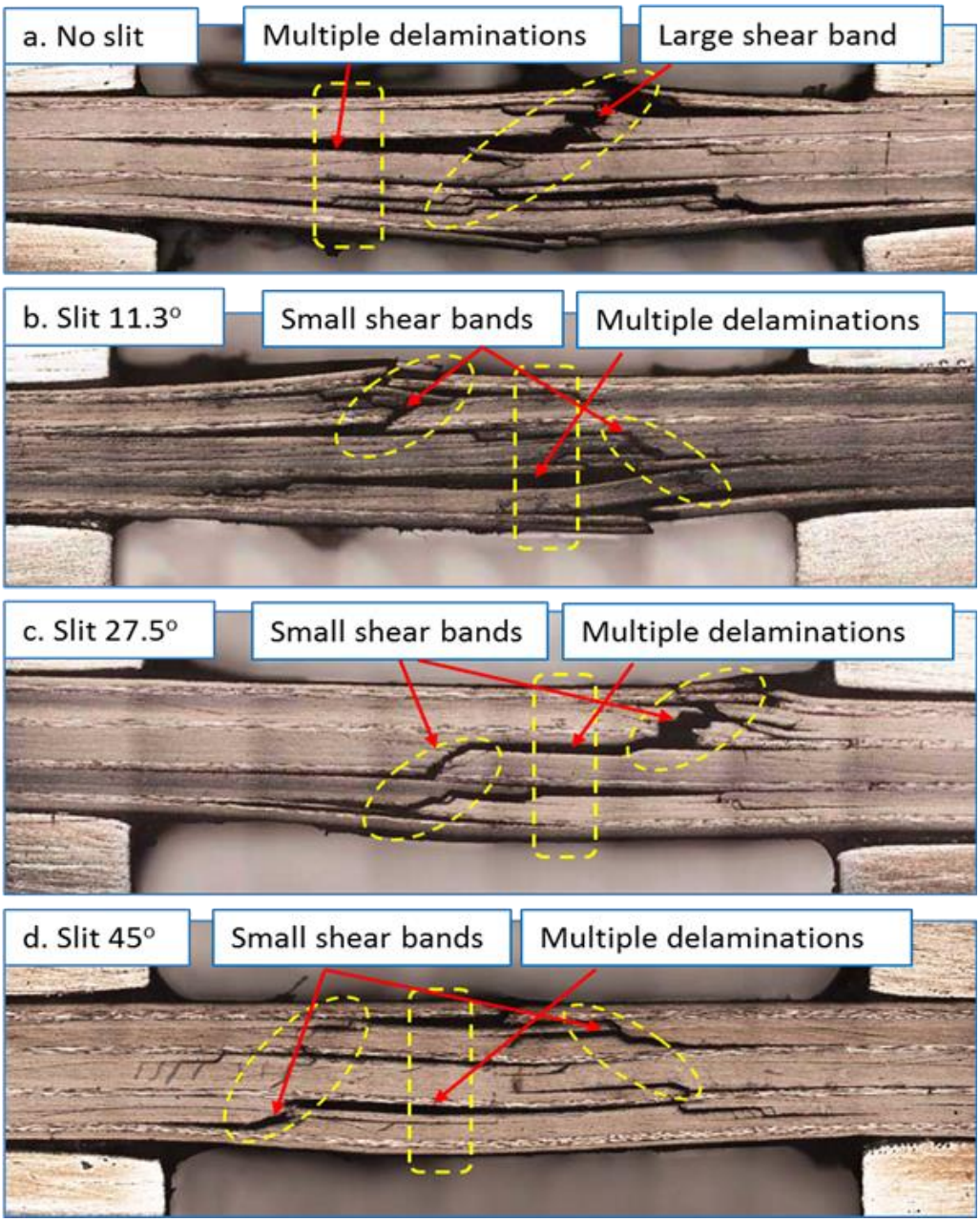

Figure 2-8: Typical images of tested specimens.

A schematic illustrating the possible failure model in the 0 ˚ ply of the specimen of bi-angle UACS laminate with slit angle ±11.3˚ is shown in Fig 2-9 to demonstrate how the slits could lead to kink band and shear band. In specimens with slit angles ±27.5˚ and ±45˚ as presented in Fig 2-8(c) and (d), matrix cracks initiated in the 90˚ and ±45˚ plies are more obvious, which leads to the laminate fracture in staggered form. A large slit angle represents long slit and then long region with high stress concentration. This is the reason why a small slit angle gives high strength value and a large slit angle tends to reduce the strength.

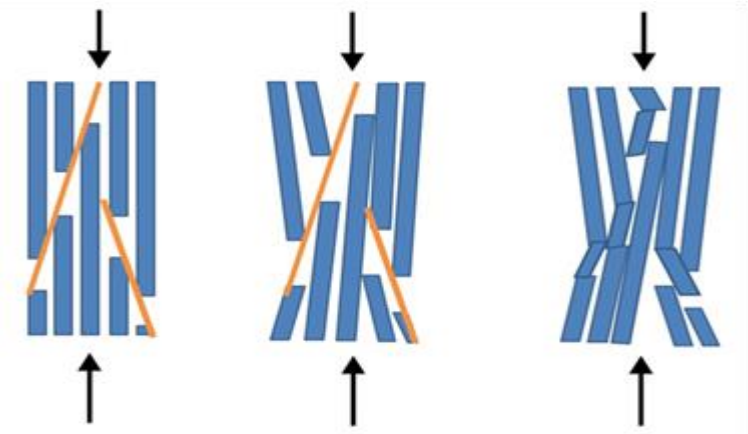

Figure 2-9: Schematic model of kinking and shear band formation in 0 ˚ ply of bi-angle UACS laminate.

2.3.2 Effects of slit angle on the progressive crushing of bi-angle UACS laminates

Progressive crushing test is different from the above static compression test and its aim is to investigate the feasibility of bi-angle UACS laminates for the application of crush box and the effects of slit angle on the energy absorption of bi-angle UACS laminates. Typical load-displacement curves for all kinds of specimens are presented in Fig. 2-10. Except for laminate without slit, all the curves for specimens of bi-angle UACS laminates illustrated a crushing up to initial peak value before 3 mm displacement and then dropped down to mean crushing state because of stress concentration around slits in UACS laminates. In contrast, the load applied on the specimen without slit quickly rose to peak value about 3.55 kN and then dropped down instantaneously and catastrophically after 3 mm displacement. Specimen with different slit angle showed different peak load. The specimen with slit angle ±11.3 ˚ gave the highest peak load of 3.69 kN, 3.8% higher than that of the specimen without slit. The specimens with ±27.5˚ and ±45˚ slit angles gave relatively low and similar peak loads. These results revealed the effect of slit angle on the peak load and progressive crushing behaviour of bi-angle UACS laminates. Furthermore, these features of load-displacement response reflect a feasibility that slit can be used as a new intralaminar trigger to initiate and control the initial and crushing failure mode, thus preventing the structure from instantaneous and catastrophic crushing failure.

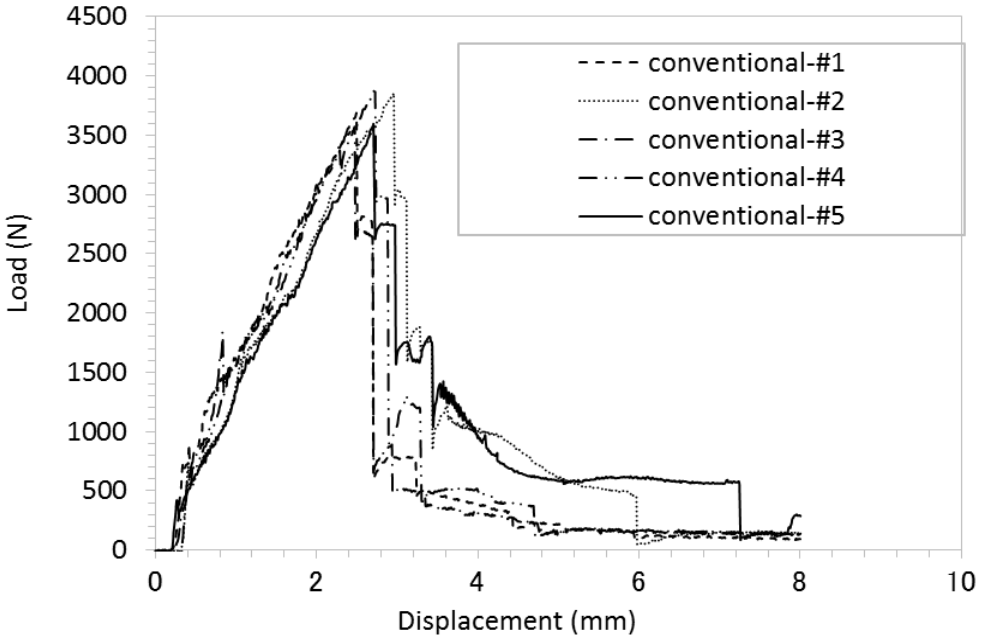

a) Conventional laminates.

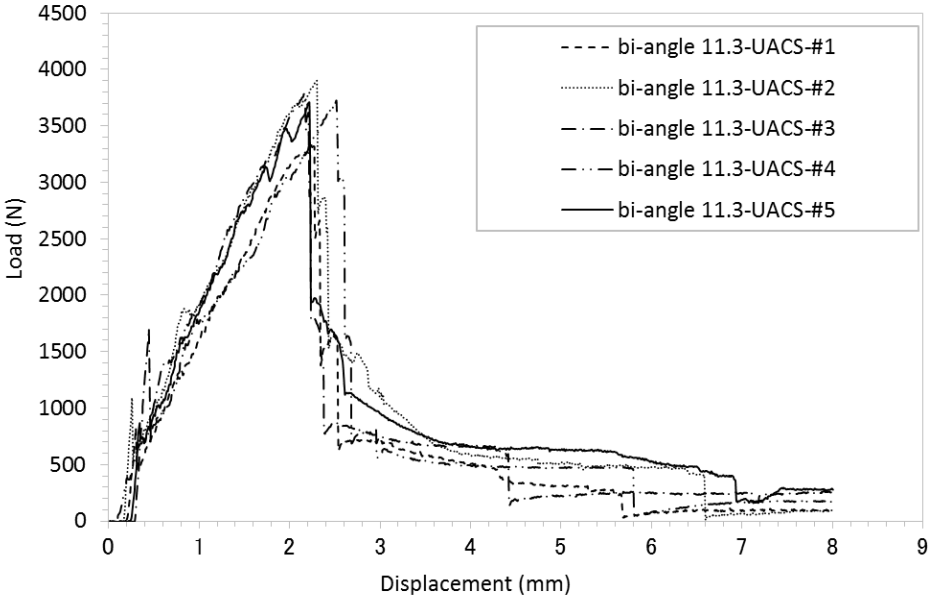

b) Bi-angle ±11.3 ˚ UACS laminates.

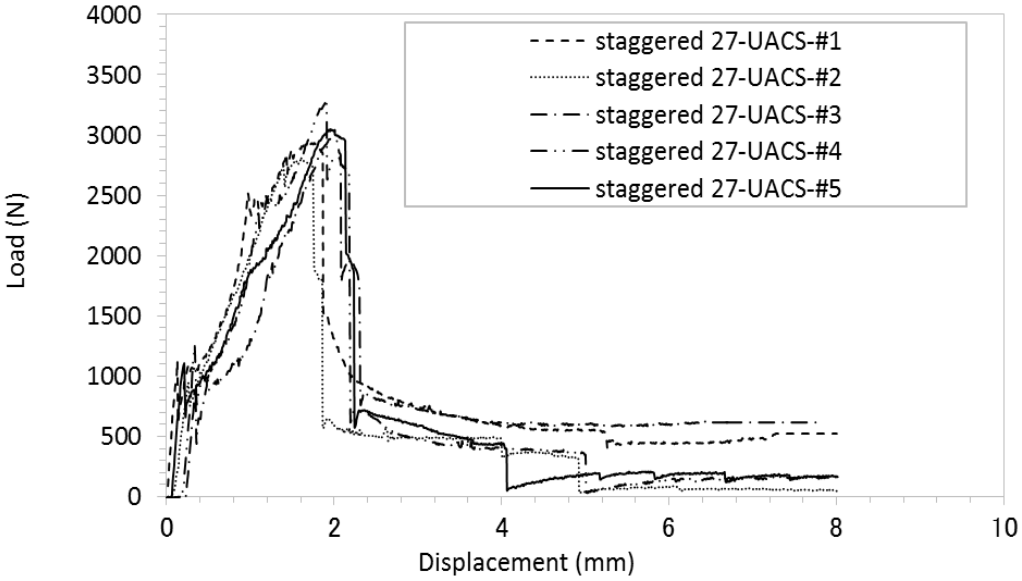

c) Bi-angle ±27.5˚ UACS laminates.

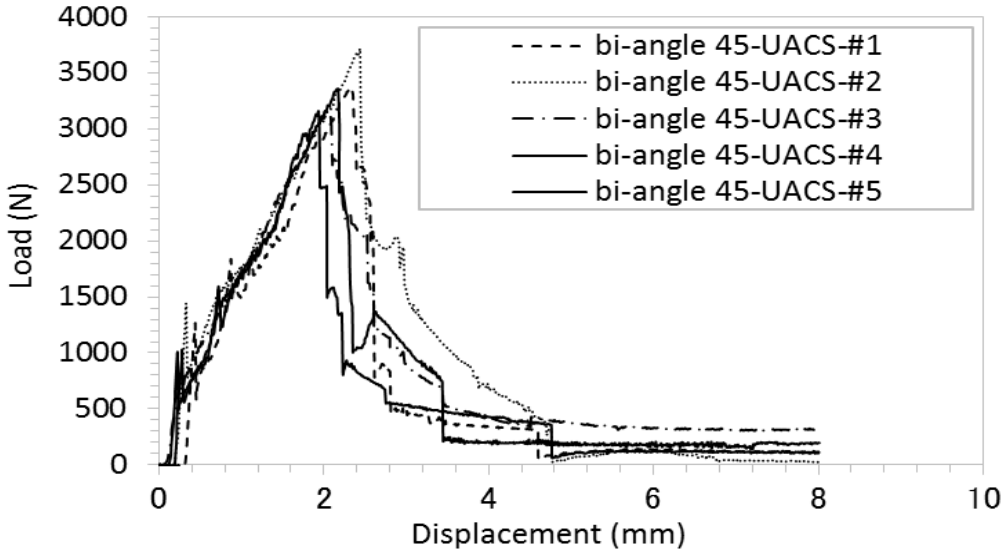

d) Bi-angle ±45˚ UACS laminates.

Figure 2-10: Load-displacement responses for various laminates.

Typical images of final crushed specimen for different angles of UACS laminates with bi-angle slit distribution are shown in Fig. 2-11. However, the crushing morphology of progressive crushing during test of specimen cannot be captured, as the view was blocked by anti-buckling jig. The specimen laminates without slit showed interlaminar splitting, multiple delamination, and bending deformation at the lower end due to the triggering mechanism of 45˚ chamfering end. We also observed that multiple long delamination propagates between interlaminar regions to reach the tab area region. As a result, it reduced the mean load of conventional specimen because of the loss of load bearing.

In contrast, three kinds of specimens with slits showed different progressive crushing behaviour. Except for bi-angle 45˚, all UACS laminates showed after the crushing of the lower chamfer-end, a single delamination could be obviously seen to propagate and suppress until the middle region. This is caused by the slits existing in this middle region. Only single delamination occurred in both bi-angle 11.3˚ and bi-angle 27.5˚, which absorbed high mean load. However, from the image, bi-angle 27.5˚ UACS laminate showed outer plies splitting and reducing mean load as it can no longer support the load bearing.

On the other hand, bi-angle 45˚ UACS laminate showed combination of conventional, bi-angle 11.3˚ UACS and bi-angle 27.5˚ UACS where multiple delamination started to propagate and then suppress at slit area. Images also showed splitting of outer laminas that reduced the mean load for bi-angle 45˚. These facts have shown that bi-angle slit in UACS laminate made weak lines, thus causing the laminate to fail from the middle region.

Specimen	Top view	Side view
Conventional CFRP		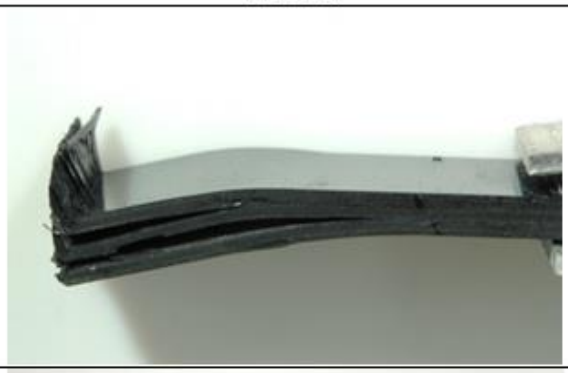
Bi-angle 11.3˚		
Bi-angle 27.5˚		
Bi-angle 45˚		

Figure 2-11: Progressive crushing failure behaviour of various laminates.

The total energy absorption, peak load and mean load for laminate without slit and bi-angle UACS laminates during progressive crushing test is presented in Fig 2-12(a), (b) and (c). The energy absorption capability of specimens is dependent on the area under load-displacement curve. The total absorbed energy from 0 mm displacement to 8 mm displacement is shown in Fig 2-12(a). Bi-angle UACS laminate with slit angle ±11.3˚ showed the highest energy absorption, which is about 95% of the laminate without slits. Laminates with slit angles ±27.5˚ and ±45˚ respectively showed relatively low energy absorption, which are about 80% and 86% of the laminate without slits. Bi-angle UACS with ±11.3˚ slit angle showed the largest peak load among all UACS laminate types followed by ±45˚ slit angle, while UACS laminate with ±27.5˚ slit angle gave the smallest value. Interestingly, all UACS laminates showed comparable mean load to conventional laminate with continuous fibres as displayed in Fig 2-12(c) and Table 2-1. From these data, ±11.3˚ slit showed constant value of maximum load, highest total energy absorption, and highest specific energy absorption among all UACS laminates. Thus, excellent formability, small diminution of mean load and energy absorption, and the ability to control the position of the initial damage implied that the bi-angle UACS laminate with ±11.3˚ slit angle may be an available material for crashworthy structure application.

The effects of slit angles on specific energy absorption (SEA) of the specimens is depicted in Fig 2-13. The bi-angle UACS laminate with slit angle ±11.3˚ has the largest SEA among all UACS laminates, while the laminate with slit angle ±27.5˚ has the smallest SEA. Generally, the larger the value of the SEA, the more efficient the energy

absorber is [8, 9]. Fig. 2-13 also indicates that a smaller angle slit in bi-angle UACS laminate leads to a significant increase in specific energy absorption.

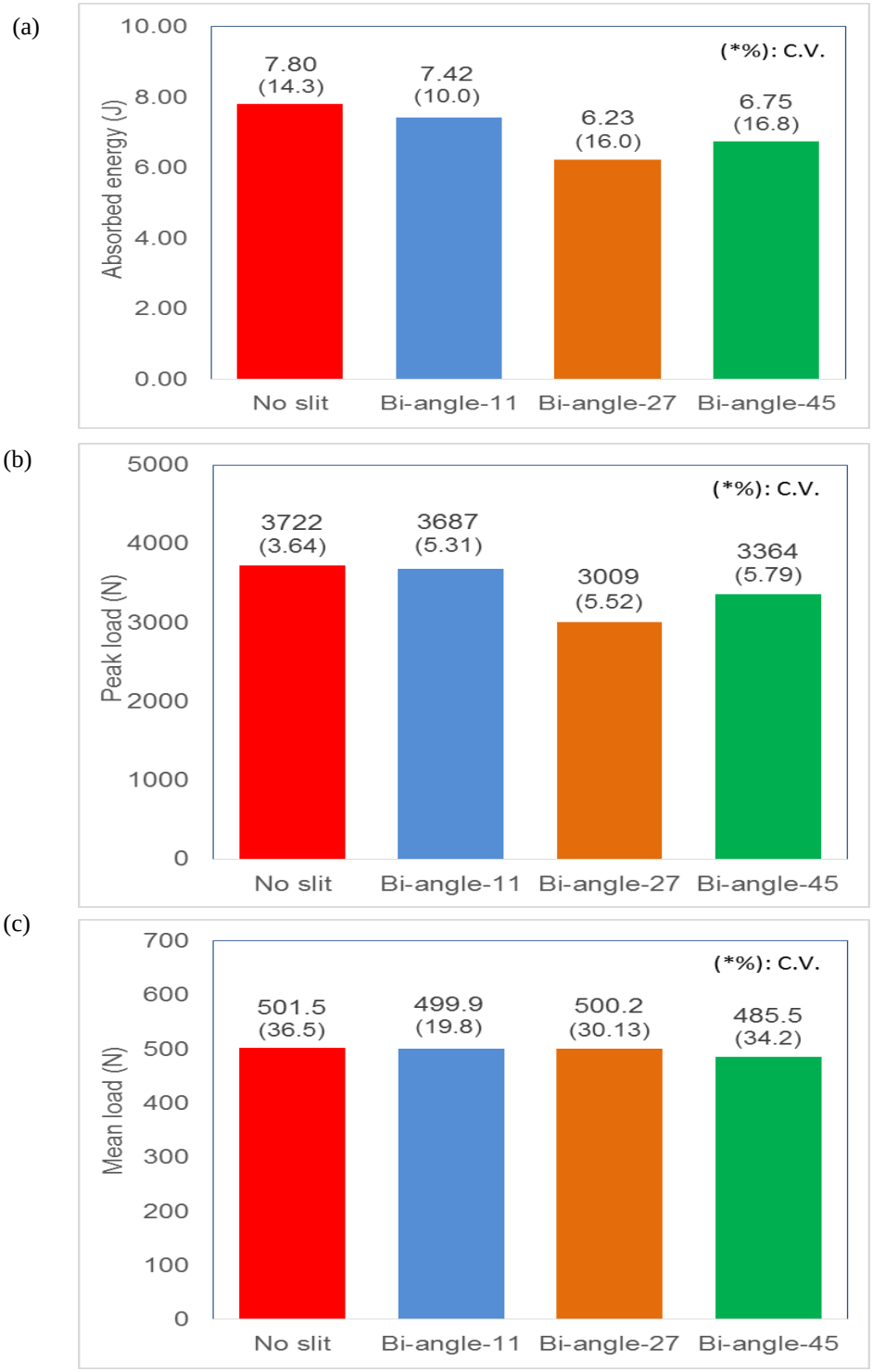

Figure 2-12: Energy absorption, maximum peak load, and mean load for various laminates.

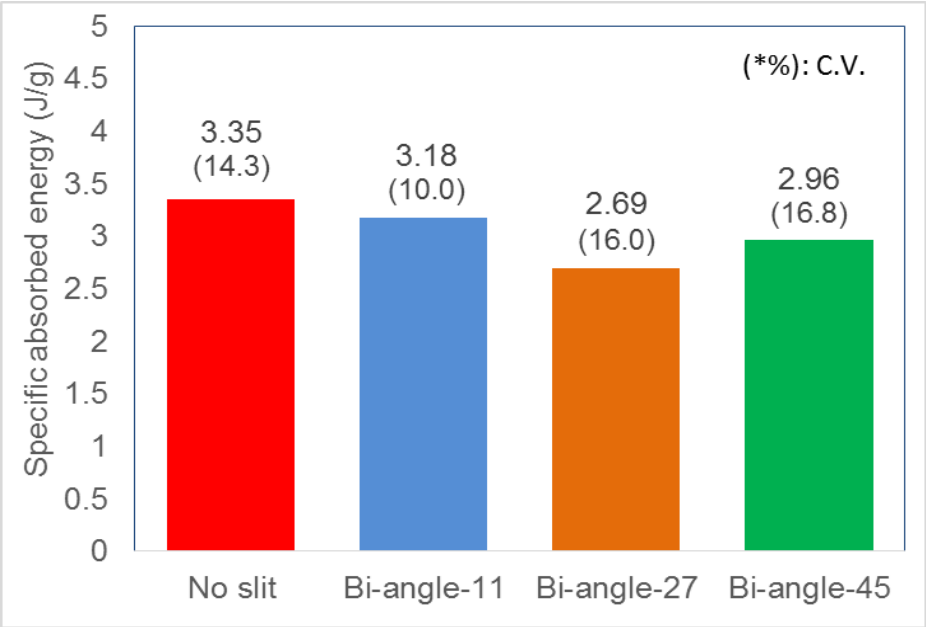

Figure 2-13: Specific energy absorption (SEA) for various laminates.

The effect of slit angle on the crush force efficiency (CFE) is depicted in Fig 2-14. It can be seen that bi-angle UACS laminate with slit angle ±27.5˚ gives the highest value of CFE about 16.6% and is followed by bi-angle UACS laminate with slit angle ±45˚, laminate without slit, and bi-angle UACS laminate with slit angle ±11.3˚ with CFE values of 14.4%, 13.5%, and 13.6%, respectively. These results implied that bi-angle UACS laminates may broaden the selection of short fibre composite materials to replace conventional laminate for crashworthy structure application. CFE is one of the most important parameters used to evaluate the performance of a material or a structure in absorbing the energy [9-15] and is related to the material effectiveness for crashworthy structure. High peak force indicates low CFE, which leads to an increase in acceleration and potential damage to the structure during frontal crush and must be avoided. Therefore, high CFE is desirable and must be maximised, and this can be obtained by decreasing the peak load [9, 13]. Introducing trigger mechanism is usually used by many researchers to

decrease the peak load to increase CFE value. However, in real application, the conventional trigger mechanism makes it difficult to adequately support and fix the chamfered end of the component at small angles or joints. Moreover, machining the component can generate local defects and micro cracks onto materials. In order to overcome those outer trigger drawbacks, bi-angle slit in UACS laminate may play a role of trigger as the slits can make weak lines in the laminate as expected. In addition, the average values of total absorbed energy, peak load, mean load, CFE, mass of the specimen, and SEA are listed in Table 2-1 for the sake of convenience.

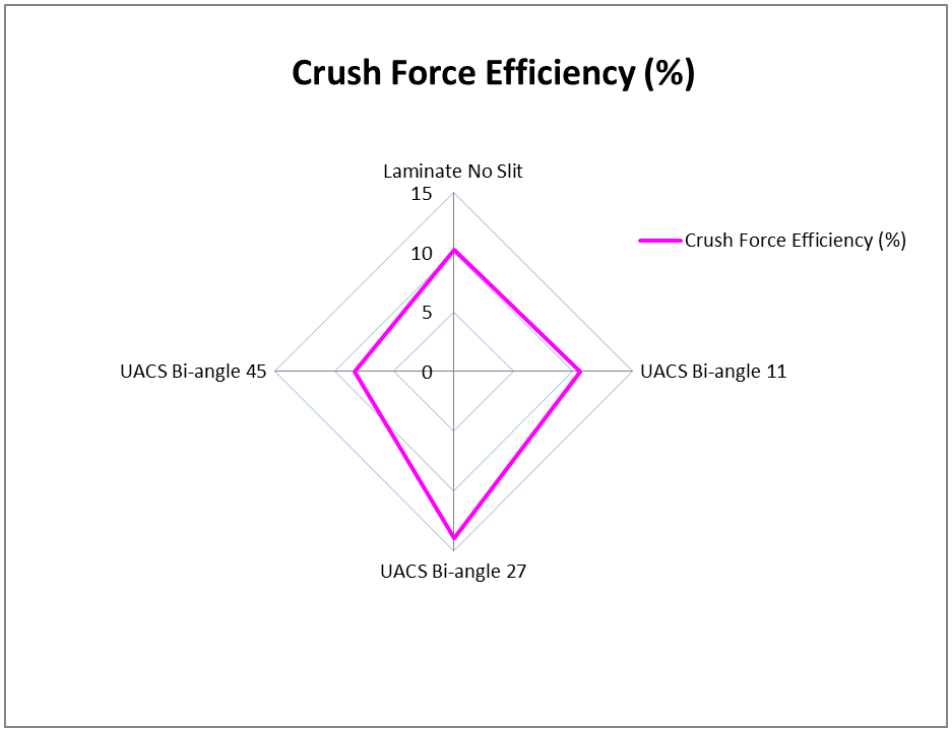

Table 2-14: Crush force efficiency (CFE) for various laminates.

Table 2-1: Test result on progressive crushing.

sample	Total energy absorbed	P_{max}	P_{mean}	weight	SEA	CFE
	(J)	(N)	(N)	(g)	(J/g)	
conventional laminate	7.80	3722.48	501.53	2.33	3.35	13.5%
bi-angle 11.3	7.42	3686.72	499.91	2.34	3.18	13.6%
bi-angle 27.5	6.23	3008.90	500.22	2.31	2.69	16.6%
bi-angle 45	6.74	3364.08	485.54	2.28	2.96	14.4%

2.4 Summary

In this chapter, static compression and progressive crushing properties of quasi-isotropic UACS laminates with bi-angle slits are investigated experimentally. Three kinds of bi-angle UACS laminates with different slit angles of ±11.3˚, ±27.5˚, and ±45˚ are fabricated and tested to investigate the effects of slit angle on the compressive and progressive crushing properties of bi-angle UACS laminates. Experimental results leads to following conclusions.

The UACS laminate with ±11.3˚ bi-angle slits gives the highest compressive strength among the three kinds of bi-angle UACS laminates, which is comparable to conventional laminate without slit, although the length of all fibres in UACS laminate with ±11.3˚ bi-angle slits are 25 mm. UACS laminates with ±45˚ and ±27˚ bi-angle slits give relatively low compressive strength compared with ±11.3˚ bi-angle slits and conventional laminate without slit. Therefore, slit angle has a significant effect to the compressive strength of bi-angle UACS laminate.

All the specimens of bi-angle UACS laminates showed a variation result on peak load, energy absorbed, mean load, and specific energy absorption, where ±11.3˚ bi-angle slits showed the highest value among all UACS types, although there was a slight decrease in mean load compared with ±27.5˚ bi-angle UACS . Here we tought that the bi-angle slits in UACS laminate made weak lines and increased concentration of stress raiser in the shorter fibre resulting in a larger number of fractured initiation sites. The energy absorption of UACS laminate with ±11.3˚ bi-angle slits is also comparable to conventional laminate without slit. In addition, bi-angle UACS laminates gave better

crush force efficiency compared with the conventional laminate. Therefore, UACS laminate with ±11.3˚ bi-angle slits is suitable for the application to structural parts that have complex shapes and require good energy absorption, since the laminate has excellent formability, comparable compressive strength and energy absorption ability, and higher crush force efficiency. However, crashworthy structure laminates require more energy absorption integrity. In the next chapter, plying strategies using UACS plies are conducted to identify the best configuration and optimisation of UACS laminate for crashworthiness structure application.

Bibliography

[1] Li H, Wang WX, Takao Y, Matsubara T. New designs of unidirectionally arrayed chopped strands by introducing discontinuous angled slits into prepreg. *Composites Part A*, 2013; 45: 127-133.

[2] Taketa I, Sato N, Kitano A, Nishikawa M, Okabe T. Enhancement of strength and uniformity in unidirectionally arrayed chopped strands with angled slits. *Composites Part A: Applied Science and Manufacturing*, 2010; 41(11): 1639–1646.

[3] Hull D. A unified approach to progressive crushing of fibre-reinforced composite tubes. *Composite Science and Tech*, 1991; 40: 377-421.

[4] Jacob GC, Feller JF, Simunovic S, Starbuck JM. Energy absorption in polymer composites for automotive crashworthiness. *Journal of Composite Materials*, 2002; 36(7): 813-850.

[5] Hou T, Pearce GMK, Prusty BG, Kelly DW, Thomson RS. Pressurised composite tubes as variable load energy absorbers. *Composite Structures*, 2015; 120: 346-357.

[6] S. Yoshiro, K. Ogi. Fracture behavior in CFRP cross-ply laminates with initially cut fibers. *Composites Part A*, 2009; 40: 938-947.

[7] Hang Li, Wen-Xue Wang, Terutake Matsubara. Multiscale analysis of damage progression in newly designed UACS laminates. *Composite Part A*, 2014; 57: 108-117.

[8] George C. Jacob, J. Michael Starbuck, John F. Fellers, S. Simunovic, R. G Boeman. Crashworthiness of various random chopped carbon fiber reinforced epoxy composite materials and their strain rate dependence. *Journal of Applied Polymer Science*, 2006; 101:1477-1486.

[9] Libo Yan, Nawasi Chouw. Crashworthiness characteristics of flax fibre reinforced epoxy tubes for energy absorption application. *Materials and Design,* 2013;51: 629-640.

[10] Alper Tasdemirci, Selim Sahin, Ali Kara, Kivanc Turan. Crushing and energy absorption characteristics of combined geometry shells at quasi-static and dynamic strain rates: Experimental and numerical study. *Thin-Walled Structure,* 2015; 86: 83-93.

[11] A. Esnaola, I. Ulacia, L. Aretxabaleta, J. Aurrekoetxea, I. Gallego. Quasi-static crush energy absorption of E-Glass/Polyester and hybrid E-Glass-basalt/polyester composite structures. *Material and Design,* 2015; 76: 18-25.

[12] T. A. Sebaey, E. Mahdi, A. Shamseldin, E. O. Eltai. Crushing behavior of hybrid hexagonal/octagonal cellular composite system: All made of carbon fiber reinforced epoxy. *Materials and Design,* 2014; 60: 556-562.

[13] Samer F, F. Tarlochan, Pooria Khalili, Hatam Samaka. Enhancement of energy absorption of thin walled hexagonal tube by using trigger mechanism. Int. J of *Research in Eng. and Tech,* 2013; vol. 2: 109-116.

[14] Louis N. S. Chiu, Brian G. Falzon, Dong Ruan, Shanqing Xu, Rodney S. Thomson, Bernard Chen, Wenyi Yan. Crush responses of composite cylinder under quasi-static and dynamic loading. *Composite Structures,* 2015; 131: 90-98.

[15] S. Palanivelu. W. V. Paepegem, J. Degrieck, J. Vantomme, D. Kakogiannis, J. V. Ackeren, D. V Hemelrijck, J. Wastiels. Crushing and energy absorption performance of different geometrical shapes of small-scales glass/polyester composites tubes under quasi-static loading conditions. *Composite Structure,* 2011;93:992-1007.

CHAPTER 3

Compression and crush responses of cross-ply laminates with UACS 0˚ plies

In this chapter, the static compression and progressive crushing properties of carbon fibre reinforced epoxy cross-ply laminates with different stacking sequence $[0/90]_{4s}$ and $[90/0]_{4s}$ and with different kinds of 0˚ plies are investigated experimentally. UACS plies with highly aligned slits of bi-angle pattern and staggered pattern are used as 0˚ ply, respectively, instead of conventional continuous fibre ply to study the effects of UACS ply on the compression and progressive crushing responses of cross-ply laminates. Effects of stacking sequence $[0/90]_{4s}$ and $[90/0]_{4s}$ and UACS 0˚ plies on the compressive strength and the progressive crushing properties, such as the maximum peak load, energy absorption, crush mean load, and crush force efficiency are clarified.

3.1 Introduction

As a new alternative material for automotive crashworthy structure application, UACS laminates require much higher specific energy absorption and better crush efficiency, while at the same time ensuring not to lose their excellent formability, as reported in previous study. If this could be achieved, UACS laminates are expected to be a novel material for crashworthiness structural application that demands complexity geometry such car's chassis/monocoque, frame, and crumple zone. Therefore, clarifying the best stacking configuration of cross-ply laminate and the best highly aligned discontinuous UACS slit pattern are necessary to determine optimum crashworthiness performance of laminate with 0˚ plies UACS.

Although many researchers have investigated the energy absorption characteristics in various continuous fibre reinforced composites and random chopped fibre reinforced composites [1-20], there is less literature available on energy absorption and crushing characteristics of highly aligned discontinuous carbon fibres. As it is important to understand relationship between compressive properties and crushing mechanism, the static compression and progressive crushing properties of carbon fibre reinforced epoxy cross-ply laminates with different stacking sequence $[0/90]_{4s}$ and $[90/0]_{4s}$ and with different kinds of UACS 0˚ plies are investigated experimentally in this chapter.

3.2 Newly intra-laminar trigger mechanism

As being discussed in the first chapter on the investigation of the earlier UACS, delamination between UACS layer is the main failure mode of UACS and it needs to be avoided. In particular, larger delamination leads to great reduction in the energy absorption ability of the laminate. Therefore, if these failure mechanisms can be controlled during crushing, composite structure is able to collapse in progressive and predictable manner that gives much higher energy to be absorbed. Almost all studies on crashworthiness indicate that energy absorption characteristics in composite structure are dependent on the crushing trigger [21,22] that usually is a weakened area at an appropriate location to initiate stable and controlled progressive failure. A chamfered end and bevel are very effective in preventing catastrophic failure, thus providing a stable initiation and propagation of collapse and reducing the initial peak load at the same time [23]. However, in real application, it is difficult to adequately support and fix the chamfered end of the component. Moreover, machining the component can generate local defect and micro cracks onto materials, which in return will influence the test result.

In order to overcome these drawbacks of the outer trigger, a new method is needed to solve the mentioned problem of chamfered trigger by creating localised weakening of specimen directly in the interior of the laminate. The stress concentration around slits may initiate stable and controllable progressive crushing, thus enhancing the crashworthiness properties of composite laminate. Previous studies on triggering the interior of the laminate by cutting the plies [21] and on UACS laminates [24-29] implicated that partially use of aligned short fibre reinforced composite plies may provide a new trigger function and make the failure process controllable. In this chapter, the

motivation is to develop a new trigger function directly in the interior of the laminate and making the failure process controllable for crashworthy structures. This is different with previous works (e.g. [28, 29]) that studied damage progression in quasi-isotropic UACS laminates ($[45/0/-45/90]_{2S}$) under tension. Present work studies the compressive resistance of cross-ply laminates $[0/90]_{4s}$ and $[90/0]_{4s}$ with UACS plies as 0˚ plies. That is, UACS plies with highly aligned slits of bi-angle pattern and staggered pattern were used as 0˚ ply in cross-ply laminates, respectively, instead of conventional continuous fibre ply to study the effects of UACS ply on the progressive crushing responses of cross-ply laminates. The effects of stacking sequence and discontinuous slit pattern on the maximum peak load, energy absorption, crush mean load, and crush force efficiency are revealed.

3.3 Experimental procedures

3.3.1 Material and fabrication of laminates

The cross-ply laminates are fabricated from carbon fibre/epoxy prepreg tape T700SC/2592 (Toray Industries, Inc.) of 0.12 mm in thickness with fibre volume fraction of 67%. In this study, two kinds of cross-ply laminates with stacking sequences of $[0/90]_{4s}$ and $[90/0]_{4s}$ were selected as baseline laminates to investigate the effect of stacking sequence on the static compression and progressive crushing properties of laminates. For each stacking sequence $[0/90]_{4s}$ or $[90/0]_{4s}$, three types of laminates with different 0˚ plies, namely, 0˚ plies of conventional continuous fibres, UACS 0˚ plies with bi-angle slit pattern, and UACS 0˚ plies with staggered slit pattern, were fabricated to explore the possibility of UACS ply as a new intra-laminar trigger mechanism for

crashworthy structures and investigate the effects of UACS plies and aligned discontinuous slit pattern on the static compression and progressive crushing properties of the cross-ply laminates. It is expected that the use of UACS ply as 0˚ ply may suppress the extension of large delamination, which causes large reduction in the critical load during the buckling and post-buckling of the laminate that finally leads to catastrophic failure of the conventional laminate [19, 22].

At first, the UACS plies were prepared by cutting sheets 250 × 250 mm out of prepreg sheet before introducing the distributed slits. However, in present work we use much smaller scale of distributed discontinuous slit with the reason to ensure much meaningful result from the effect of slit on a small width of specimen. This simple solution avoids the problem of a lack of resin on new trigger because the small length of slit and their gap are easily filled by an excess of the resin in the prepreg. Moreover, unlike the outer conventional trigger configuration, this new idea involves the use of very narrow trigger (only 12.5 mm length and 5 mm width) constantly in laminate instead of front structure in order to increase the specific energy absorb. Figs. 3-1(a) and 3-1(b) illustrate the images of UACS plies with bi-angle slit pattern and staggered slit pattern, respectively.

Similar with our previous work, the slit was carefully introduced into the prepreg sheet by hand using a conventional paper cutter based on a printed slit pattern. In the bi-angle UACS ply, the angle between the slit and fibre direction was chosen to be at 11.3 degrees according to previous studies [26, 28, 29]. In contrast, the slit in the staggered UACS ply is perpendicular to the fibre. To insure that there is at least one slit within 10 mm gauge length of specimens for static compressive test, all the fibres in 0˚UACS plies were cut into 12.5 mm length although the fibre's length of the original UACS plies [26, 28, 29] is

25 mm, while all the 90˚ plies in cross-ply laminates remained continuous fibres. The reason is that 90˚ plies play an important role in supporting adjacent 0˚ plies and enhancing the buckling capability of 0˚ plies. If slits are also introduced into 90˚ plies, the 0˚ plies may lose their load carrying capability significantly. After introducing the slits into the prepreg sheet, 0˚ UACS ply with aligned short fibres and 90˚ply with continuous fibres were stacked into cross-ply laminates of $[0/90]_{4s}$ and $[90/0]_{4s}$. Then, the stacked laminates were cured using an autoclave. The cure temperature and pressure were 135˚C and 0.3 MPa following the cure cycle given by manufacturer. The average thickness of cured laminate was 2.0 mm. It is obviously seen on the surfaces of $[0/90]_{4s}$ laminates that slits were filled by resin.

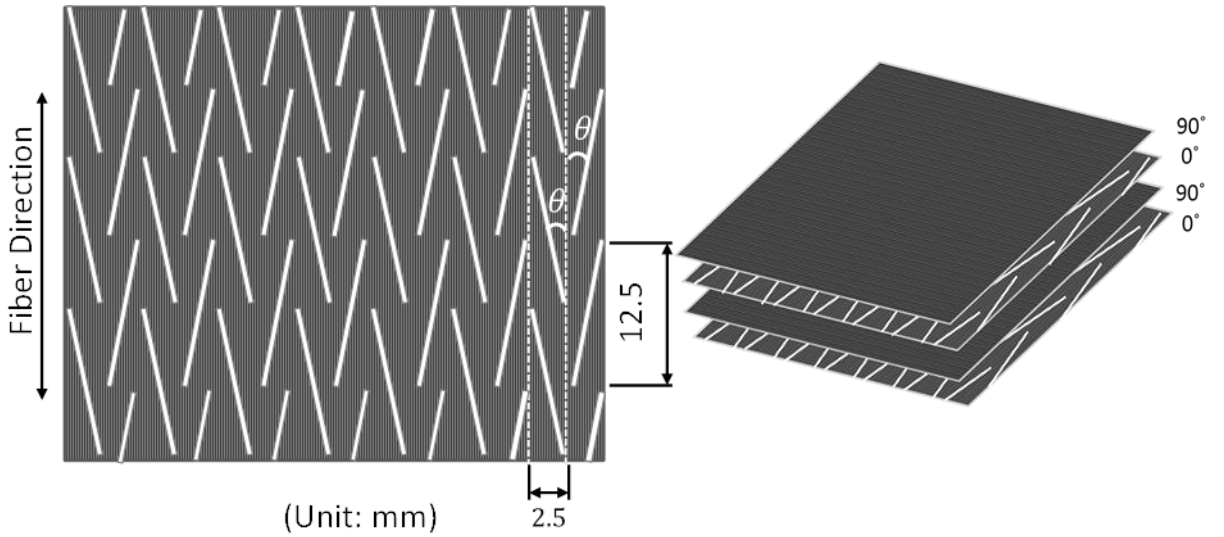

(a) UACS ply with bi-angle slit pattern (left) and cross-ply laminate with bi-angle UACS plies (right).

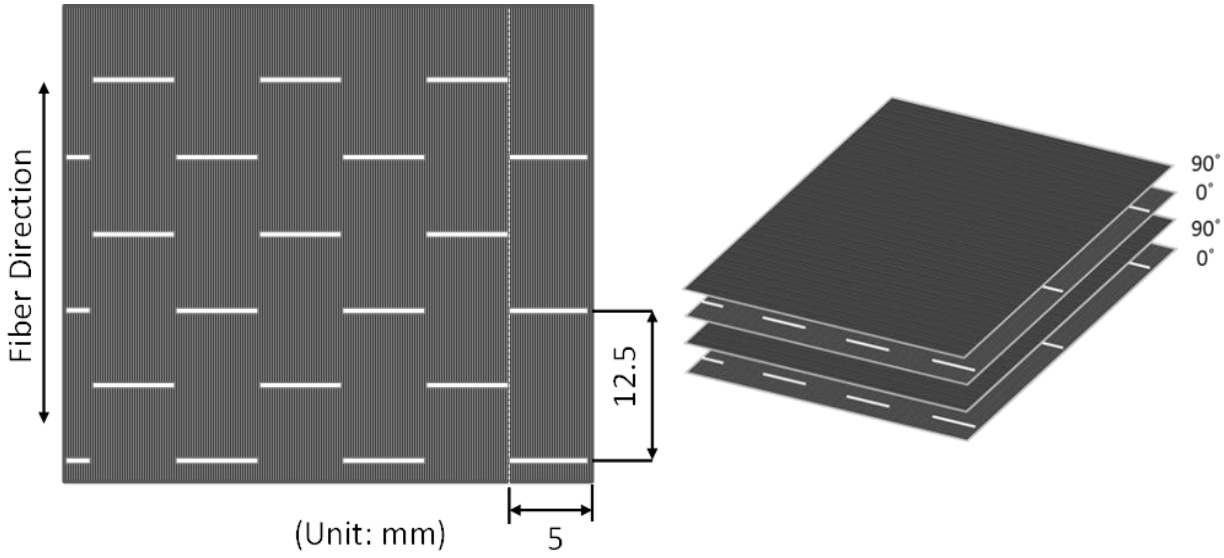

(b) UACS ply with staggered slit pattern (left) and cross-ply laminate with staggered UACS plies (right).

Figure 3-1: Illustrations of two kinds of UACS plies and cross-ply laminates with 0˚ UACS plies.

3.3.2 Specimens and testing procedures

Geometries of specimens for static compression and progressive crushing tests are illustrated in Fig 3-2 based on ASTM D3410 and previous papers [12]. Thickness and width of specimens are 2 mm and 10 mm, respectively. Aluminium tabs of 1 mm in thickness were bonded to the ends of specimens. The gauge length of specimens for static compression test is 10 mm and a strain gauge was bonded on the specimen surface to measure the axial strain. The gauge length of specimens for progressive crushing test is 20 mm with a 45˚ chamfered end. Static compression and progressive crushing tests were conducted using a MTS-810 testing system.

In order to measure the compressive strength of laminates, the static compression tests were carried out. The loading rate used for static compression is 1 mm/min at constant loading rate. The loading stress and strain were recorded for each specimen. After static compression testing, the side edges of tested specimens were polished and the microstructures were observed using optical microscope to identify the failure mechanisms involved during static compression testing. On the other hand, the progressive crushing tests were carried out to investigate the crashworthiness properties of laminates. In order to use the same strain rate with the static compression tests, we used the loading rate of 2 mm/min for progressive crushing test because the length of specimens for progressive crushing test is 20 mm. A video system was employed to record the whole crushing process during the progressive crushing test. The progressive crushing testing was carried out until the crushed displacement reaches 10 mm. The loading force-displacement response was recorded for each specimen to analyse the crashworthiness properties of the specimen. Five specimens were tested for each laminate

type according to ASTM D3410 and with the consideration of experimental cost. All the laminate types and nominal dimensions of specimens for static compression and progressive crushing tests are listed in Table 3-1 and Table 3-2.

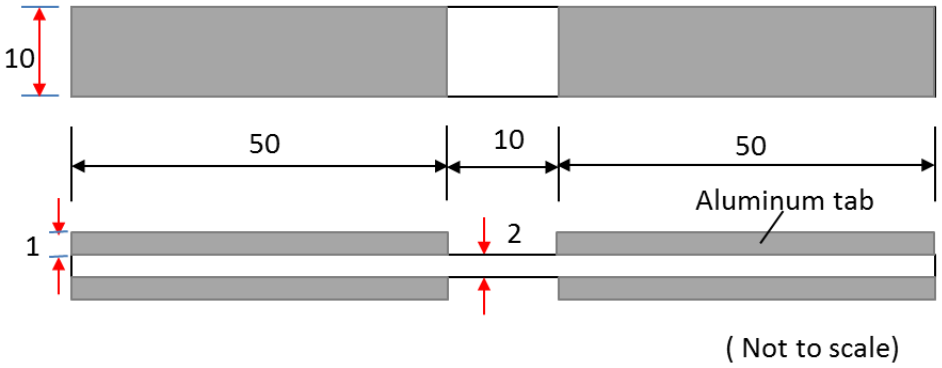

a) Specimen geometry for static compressive test

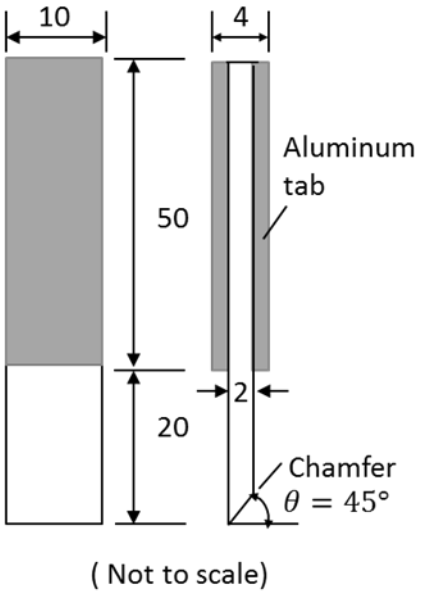

b) Specimen geometry for progressive crushing test

Figure 3-2: Geometries of two kinds of specimens.

Table 3-1: Laminate types and nominal and weight of specimens for static compression test.

Laminate types	**0˚ - ply types**	**Nominal dimension of specimens for static compression test**		
		Gauge length (mm)	Width (mm)	Thickness (mm)
[0/90/0/90/0/90/0/90]s	conventional	10	10	2
[0*/90/0*/90/0*/90/0*/90]s	0*-bi-angle UACS	10	10	2
[0*/90/0*/90/0*/90/0*/90]s	0*-staggered UACS	10	10	2
[90/0/90/0/90/0/90/0]s	conventional	10	10	2
[90/0*/90/0*/90/0*/90/0*]s	0*-bi-angle UACS	10	10	2
[90/0*/90/0*/90/0*/90/0*]s	0*-staggered UACS	10	10	2

Table 3-2: Laminate types and nominal and weight of specimens for progressive crushing test.

Laminate types	**0˚ - ply types**	**Nominal dimension and weight of specimens for progressive crushing test**			
		Gauge length (mm)	Width (mm)	Thickness (mm)	Weight (g)
[0/90/0/90/0/90/0/90]s	Conventional	20	10	2	2.1
[0*/90/0*/90/0*/90/0*/90]s	0*-bi-angle UACS	20	10	2	2.1
[0*/90/0*/90/0*/90/0*/90]s	0*-staggered UACS	20	10	2	2.1
[90/0/90/0/90/0/90/0]s	Conventional	20	10	2	2.1
[90/0*/90/0*/90/0*/90/0*]s	0*-bi-angle UACS	20	10	2	2.1
[90/0*/90/0*/90/0*/90/0*]s	0*-staggered UACS	20	10	2	2.1

3.4 Results and discussions

3.4.1 Results of static compression tests

Results of static compression tests are presented in Figs. 3-3 to 3-7. Compressive stress-strain responses are depicted in Fig. 3-3 for various laminates. All specimens showed linear response initially and then nonlinear response until failure. Cross-ply laminates of $[90/0]_{4s}$ with conventional 0˚ plies, with bi-angle UACS 0˚ plies, and with staggered UACS 0˚ plies showed better compressive properties than corresponding $[0/90]_{4s}$ laminates, respectively. Detailed results of average values of compressive strength are described in Fig. 3-4 for various laminates based on five specimens. Standard deviation value is given in round bracket. The coefficient of variations (the ratio of standard deviation to averaged value) is in the range of 1.3% – 9.7%. This scattered range is generally acceptable for the strength values of composite laminates [24]. Naturally, to improve the statistic reliability of test results, tests for more than five specimens are desirable, although the five is the minimum number of specimens specified by standard testing method ASTM D3410. Nevertheless, conventional $[90/0]_{4s}$ laminate gave the highest strength with a reading of 731 MPa, about 4% higher than conventional $[0/90]_{4s}$ laminate. Cross-ply laminate of $[90/0]_{4s}$ with bi-angle UACS 0˚ plies gave compressive strength of about 664 MPa, only 9% lower than conventional $[90/0]_{4s}$ laminate, although all the fibres were cut into 12.5 mm in bi-angle UACS 0˚ plies, and 16% higher than $[0/90]_{4s}$ laminate with bi-angle UACS 0˚ plies. In contrast, Cross-ply laminate of $[90/0]_{4s}$ with staggered UACS 0˚ plies gave compressive strength of about 420 MPa that is 57% of the strength of conventional $[90/0]_{4s}$ laminate and slightly higher than $[0/90]_{4s}$ laminate with staggered UACS 0˚ plies. These results revealed that slit patterns in the UACS ply

have significant influence on the compressive strength of cross-ply laminates, which is consistent with previously reported results [26]. On the other hand, the difference of the compressive strength values between $[90/0]_{4s}$ and $[0/90]_{4s}$ laminates was not significant, except for the case of cross-ply laminates with bi-angle UACS 0˚ plies.

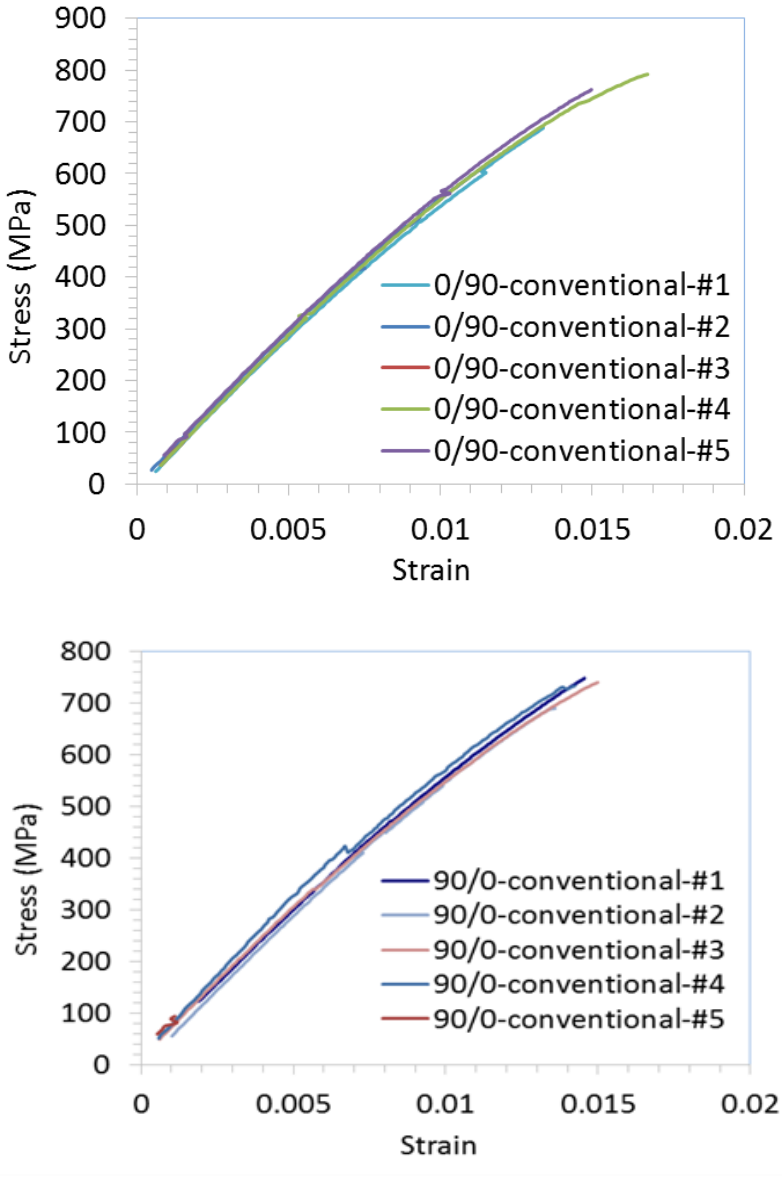

Figure 3-3: a) Compressive stress-strain responses of conventional $[0/90]_{4s}$ and $[90/0]_{4s}$ laminates .

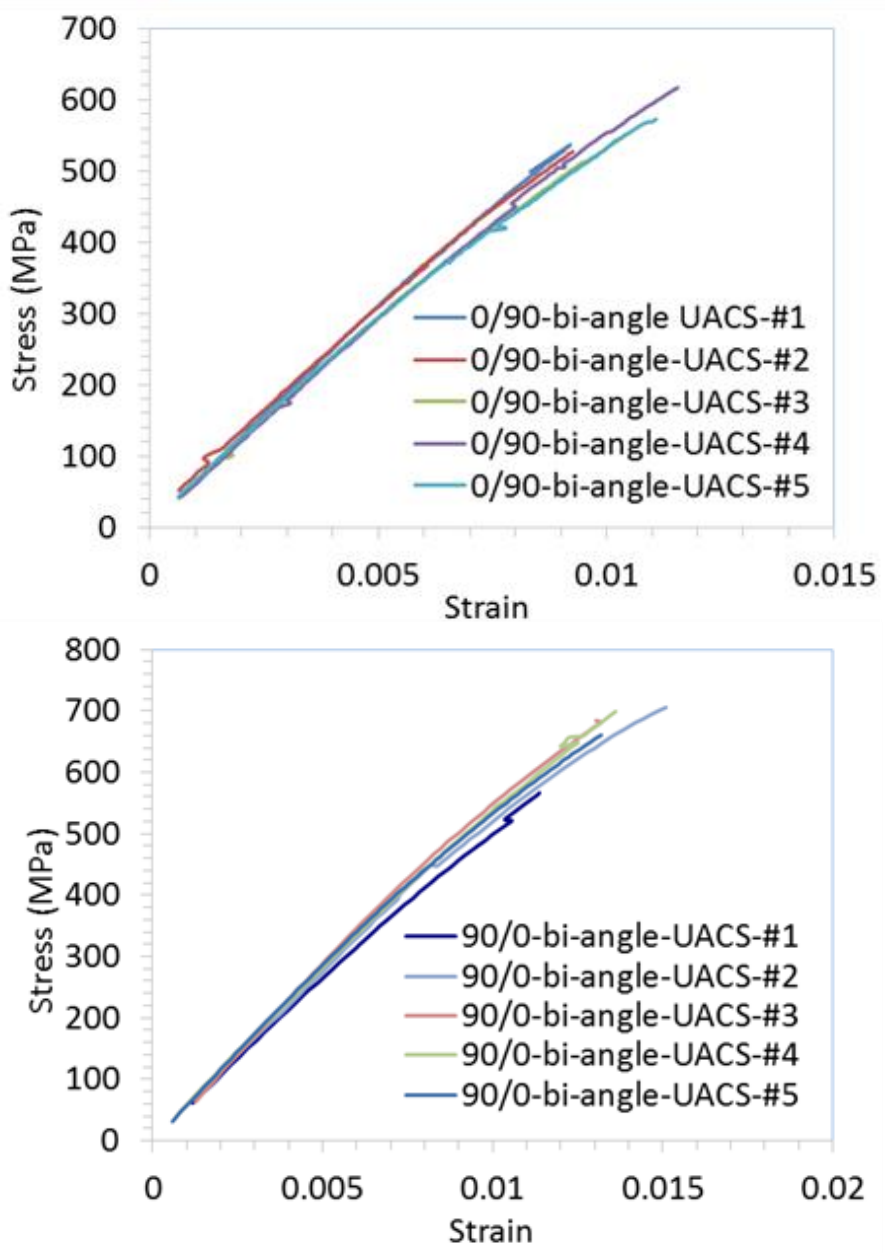

Figure 3-3: b) Compressive stress-strain responses of bi-angle UACS $[0/90]_{4s}$ and $[90/0]_{4s}$ laminates.

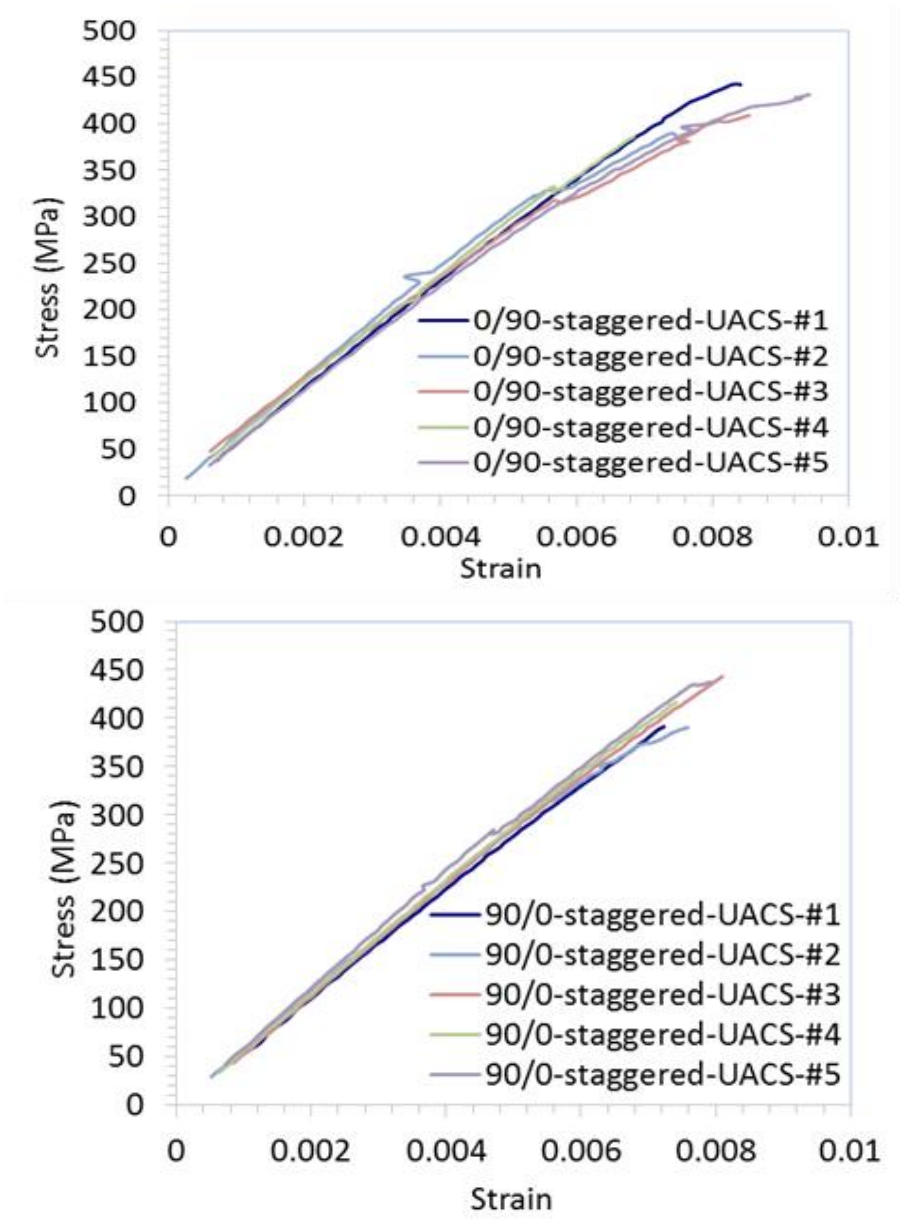

Figure 3-3: c) Compressive stress-strain responses of Staggered UACS $[0/90]_{4s}$

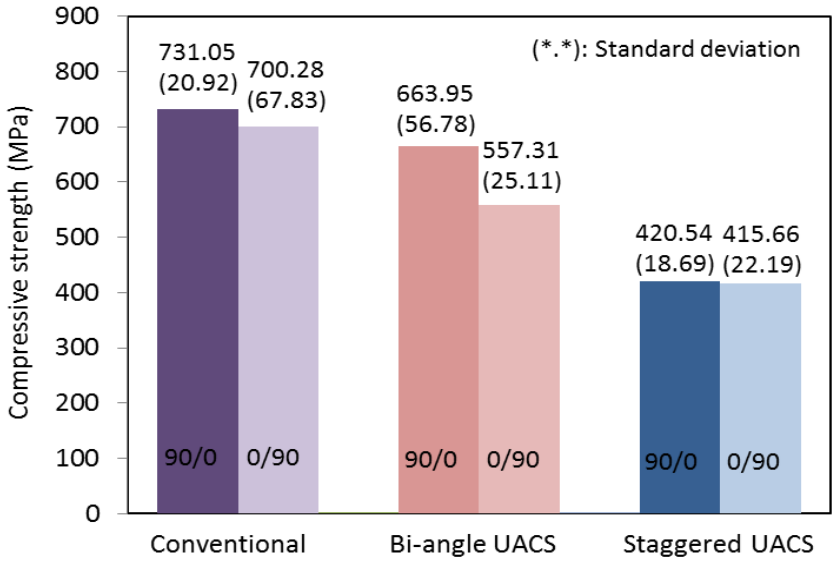

Figure 3-4: Average values of compressive strength for various laminates.

Typical images of failed specimens are presented in Figs. 3-5 to 3-7. Images of conventional $[0/90]_{4s}$ and $[90/0]_{4s}$ laminates are shown in Fig. 3-5(a) and Fig. 3-5(b). Large shear failure and then large multi-delamination were observed. It is seen that two cross-ply laminates showed similar failure images. In Fig. 3-6, multiple shear failure regions and relatively small delamination are observed. These images are different from those shown in Fig. 3-5 for conventional cross-ply laminates. Regarding to this reason, it was thought that slits in UACS 0˚ plies not only limited the shear failure to small regions but also suppressed the extension of large delamination. In the cases of cross-ply laminates with staggered UACS 0˚ plies (see Fig. 3-7), multiple shear failure regions and relatively large delaminations were observed. These facts implicate that the present staggered slits perpendicular to the fibres cannot effectively suppress the extension of large delamination. High shear stress concentration at interface around the slit ends easily initiated delamination and promotes rapid delamination extension [26], which was the

main reason for the large reduction in the compressive strength compared with the cross-ply laminates with bi-angle UACS 0˚ plies.

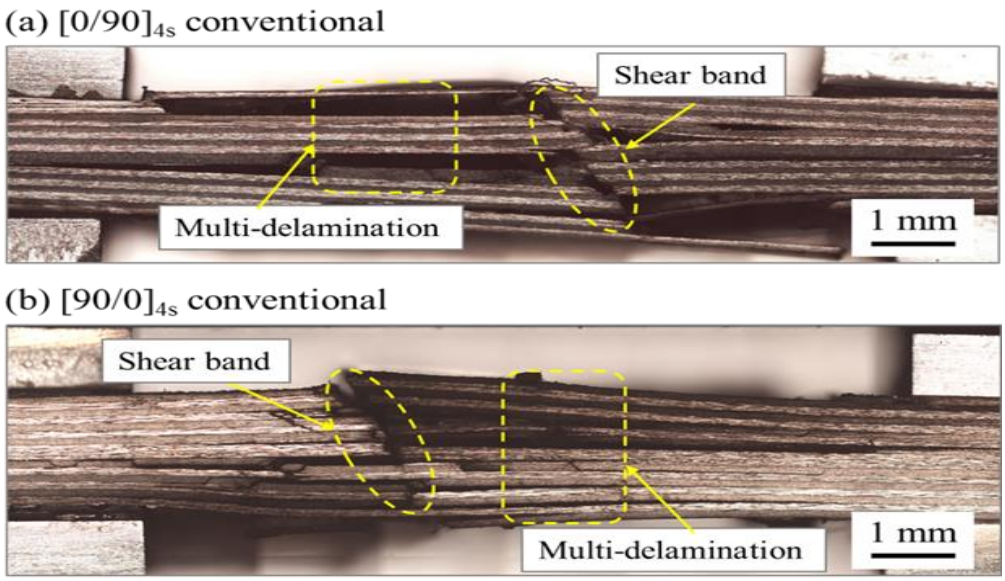

Figure 3-5: Typical images of failed specimens of conventional cross-ply laminates.

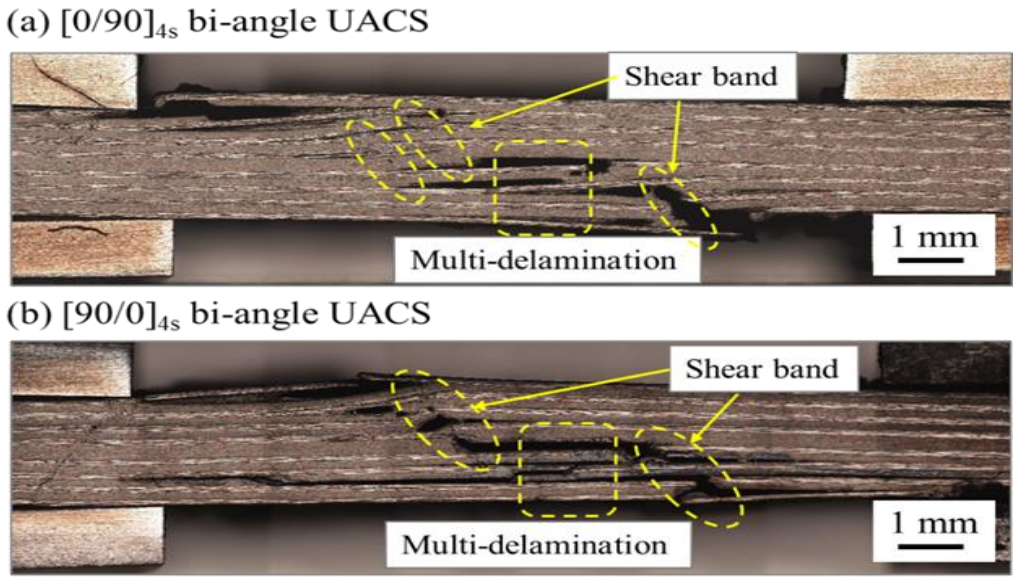

Figure 3-6: Typical images of failed specimens of cross-ply laminates with bi-angle UACS 0˚plies.

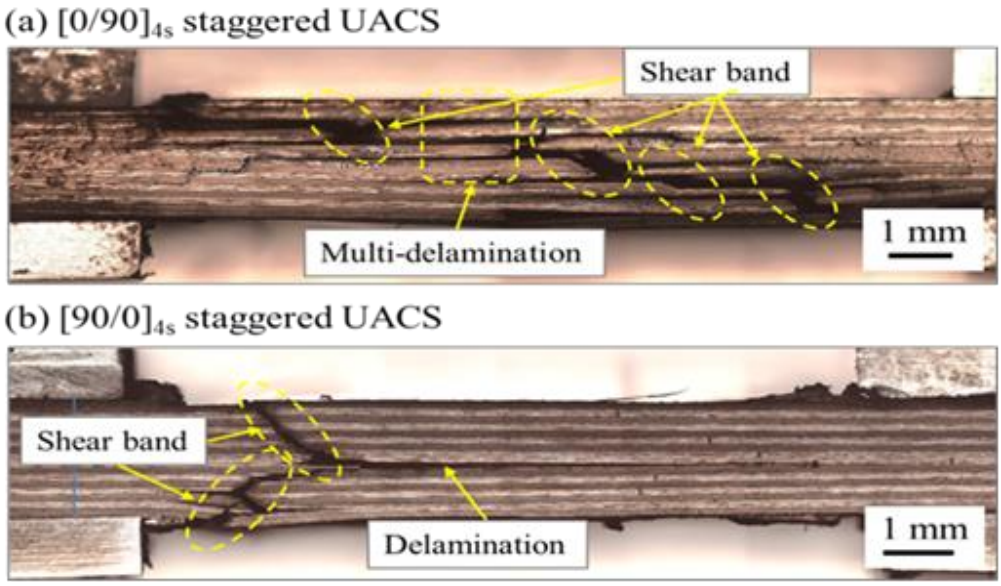

Figure 3-7: Typical images of failed specimens of cross-ply laminates with staggered UACS 0˚plies.

3.4.2 Results of progressive crushing tests

In general, crashworthiness of composite materials was classified according to how they deform, fail, and absorb crushing energy in controllable behaviour [12, 33, 34]. In axial crushing of conventional composite plate the crushing was absorbed by four main crushing modes including fragmentation, lamina bending, brittle fracturing and local buckling [14], and their combination during progressive crushing failure. Present results of progressive crushing tests are shown in Fig. 3-8 to Fig. 3-14. Load-displacement responses and the average values of maximum peak load are depicted in Fig. 3-8 for various laminates. All curves firstly showed an increase in load with the increase of displacement until the load reaches its maximum peak value.

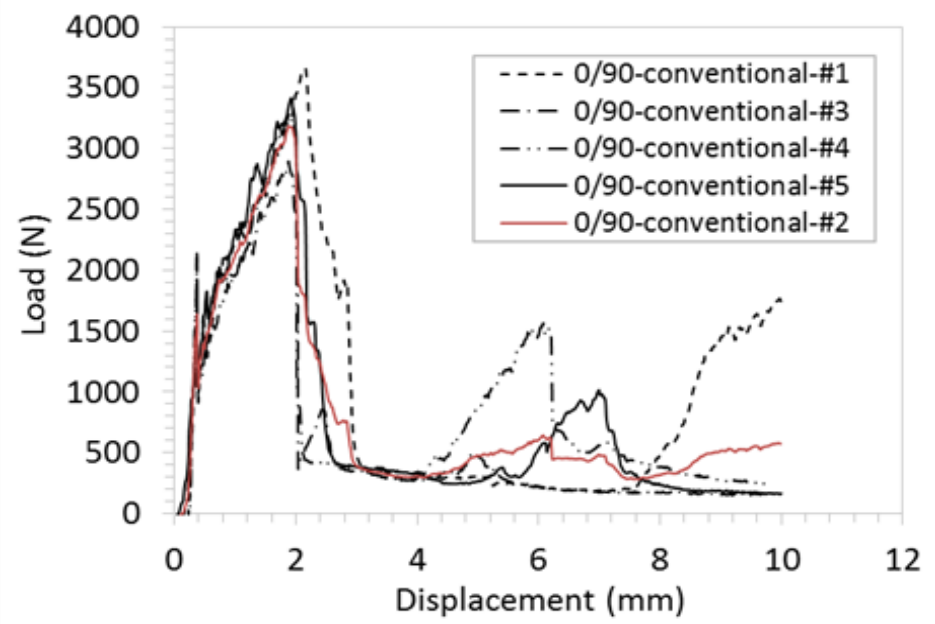

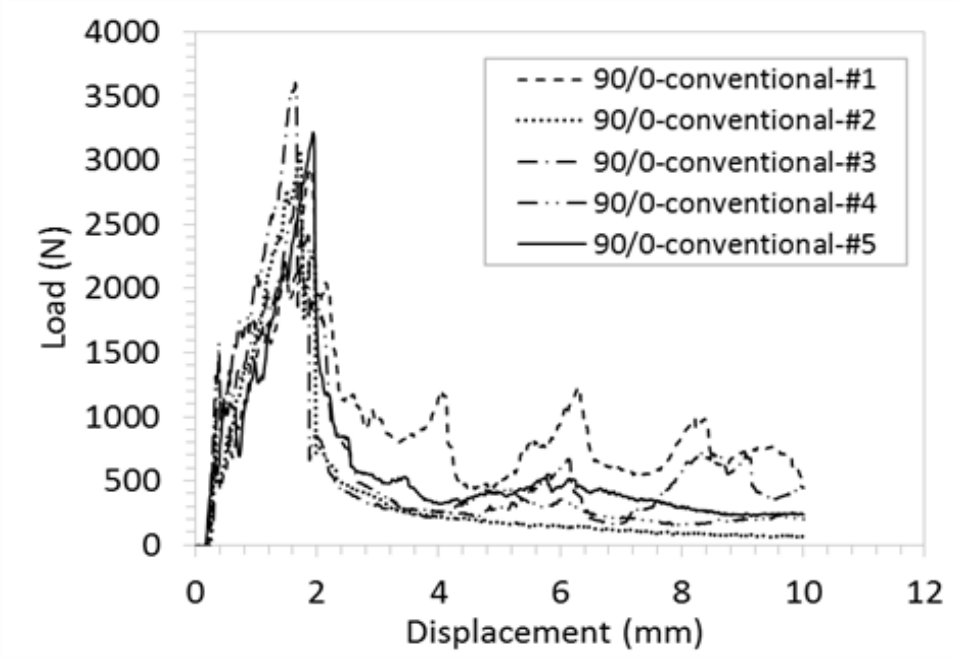

Figure 3-8: a) Load-displacement responses of conventional $[0/90]_{4s}$

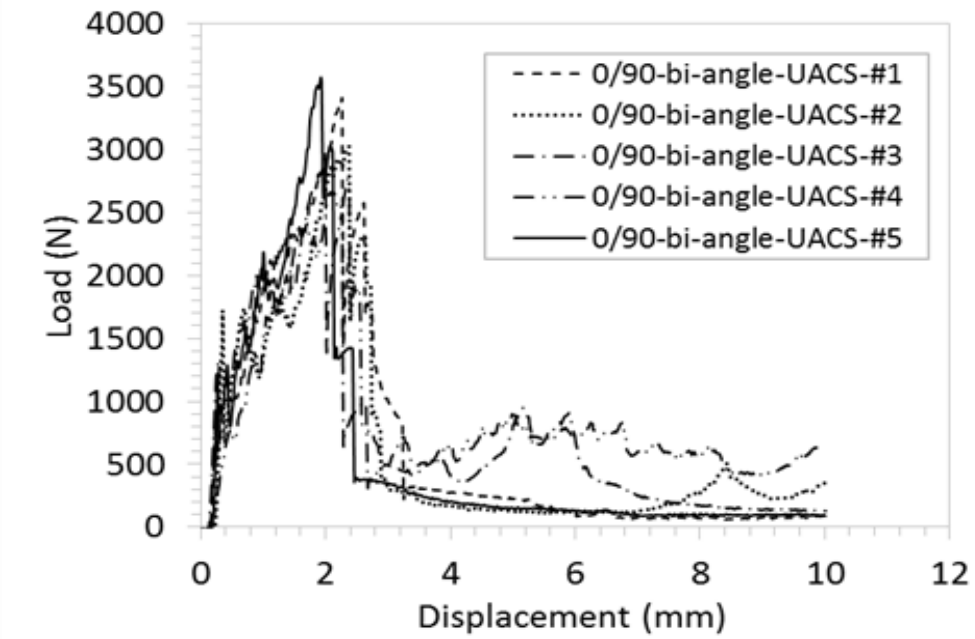

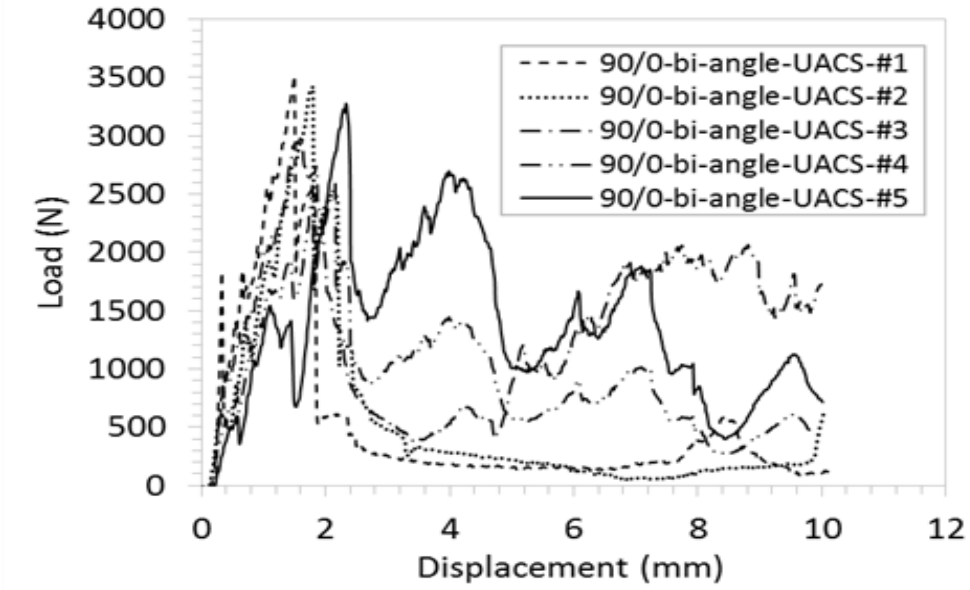

Figure 3-8: b) Load-displacement responses of bi-angle UACS $[0/90]_{4s}$ and $[90/0]_{4s}$ laminates.

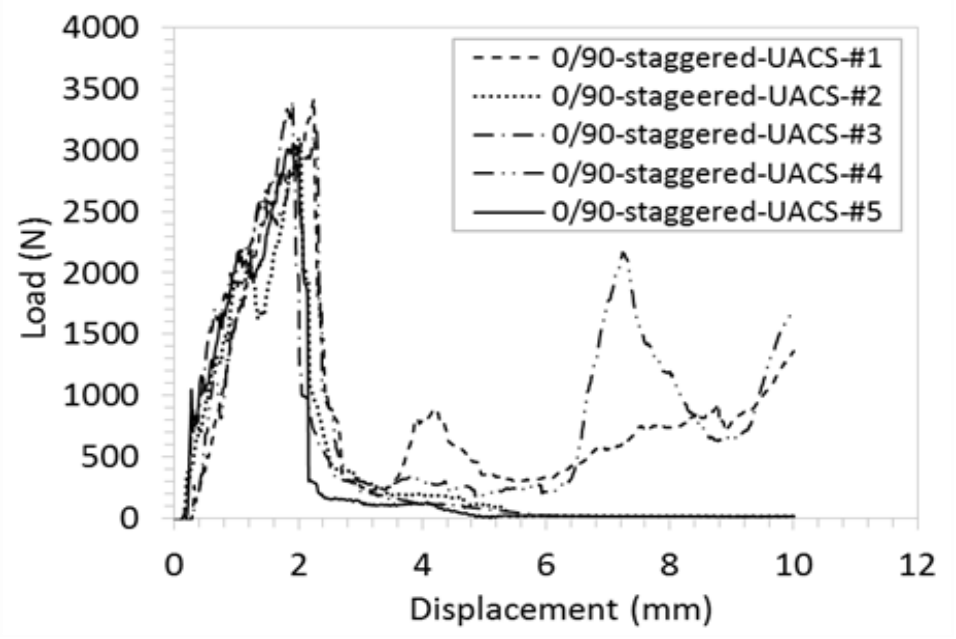

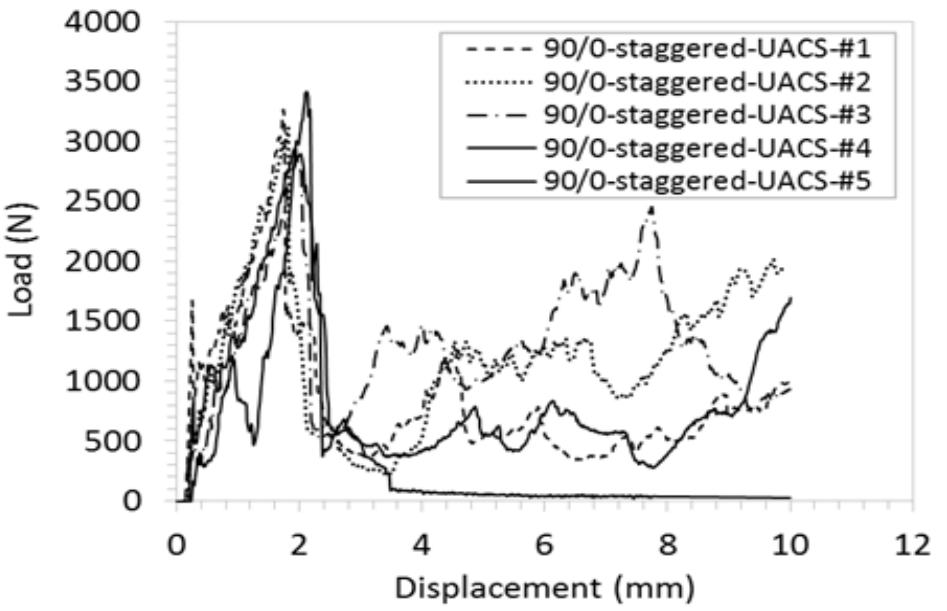

Figure 3-8: c) Load-displacement responses of staggered UACS $[0/90]_{4s}$

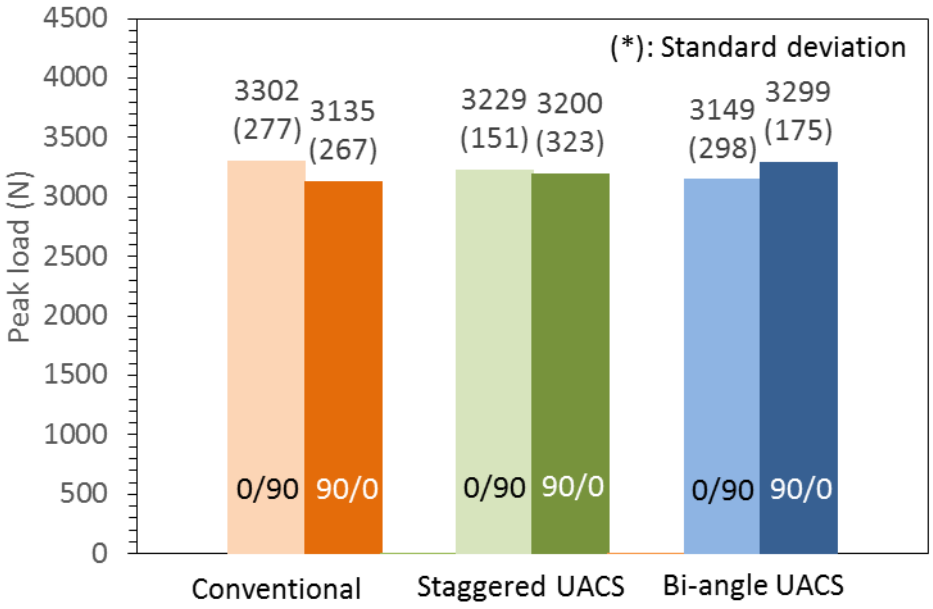

Figure 3-8: d) Averaged value of peak load for various laminated.

It is noted that the initial compression is dominated by the surface ply of laminates due to the influence of chamfered end. Therefore, in the case of $[0/90]_{4s}$, the specimens of conventional and bi-angle UACS showed an initial jump since the 0˚ surface ply dominated specimens of these two laminates had much higher compressive strength. The average values of maximum peak load are presented in Fig. 3-8(d). The coefficients of variation are in the range of 4.6% – 10.0%. All the laminates showed close average peak values, this feature is different from that of the static compressive strength values. The reason is that the deformation in the progressive crushing testing is not uniaxial compression and is the combination of compression and bending due to the influence of chamfered end and the splitting of laminate. After the maximum peak load, different trends are observed from $[0/90]_{4s}$ and $[90/0]_{4s}$ laminates. Relatively large fluctuation with

multiple peaks are observed in the curves of $[90/0]_{4s}$ laminates compared with the curves of $[0/90]_{4s}$ laminates, especially in the curve of $[90/0]_{4s}$ laminate with bi-angle UACS 0˚ plies. These results implicate that $[90/0]_{4s}$ laminates can absorb much more energy than $[0/90]_{4s}$ laminates during the crush process, especially after the maximum peak load, since the energy absorption capability of the laminate is dependent on the area under load-displacement curve.

Typical values of energy absorption and specific energy absorption of various laminates are shown in Fig. 3-9. The coefficients of variation are in the range of 11.6% – 21.1%, which is larger than that of maximum peak values due to the influence of crush behaviour after the maximum peak values. $[0/90]_{4s}$ laminates with UACS 0˚plies laminates show slightly drop off in energy absorption capability. In contrast, two kinds of UACS 0˚plies with $[90/0]_{4s}$ laminates showed an increasing in total energy absorbed than those conventional $[90/0]_{4s}$ laminate. $[90/0]_{4s}$ laminate with staggered UACS 0˚ plies gave the largest energy absorption of 9.14 J and specific energy absorption reading of 4.31 J/g, in which these values are 29% higher than those of conventional $[90/0]_{4s}$ laminate, respectively. In addition, $[90/0]_{4s}$ laminate with bi-angle UACS 0˚ plies gave energy absorption of 8.58 J and specific energy absorption reading of 4.1 J/g, in which these values are 24% and 25%, respectively higher than those of conventional $[90/0]_{4s}$ laminate.

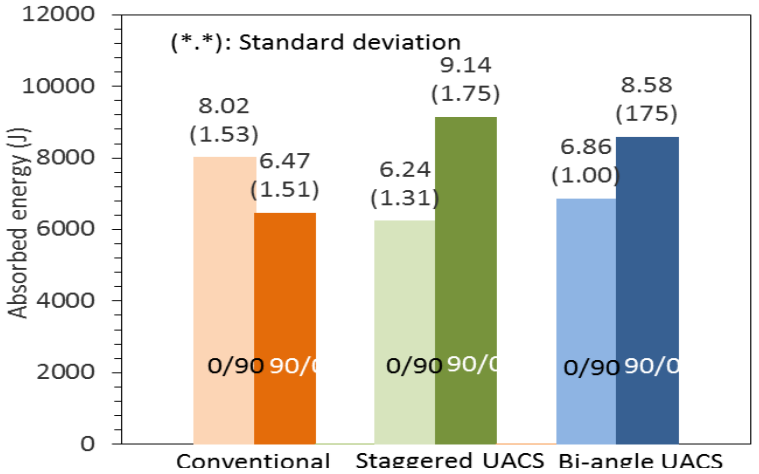

(a) Energy absorption

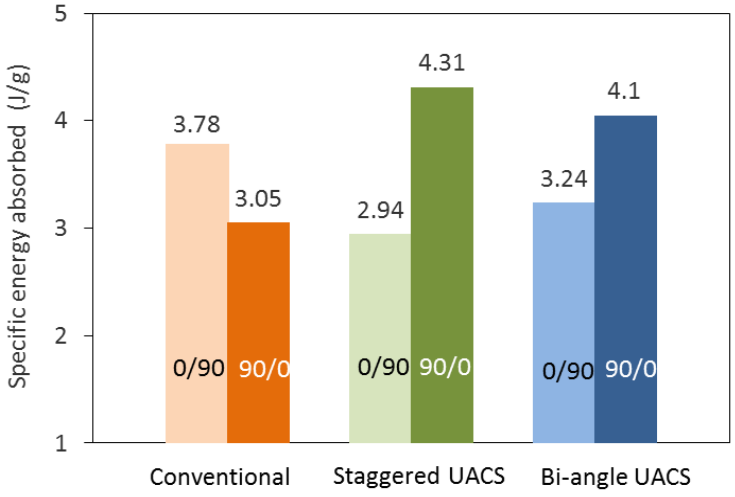

(b) Specific energy absorption

Figure 3-9: Energy absorption and specific energy absorption of various laminates.

Variations of energy absorption with crushed displacement are shown in Figs. 3-10(a) and 3-10(b) for $[0/90]_{4s}$ and $[90/0]_{4s}$ laminates, respectively. The energy absorption of three kinds of $[0/90]_{4s}$ laminates similarly grew with the increase of crushed displacement. In contrast, the $[90/0]_{4s}$ laminate with bi-angle UACS 0˚ plies showed the highest increase with the increase of crushed displacement. From these energy absorption results, it is noticeable that the $[90/0]_{4s}$ laminate with bi-angle UACS 0˚ plies is effective instead

of conventional laminate for the crashworthy structure application due to its relatively steady crushing behaviour.

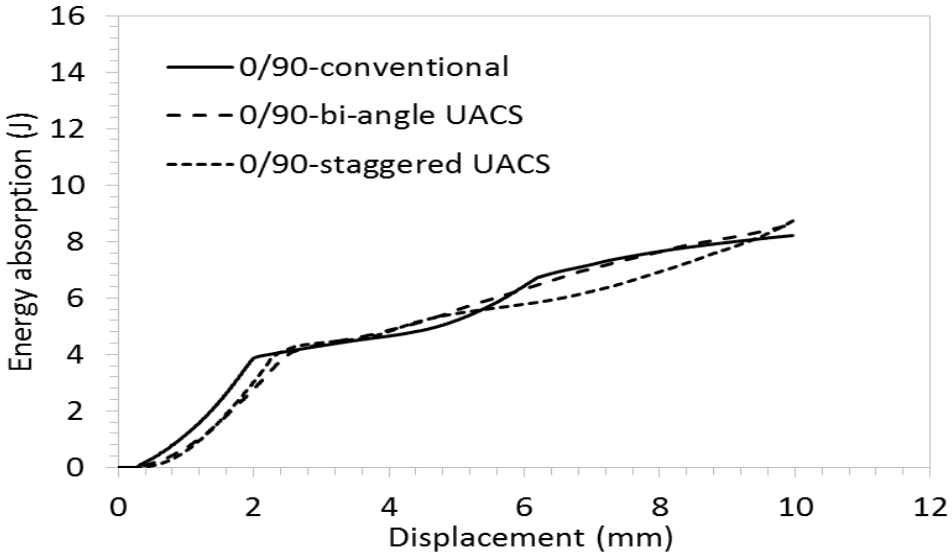

(a) $[0/90]_{4s}$

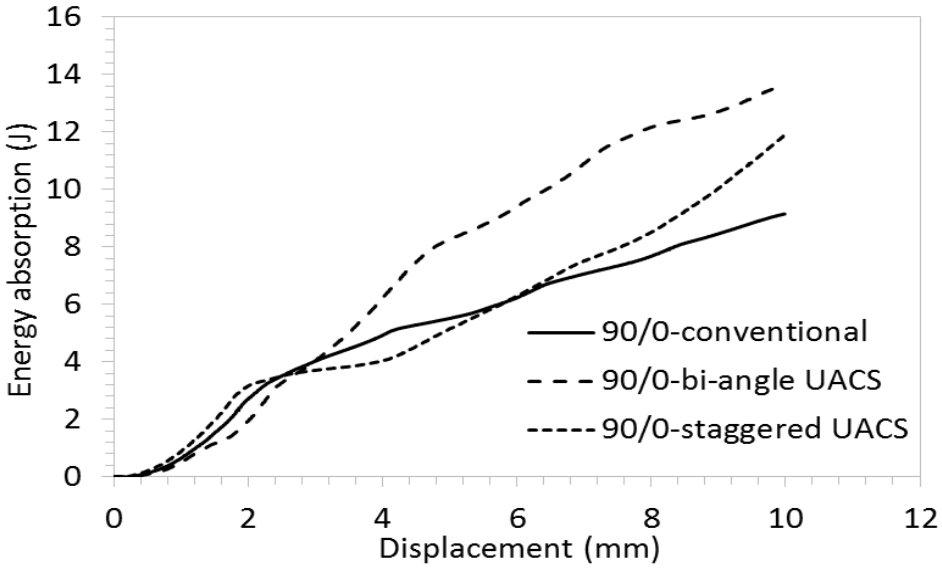

(b) $[90/0]_{4s}$

Figure 3-10: Energy absorption-displacement curves of various laminates.

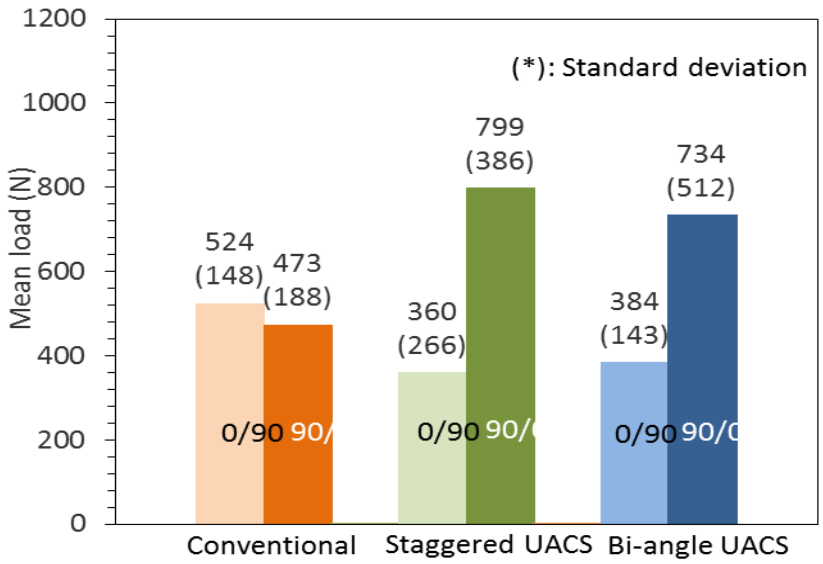

Figure 3-11: Mean loads of various laminates.

The mean load, which is defined by the ratio of the absorbed energy to the crushed length during the post crush process (after the maximum peak load), is a useful parameter to evaluate the energy absorption capability of a material for the crashworthy structure application. Detailed mean loads of various laminates are presented in Fig. 3-11. In the case of $[0/90]_{4s}$ laminates, two kinds of $[0/90]_{4s}$ laminates with staggered UACS 0˚ plies and with bi-angle UACS 0˚ plies showed 360 N and 384 N mean loads, respectively, which are decline about 28% and 17% lower than those of conventional $[0/90]_{4s}$ laminate, respectively. In contrast, in the case of $[90/0]_{4s}$ laminates, two kinds of $[90/0]_{4s}$ laminates with staggered UACS 0˚ plies and with bi-angle UACS 0˚ plies showed 799 N and 734 N mean loads, which are 40% and 36% higher than those of conventional $[90/0]_{4s}$ laminate.

Another important measurement of crush performance effectiveness is the crush force efficiency (CFE), which is defined as the ratio of the mean load to the maximum peak load [35]. The percentage of CFE is a considerable value to describe the failure mechanism of composite namely catastrophic or progressive failure. Low value CFE reflects high peak force, which leads to the increase in acceleration and potential damage to the structure during crush process and is expected to be avoided. Therefore, high value of CFE is desirable to the laminate for the crashworthy structure application. The diagram of CFE percentage of various laminates is depicted in Fig. 3-12. Three kinds of $[0/90]_{4s}$ laminates showed CFE values of around 11% - 16%, which are lower than the CFE values of the three kinds of $[90/0]_{4s}$ laminates. Furthermore, $[90/0]_{4s}$ laminates with bi-angle UACS 0˚ plies and with staggered UACS 0˚ plies showed 22.3% and 25% CFE values, which are much higher than the CFE value (15.1%) of conventional $[90/0]_{4s}$ laminate.

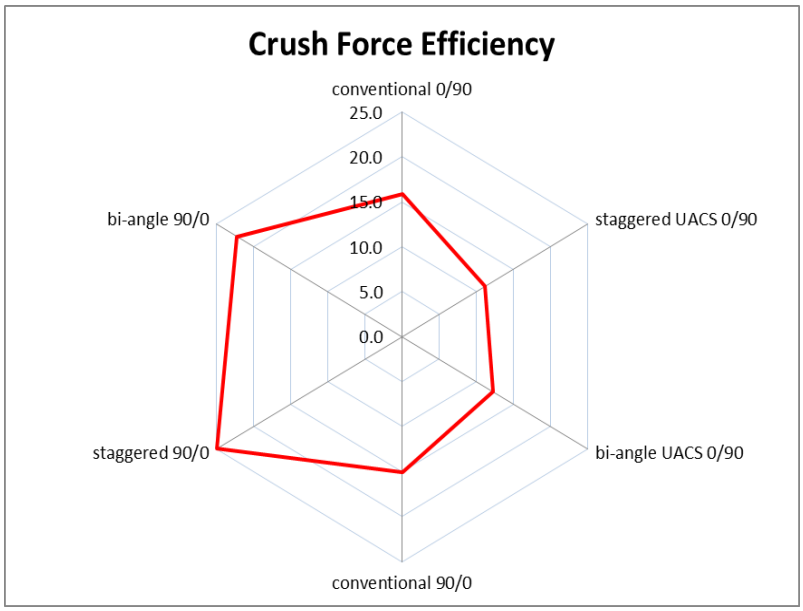

Figure 3-12: Crush force efficiency of various laminates.

Typical progressive crushing images taken out from the digital video camera for various laminates are presented in sequence in Figs. 3-13. In all cases of laminates, the crush began from the chamfered tip of the laminate under compressive load and then outer plies of the laminate were pushed outwards. Afterwards, the chamfered part was completely crushed, and multiple delamination occurred from the end of the crushed laminate. All laminates showed roughly steady progressive crushing behaviour, except for the $[0/90]_{4s}$ laminate with staggered UACS 0˚ plies, which showed global buckling. Large delamination and bending into large radius of curvature during buckling and post buckling were observed in $[0/90]_{4s}$ laminates with conventional 0˚ plies and with bi-angle UACS 0˚ plies, and $[90/0]_{4s}$ laminates with conventional 0˚ plies and with staggered UACS 0˚ plies. Relatively small delamination was seen in the $[90/0]_{4s}$ laminate with bi-angle UACS 0˚ plies.

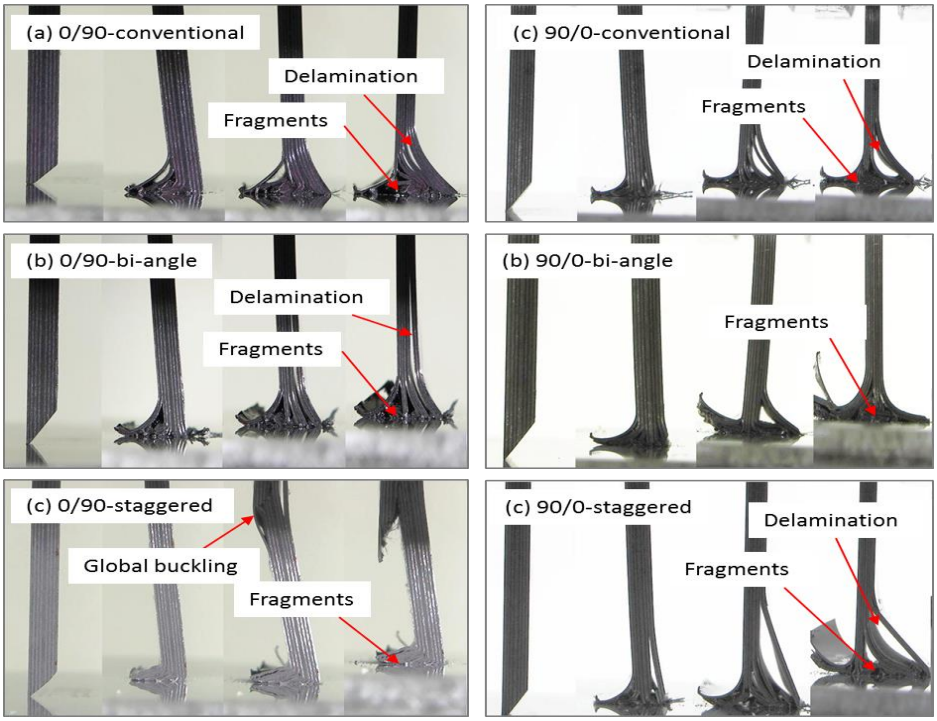

Figure 3-13: Typical images of progressive crushing behaviour of various laminates

For comparison, the enlarged images of the crushing regions for $[90/0]_{4s}$ laminates with conventional 0˚ plies and with bi-angle UACS 0˚ plies are presented in Fig. 3-14. Large delamination was clear in the conventional $[90/0]_{4s}$ laminate, which significantly reduced the bending stiffness and critical loads of buckling and post buckling of the laminate and led to low energy absorption capability. In contrast, small delamination was seen in the $[90/0]_{4s}$ laminate with bi-angle UACS 0˚ plies because the angled and discontinuous slits in the UACS 0˚ plies easily fractured the laminate at the locations of slits and then suppressed the delamination extension. Large crushing load and energy were required to force the splayed fronds bending into small radius of curvature [36]. Therefore, the $[90/0]_{4s}$ laminate with bi-angle UACS 0˚ plies showed the most desirable steady progressive crushing behaviour.

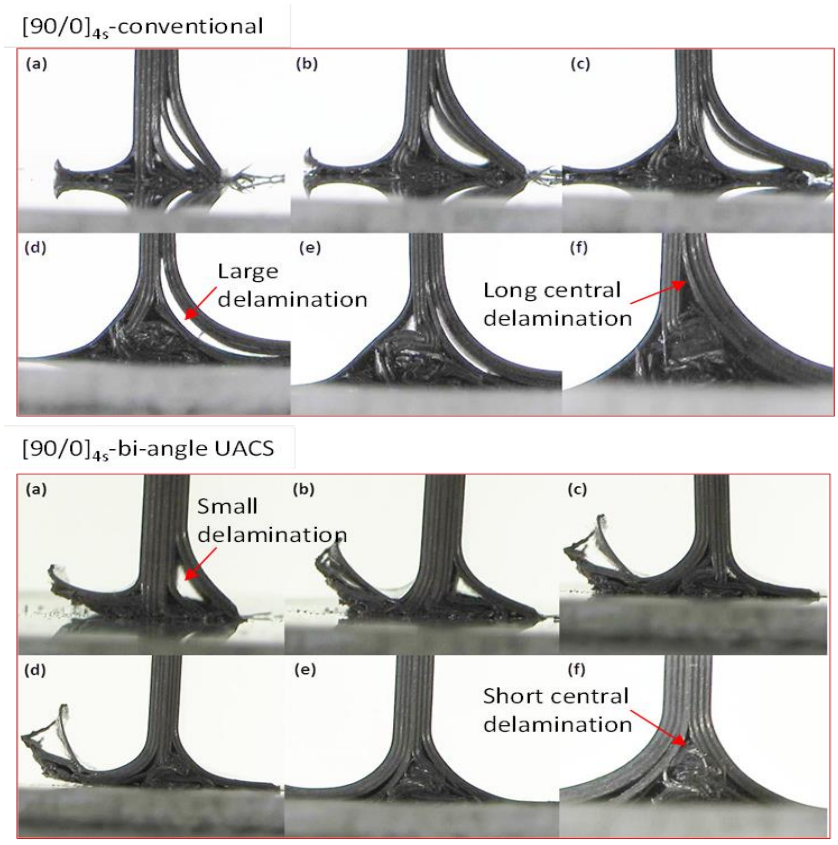

Figure 3-14: Comparison of crush behaviours between $[90/0]_{4s}$ laminates with conventional 0˚plies and bi-angle UACS 0˚plies.

3.5 Summary

In this chapter, the static compression and progressive crushing properties of carbon fibre reinforced epoxy cross-ply laminates with different stacking sequence $[0/90]_{4s}$ and $[90/0]_{4s}$ and with different kind of 0˚ plies are investigated experimentally. Effects of stacking sequence $[0/90]_{4s}$ and $[90/0]_{4s}$ and UACS 0˚ plies with different slit patterns on the compressive strength and the progressive properties are clarified. The main experimental results are concluded as follows:

1. Three kinds of $[90/0]_{4s}$ laminates showed a little higher compressive strength than the three kinds of $[0/90]_{4s}$ laminates. In contrast, the slit pattern in UACS 0˚ ply had a significant influence on the compressive strength. $[90/0]_{4s}$ laminates with bi-angle UACS 0˚ plies and with staggered UACS 0˚ plies demonstrated the values of compressive strength of 9%, and 58% lower than the conventional $[90/0]_{4s}$ laminate, respectively. Shear failure and delamination were the main compressive failure modes.

2. $[0/90]_{4s}$ laminates and $[90/0]_{4s}$ laminates demonstrated different crush load-displacement responses. After the maximum peak load, relatively large fluctuation with multiple peaks were observed in the crush load-displacement curves of $[90/0]_{4s}$ laminates compared with the curves of $[0/90]_{4s}$ laminates, especially in the curve of $[90/0]_{4s}$ laminate with bi-angle UACS 0˚ plies. That is, $[90/0]_{4s}$ laminates had better post progressive crushing properties.

3. Three kinds of $[90/0]_{4s}$ laminates showed quite different crush energy absorption capability. $[90/0]_{4s}$ laminate with staggered UACS 0˚ plies gave the largest energy absorption 9.14 J and specific energy absorption 4.31 J/g, in which these values are 29% higher than those of the conventional $[90/0]_{4s}$ laminate. In addition, $[90/0]_{4s}$ laminate with

bi-angle UACS 0˚ plies gave energy absorption of about 8.58 J and specific energy absorption reading of 4.1 J/g, in which these values are 24% and 25%, respectively higher than those of the conventional $[90/0]_{4s}$ laminate.

4. Regarding the mean load, which is a useful parameter to evaluate the energy absorption capability of a material for the crashworthy structure application, three kinds of $[90/0]_{4s}$ laminates demonstrated much higher mean loads than the relative three kinds of $[0/90]_{4s}$ laminates. Furthermore, two kinds of $[90/0]_{4s}$ laminates with staggered UACS 0˚ plies and with bi-angle UACS 0˚ plies showed 799 N and 734 N mean loads, which are 40% and 36% higher than those of the conventional $[90/0]_{4s}$ laminate.

5. Three kinds of $[0/90]_{4s}$ laminates showed CFE values of around 11% - 16%, which are lower than the CFE values of the three kinds of $[90/0]_{4s}$ laminates. Moreover, $[90/0]_{4s}$ laminates with bi-angle UACS 0˚ plies and with staggered UACS 0˚ plies showed 22.3% and 25% CFE values, which are much higher than the CFE value (15.1%) of the conventional $[90/0]_{4s}$ laminate.

6. Conventional $[90/0]_{4s}$ laminate demonstrated large delamination and bending into large radius of curvature during buckling and post buckling due to the high bending strength of conventional 0˚ plies with continuous fibres, which significantly reduced the bending stiffness and critical loads of buckling and post buckling of the laminate and led to low energy absorption capability. In contrast, small delamination is seen in the $[90/0]_{4s}$ laminate with bi-angle UACS 0˚ plies that demonstrated small delamination because the angled and discontinuous slits in the UACS 0˚ plies reduced the bending strength of the laminate and then suppressed the delamination extension. Large crushing load and energy are required to force the splayed fronds bending into small radius of curvature. Therefore,

the $[90/0]_{4s}$ laminate with bi-angle UACS 0˚ plies showed the most desirable steady progressive crushing behaviour.

Bibliography

[1] Lukaszewicz D.H.-J.A. A. Automotive Composite Structures for Crashworthiness. Chapter 5: in Advanced composite materials for automotive applications : structural integrity and crashworthiness (Edited by Ahmed Elmarakbi) . New Delhi: John Wiley & Sons Ltd; 2014.

[2] Mahdia E, Hamoudab AMS, Saharib BB, Khalidb YA. Experimental quasi-static axial crushing of cone–tube–cone composite system. *Composites Part B: Engineering*, 2003; 34: 285–302.

[3] Duan S, Tao Y, Han X, Yang X, Hou X, Hu Z. Investigation on structure optimization of crashworthiness of fiber reinforced polymers materials. *Composites Part B: Engineering*, 2014; 60: 471–478.

[4] Bussadori BP, Schuffenhauer K, Scattina A. Modelling of CFRP crushing structures in explicit crash analysis. *Composites Part B: Engineering*, 2014; 60: 725–735.

[5] Liu Q, Ou Z, Mo Z, Li Q, Qu D. Experimental investigation into dynamic axial impact responses of double hat shaped CFRP tubes. *Composites Part B: Engineering*, 2015; 79: 494-504.

[6] Luo H, Yan Y, Meng X, Jin C. Progressive failure analysis and energy-absorbing experiment of composite tubes under axial dynamic impact. *Composites Part B: Engineering*, 2015; 87: 1-11.

[7] Mamalis AG, Manolakos DE, Ioannidis MB, Papapostolou DP. On the experimental investigation of crash energy absorption in laminate splaying collapse mode of FRP tubular components. *Composite Structures*, 2005; 70: 413-429.

[8] Yokozeki T, Ogasawara T, Ishikawa T. Nonlinear behavior and compressive strength of unidirectional and multidirectional carbon fiber composite laminates. *Composite Part A*, 2006; 37: 2069-2079.

[9] Israr HA, Rivallant S, Barrau JJ. Experimantal investigation on mean crushing stress characterization of carbon-epoxy plies under compressive crushing mode. *Composite structures*, 2013; 96: 357-364.

[10] Louis NSC, Falzon BG, Dong R, Shanqing X, Rodney ST, Bernard C, Wenyi Y. Crush responses of composite cylinder under quasi-static and dynamic loading. *Composite Structures*, 2015; 131: 90-98.

[11] Jumahat A, Soutis C, Jones FR, Hodzic A. Fracture mechanisms and failure of carbon fibre/toughned epoxy composite subjected to compressive loading. Composite Structures, 2010; 92: 295-305.

[12] Israr HA, Rivallant S, Bouvet C, Barrau JJ. Finite element simulation of 0/90 CFRP laminated plates subjected to crushing using a free-face-crushing concept. *Composite Part A*, 2014; 62: 16-25.

[13] Tao WH, Robertson RE, Thornton PH. Effect of material properties and crush conditions on the crush energy absorption of fiber composite rods. *Composite Science and Technology*, 1993; 47: 405-418.

[14] Hull D. A unified approach to progressive crushing of fibre-reinforced composite tubes. *Composite Science and Tech*, 1991; 40: 377-421.

[15] Vinod MS, Sunil BJ, Vinay N, Raghavendra S, Murali MS, Nafidi A. Fractography of compression failed carbon fiber reinforced plastic composite laminates. *Journal of Mechanical Engineering Research*, 2010; 2(1): 001-009.

[16] Yin Y., Yu T., Bui T.Q., Xia S., Hirose S. A cutout isogeometric analysis for thin laminated composite plates using level sets. *Composite Structures,* 2015; 127: 152–164.

[17] Liu P, Bui TQ, Zhu D, Yu TT, Wang JW, Yin, Hirose S. Buckling failure analysis of cracked functionally graded plates by astabilized discrete shear gap extended 3-node triangular plate element. *Composites Part B: Engineering,* 2015; 77: 179-193.

[18] Yu T, Bui TQ, Yin S, Doan DH, Wu CT, Do TV, Tanaka S. On the thermal buckling analysis of functionally graded plates within thermal defects using extended isogeometric analysis. *Composite Structures,* 2016;136: 684–695.

[19] Zuleyha A, Mustafa S. Buckling behavior and compressive failure of composite laminates containing multiple large delaminations. *Composite Structure,* 2009; 89: 382-390.

[20] Tampas SA, Greenhalgh GS, Ankersen J, Curtis PT. On compressive failure of multidirectional fibre-reinforced composites: A fractographic study. *Composite Part A: Applied Science and Manufacturing,* 2012; 43: 454-468.

[21] Troiani E, Donati L, Molinari G, Sante RD. Influence of plying strategies and trigger types on crashworthiness properties of carbon fiber laminates cured through autoclave processing. *Journal of Mechanical Engineering,* 2014; 60: 375-381.

[22] Thuis HGSJ, Metz VH. The influence of trigger configurations and laminate lay-up on the failure mode of composite crush cylinders. Composite Structures, 1994; 28: 131-137.

[23] Palanivelu P, Paepegem WV, Degrieck J, Ackeren JV, Kakogiannis D, Hemelrijck DV, Wastiels J, Vantomme J. Experimental study on the axial crushing behavior of pultruded composite tubes. *Polymer Testing*, 2010; 29: 224-234.

[24] Taketa I, Okabe T, Kitano A. A new compression-molding approach using unidirectionally arrayed chopped strands. *Composite Part A*, 2008; 39: 1884-1890.

[25] Taketa I, Okabe T, Kitano A. Strength improvement in unidirectional arrayed chopped strands with interlaminar toughening. *Composite Part A*, 2009; 40: 1174-1178.

[26] Taketa I, Sato N, Kitano A, Nishikawa M, Okabe T. Enhancement of strength and uniformity in unidirectionally arrayed chopped strand with angled slits. *Composite Part A*, 2010; 42: 1639-1646.

[27] Taketa I, Okabe T, Matsutani H, Kitano A. Flowability of unidirectionally arrayed chopped strands in compression molding. *Composite Part B: Engineering*, 2011; 42: 1764-1769.

[28] Li H, Wang WX, Takao Y, Matsubara T. New designs of unidirectionally arrayed chopped strands by introducing discontinuous angled slits into prepreg. Compos Part A 2013;45:127-133.

[29] Li H, Wang WX, Matsubara T. Multiscale analysis of damage progression in newly designed UACS laminates. *Composite Part A*, 2014; 57: 108-117.

[30] Reddy S, Abbasi M. Multi-cornered thin walled sheet metal members for enhanced crashworthiness and occupant protection. *Thin-Walled Structures*, 2015; 94: 56-66.

[31] Dayyani I, Shaw AD, Flores EIS, Friswell MI. The mechanics of composite corrugated structures: A review with application morphing aircraft. *Composite Structure*, 2015; 133: 358-380.

[32] Grauers L, Olsson R, Gutkin R. Energy absorption and damage mechanism in progressive crushing of corrugated NFC laminates: Fractographic analysis. *Composite Structures,* 2014; 110; 110-117.

[33] Ghafari-Namini N, Ghasemnejad H. Effect of natural stitched composite on the crashworthiness of box structures. *Material and Design*, 2012; 39: 484-494.

[34] Libo Y, Nawasi C. Crashworthiness characteristics of flax fibre reinforced epoxy tubes for energy absorption application. *Materials and Design*, 2013; 51: 629-640.

[35] Ataollahi S, Taher ST, Eshkoor RA, Ariffin AK, Azhari CH. Energy absorption and failure response of silk/epoxy composite square tubes: Experimental. *Composite Part B: Engineering*, 2011; 43: 542-548.

[36] Savona SC, Hogg PJ. Investigation of plate geometry on the crushing of flat composite plates. *Composite Science and Technology,* 2006; 66: 1639-1650.

CHAPTER 4

Crashworthiness characteristics of composite circular tube with 0˚ plies of UACS

In this chapter, the effects of UACS 0˚ plies with two different slit distributions on circular laminate tubes are investigated to evaluate failure mechanism and improve crashworthiness properties of tubular structures. UACS plies with slits of bi-angle pattern and staggered pattern were used as 0˚ ply, respectively, instead of conventional continuous fibre ply to study the relationship between crashworthiness parameter and the failure mechanism of two kinds of tubes with different 0˚ UACS plies. For all cases of laminated tubes, four tubes for each kind of UACS 0˚ plies were fabricated and tested. For a benchmark, conventional continuous fibre laminated tubes were also fabricated and tested. Furthermore, for a comparison with conventional steel and glass fibre reinforced composite, steel circular tube and E-glass/polyester composite square tube were also tested.

4.1 Introduction

Crashworthiness performance is based largely on absorbing energy through structural deformation or controlled failure mechanisms during crushing. Due to the complex failure mechanisms that occur in composite materials during crush, crush testing of simple specimen geometries including tube remains as a popular method of determining energy absorbing characteristics because they are easy to fabricate and close to the geometry of the actual crashworthy structures. Moreover, composite tubes can be easily designed for stable crushing and to absorb impact energy in a controlled manner by providing a trigger to initiate progressive crushing [1-3]. Therefore, it is important to study the effects of 0˚ plies UACS laminates by scaling up from small coupon/plate tests to larger scale structures in determining the crashworthiness characteristics and performance of the material.

Previous research has shown that the energy absorption of composite tube structure relies on testing variables including cross-sectional geometry, shape, stacking sequence, trigger type, and fibre architecture, which is relatively well understood [4-12]. While almost all of these researches focused on continuous fibre and conventional short fibre tube, there is no literature available on the energy absorption and crushing characteristics of highly aligned discontinuous fibre composite tubes. Owing the fact that they are important because of the superior flowability to allow fabrication on complex geometry structural shape and together with high specific strength and stiffness, an attempt was

made to investigate and characterise the effects of the two different kinds 0˚ plies UACS laminate tube on crashworthiness performance. In present work, a circular tube geometry shape was selected to facilitate their testing on the basis of stability, ease fabrication, and giving optimum energy absorption than tube with planar section [5, 10, 13-14].

As described in Chapter 3, both discontinuous slits pattern in 0˚ plies UACS laminate plate were successful triggering and propagating laminate to crush in a controllable manner and at the same time suppressing the extension of delamination. As a result 0˚ plies UACS laminate had improved 29% in energy absorption of their conventional laminate. This was attributed to the smallest curvature radius and short central delamination. However, this phenomenon and performance might be different for specimen with non-planar section and tube. Therefore, to investigate the crashworthiness performance and crushing behaviour of circular tube with 0˚plies UACS laminate, quasi-static progressive crushing tests with three different kinds tube were conducted in this chapter.

4.2 Experimental procedures

4.2.1 Material and fabrication of circular laminate tube

Similar to the compression test as described in chapters 2 and 3, the conventional CFRP prepreg of T700SC/2592 by Toray Industries, Inc. was also used in this experiment. The thickness of the separate lamina is 0.125 mm and fibre volume fraction of 67%. In this study, three different kinds of circular tubes were fabricated from the three types of cross-ply laminates with different 0˚ plies, namely, 0˚ plies of conventional continuous fibres, UACS 0˚ plies with bi-angle slit pattern, and UACS 0˚ plies with staggered slit pattern to explore the potential of UACS ply to be used for crashworthy structural application and investigate the effects of UACS plies and slit pattern under quasi-static progressive crushing test.

The UACS plies are prepared by cutting sheets of 280 x 220 mm out of prepreg sheet for 0° and 90° plies before introducing the distributed slits as shown in Fig. 4-1(a). A smaller scale of slit similar to the one in chapter 3 was used. The slit angle between the slit and the fibre direction is 11.3 degrees and the length of chopped strands is 12.5 mm. Figs. 4-2(a) and 4-2(b) illustrate the images of UACS plies with bi-angle slit pattern and staggered slit pattern, respectively. White solid lines denote slits. The slit was carefully introduced into the prepreg sheet by hand using a conventional paper cutter based on a printed slit pattern as presented in Fig. 4-1(b). It is seen that all the fibres in UACS plies were cut into 12.5 mm length while all the 90˚ plies in cross-ply laminates remained continuous fibres. In the bi-angle UACS ply, the angle between the slit and fibre direction was chosen to be 11.3 degrees according to the previous studies [15-17]. In contrast, the

slit in the staggered UACS ply is perpendicular to the fibre. After introducing the slits into the prepreg sheet, 0˚ UACS ply with highly aligned short fibres and 90˚ply with continuous fibres were stacked into cross-ply laminate of $[90/0]_{4s}$ as illustrated on the right side image of Fig. 4-2(a-b).

The circular tube was selected on the basis of optimum energy absorption and ease of fabrication [3, 14], as shown in Fig. 4-3. The tubes were fabricated by wrapping the prepreg sheet around a circular aluminium pipe of 40 mm in diameter followed by overwrapping with release film and alloy steel sheet, as shown in Fig. 4-1(c), (d) and (e). After vacuum bagging preparation was completed, assembly was cured using an autoclave as in image shown in Fig. 4-1(f)-(g) under modified curing cycle by manufacturer to prevent too large pressure of alloy sheet on laminate's surface that could bring weld line defect to the tube. The curing cycle consisted with pressure inside autoclave of 0.1 MPa instead of 0.3MPa, then the temperature was raised from room temperature up to 135ºC. The laminate tube was cured for 120 minutes upon the temperature of 135ºC. Once the curing process was completed, the pressure inside the autoclave was released and the stacking was cooled down to about 60ºC in 30 minutes. The cured of laminate tubes is shown in Fig. 4-1(h).

Fig. 4-4(a) and 4-4(b) illustrated modified curing cycle diagram and schematic vacuum bag system for UACS tube, respectively. It was expected that the slit was filled by an excess of resin in the UACS 0˚ plies and might suppress the extension of large delamination and propagate controllable failure. The cured laminate tubes then were cut by diamond cutter machine with a specimen length of 100 mm and outer diameter of 44 mm. The average thickness of cured laminate tubes was 2.0 mm. All kind of specimen

tubes were bevelled with an angle of 45˚ for one end to give a trigger for progressive crushing failure.

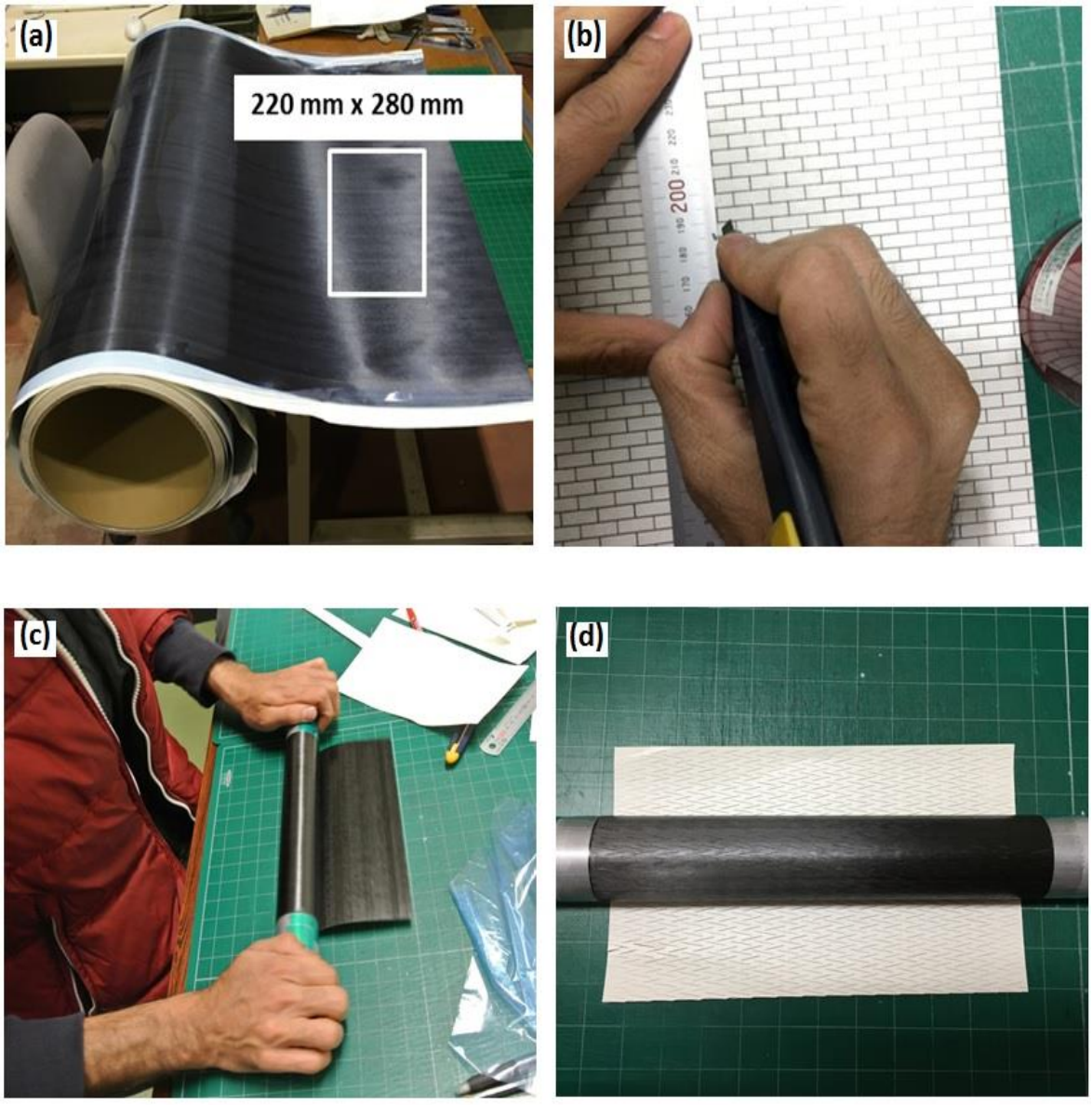

Figure 4-1: Fabrication procedure of circular tube with 0˚plies UACS laminate; a)cut-out of prepreg, b)introduces slit, c)wrapping prepreg onto hollow pipe, d) images of stacked laminate .

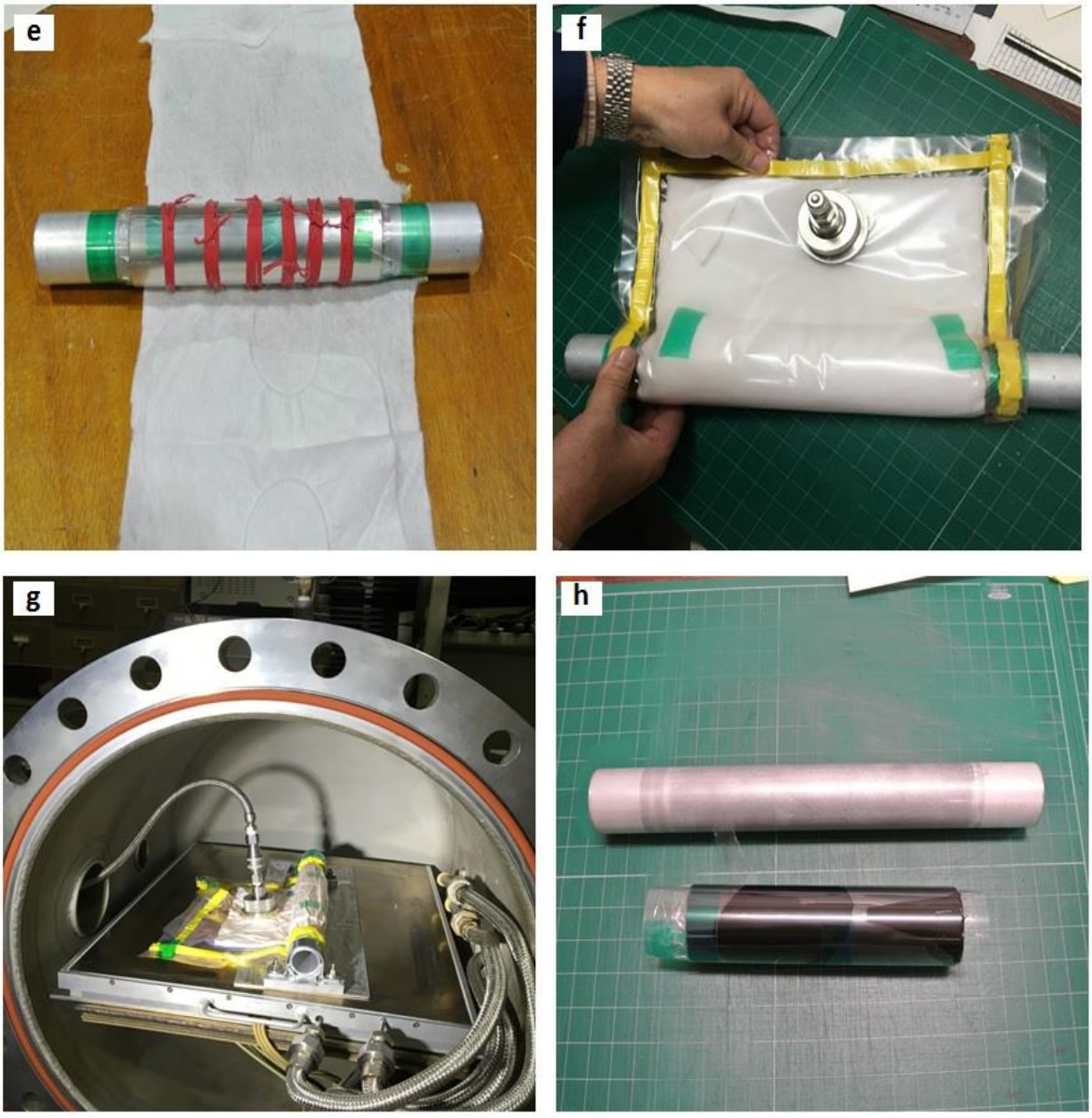

Figure 4-1: Fabrication procedure of circular tube laminate; e) wrapping stacked laminate with steel, f)vacuum bagging preparation, g)autoclave curing process, h) remove cured laminate.

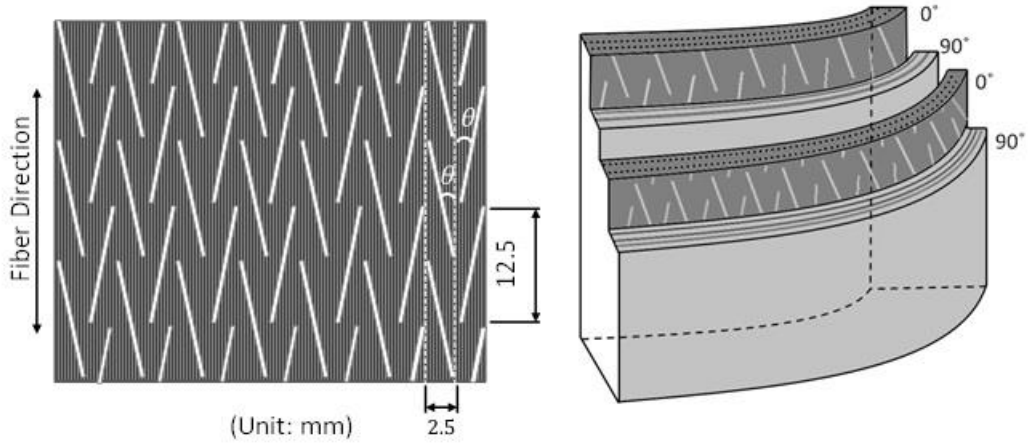

(a) UACS ply with bi-angle slit pattern and circular tubes stacking with bi-angle 0° plies UACS

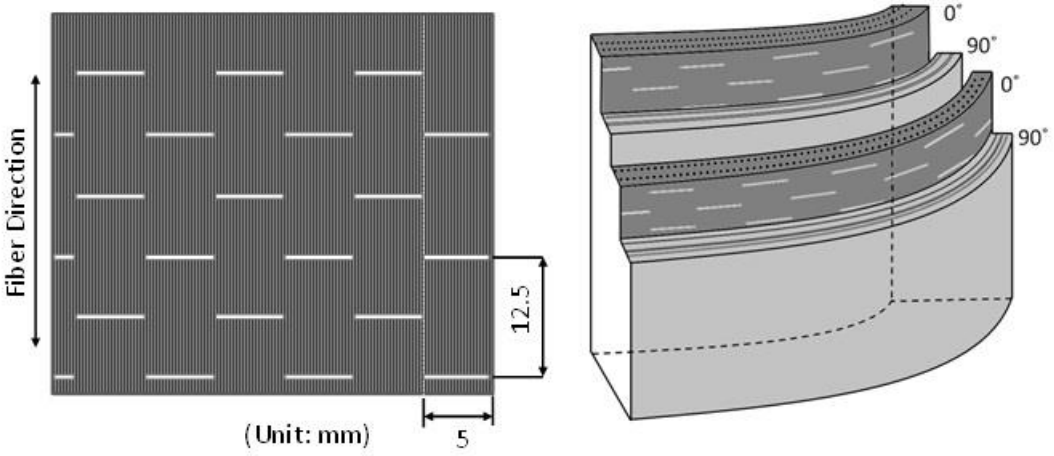

(b) UACS ply with staggered slit pattern and tube stacking with staggered 0° plies UACS

Figure 4-2: Illustrations of two kinds of UACS plies (left) and circular tube stacking sequence with 0˚ UACS plies (right).

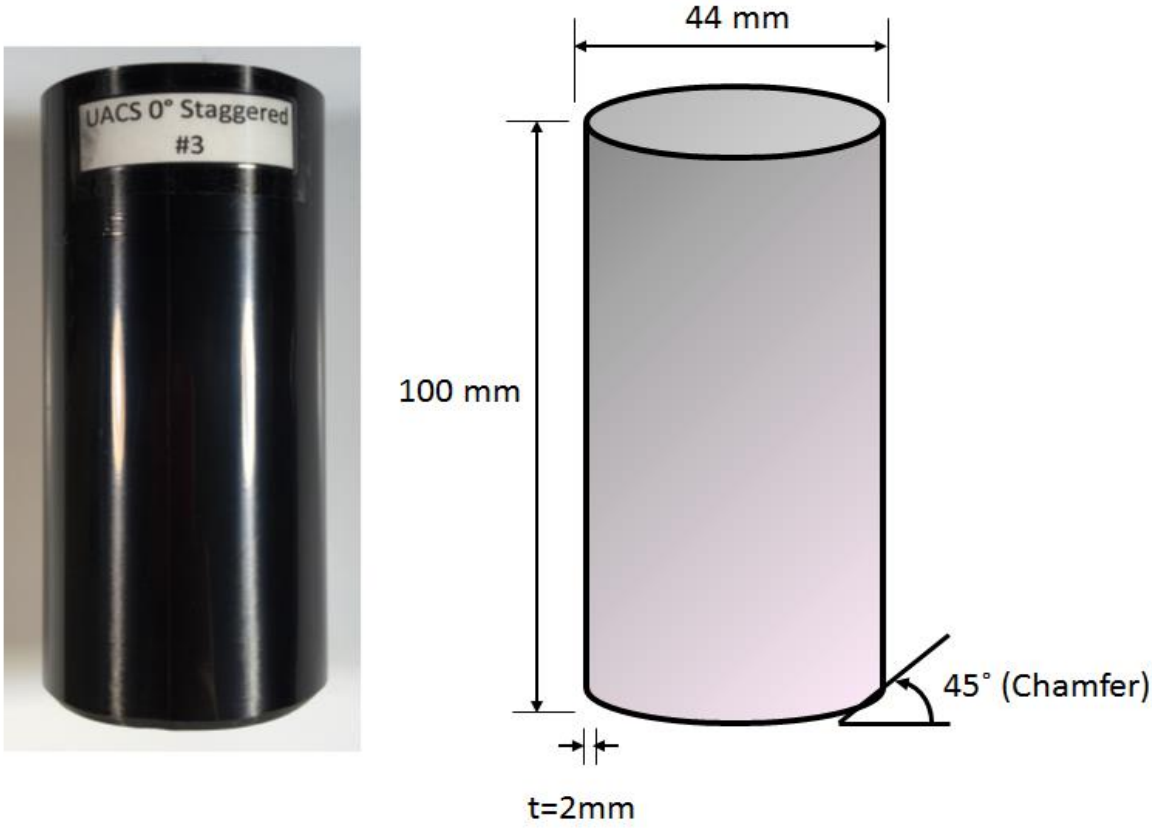

Figure 4-3: Illustrations of tested specimen tube (above) and geometries of the specimen tube.

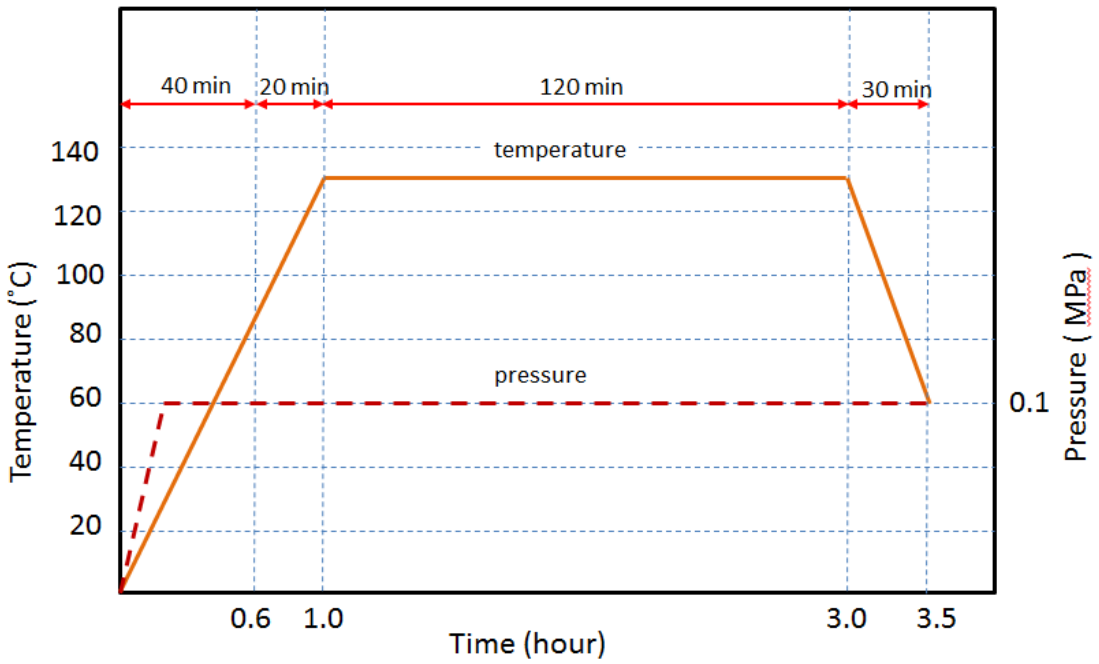

a) modified curing cycle diagram

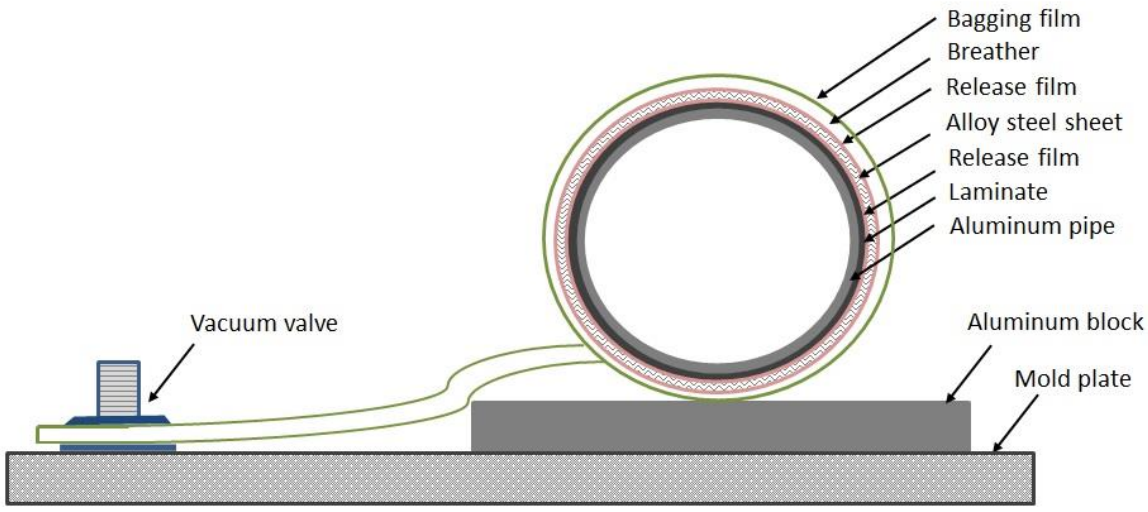

b) Vacuum bagging layout

Figure 4-4: Diagram of Autoclave process for composite tubes. a) modified curing cycle, b) vacuum bag layout.

4.2.2 Quasi-static crushing test

Quasi-static crushing tests were conducted using a 100 kN capacity MTS-810 testing system to investigate the crashworthiness properties of cross-ply laminated circular tubes with UACS 0° plies. During crushing test, the tube specimen was placed between two platen plates, in which the upper side platen was designed to clamp and hold the top of the specimen (see Fig 4-5). The plates were kept parallel to the tube in the centre. All tubes were compressed until the load increased rapidly by stacking of debris inside them at a loading rate of 10 mm/min as followed with reference [14] and each testing was carried out until the crushed displacement reaches 80 mm. The automatic data acquisition system of MTS-810 was used to obtain the load-displacement curve of the crushing test. On the other hand, a video system was employed to record the whole crushing process during the progressive crushing testing to obtain overall view of crushed tube. Four tube specimens were tested for each type. Fig. 4-6 shows the specimens at the end of quasi-static crushing test. In addition, after compression testing, the vertical-section views of crushed tube were obtained by using a diamond cutting machine as shown in Fig. 4-7. Microstructures of vertical-sectional then were observed to identify the failure mechanisms involved during quasi-static crushing process.

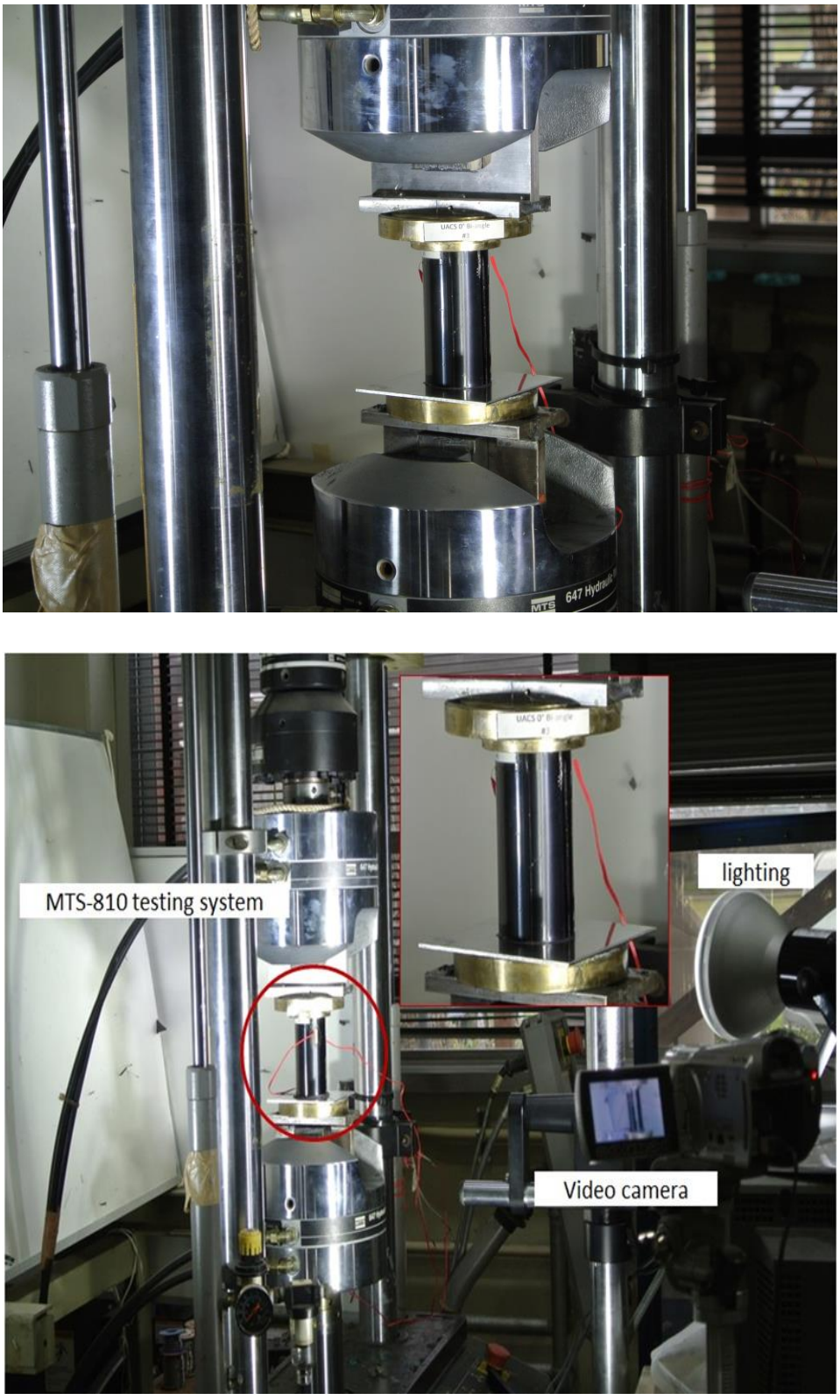

Figure 4-5: Test setup for quasi-static crush test.

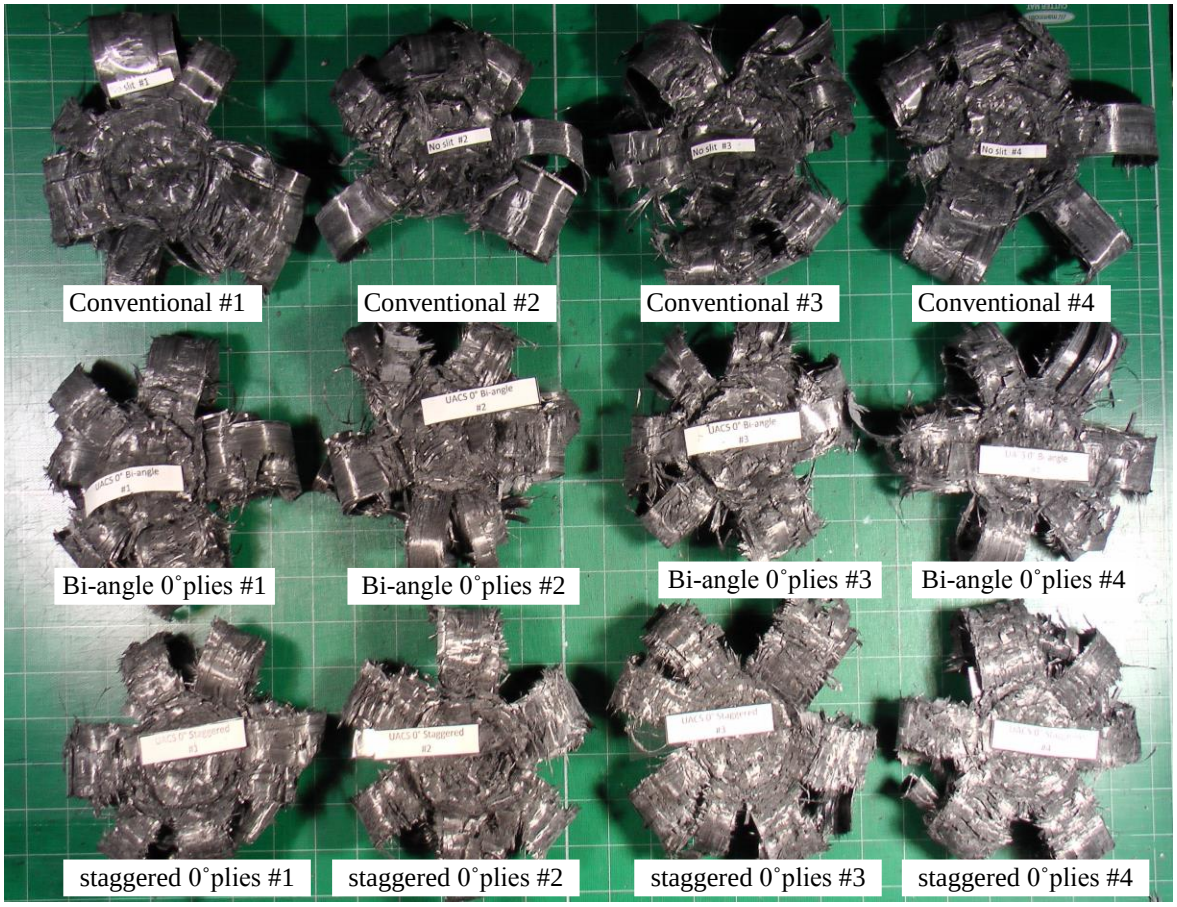

Figure 4-6: Specimens tube after quasi-static crushing tests.

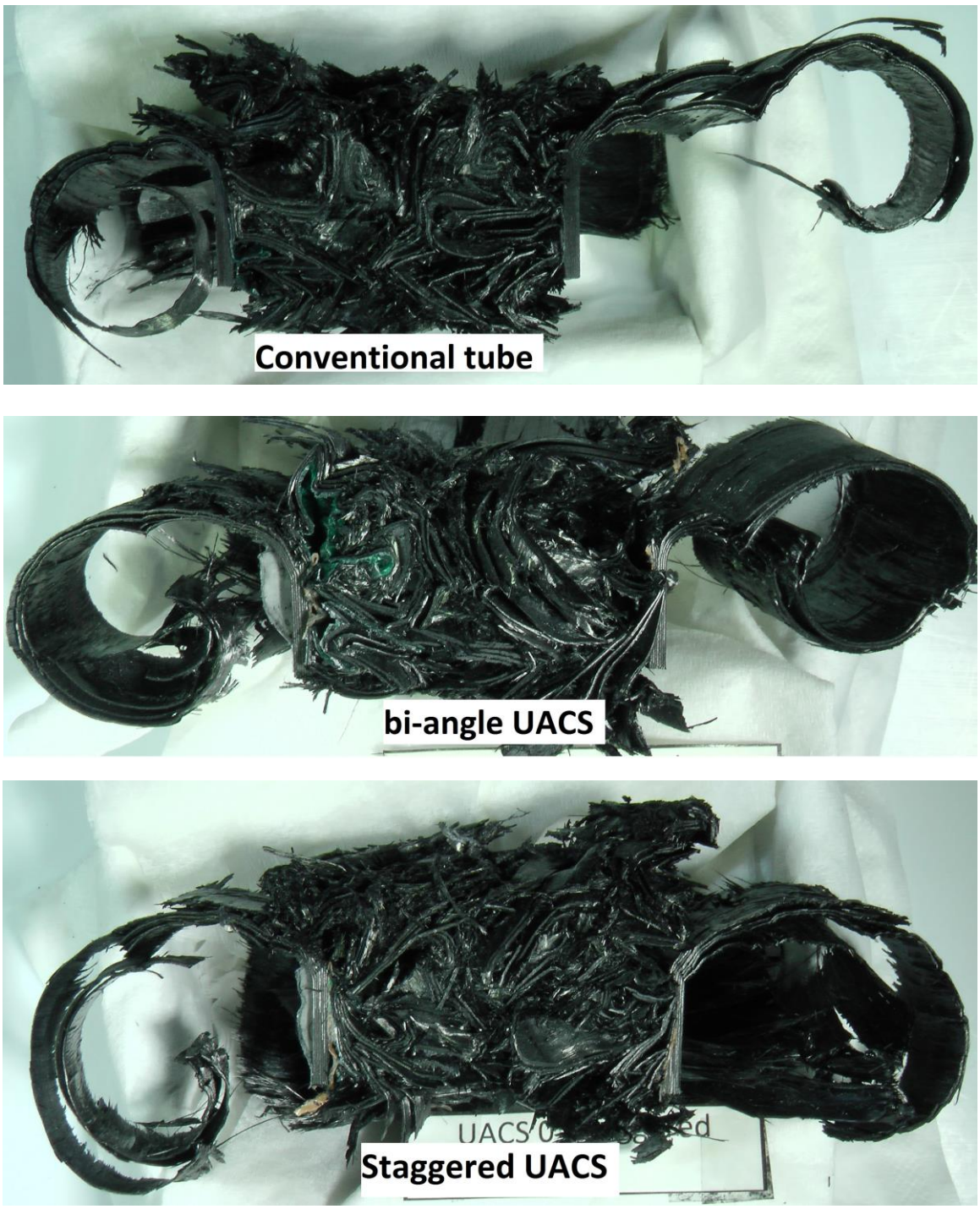

Figure 4-7: Cross-sectional view of final crushed specimen tubes.

4.3 Results and discussions

4.3.1 Load-displacement responses of tubes with UACS 0˚plies

The load-displacement curves of conventional laminated tubes, laminated tubes with staggered UACS 0˚ plies, and laminated tubes with bi-angle UACS 0˚ plies are shown in Fig. 4-8(a), (b) and (c), respectively. The load-displacement curves of Fig. 4-8 describe the crushing responses of the four specimens for each kind of laminated tube. It can be seen that there was a small scattered range pattern between the responses of four specimens. From Fig. 4-8, it is obvious shown that the peak forces of tubes with UACS 0˚ plies were found to be close to the mean crush force for both tubes with bi-angle UACS 0˚plies and staggered UACS 0˚plies, which is comparable to conventional tube, whereas the tubes with bi-angle UACS 0˚plies showed the highest mean load. This phenomenon is desirable since too large drop of peak load showed a catastrophic failure that needed to be avoided when designing a crashworthy structure. In particular, there is almost no catastrophic failure and load scatter is constant along the crushing process for tubes with staggered UACS 0˚plies. This proves that UACS 0˚ plies with staged pattern give much more stable energy absorption at post-crushing stage. All kinds of tubes exhibited typical splaying crushing mode, however for tubes with UACS 0˚ plies, it was shown that outward splaying of crushed tubes are much in combination of splaying and brittle fracture with many tearing laminate as we can see in crash morphology of Fig 4-9. Details of crushing behaviour mechanism will be discussed in 4.3.3.

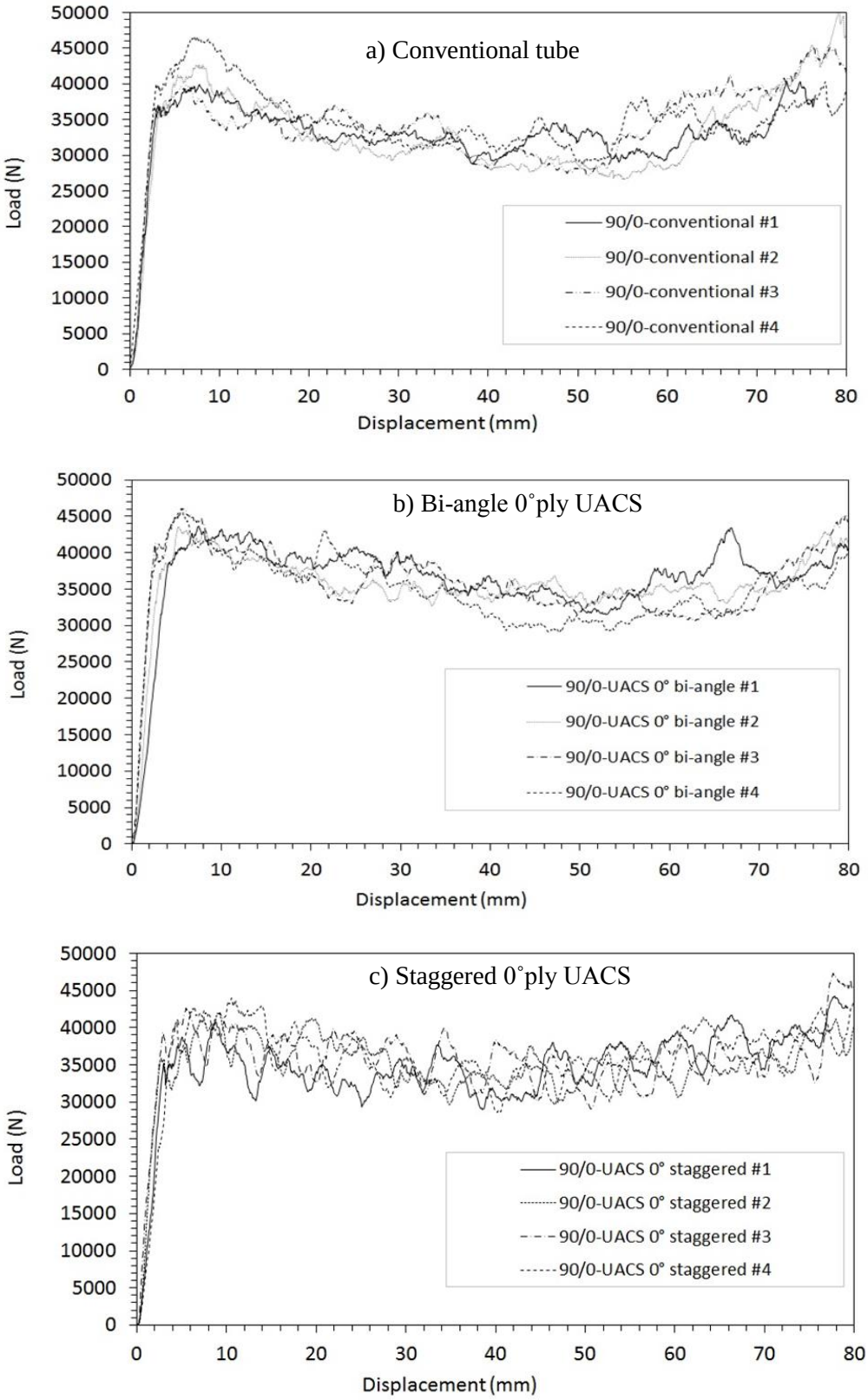

Figure 4-8: Typical load-displacement response of a) conventional tube, b) 0˚ plies bi-angle UACS tubes, c) 0˚ plies staggered UACS tubes.

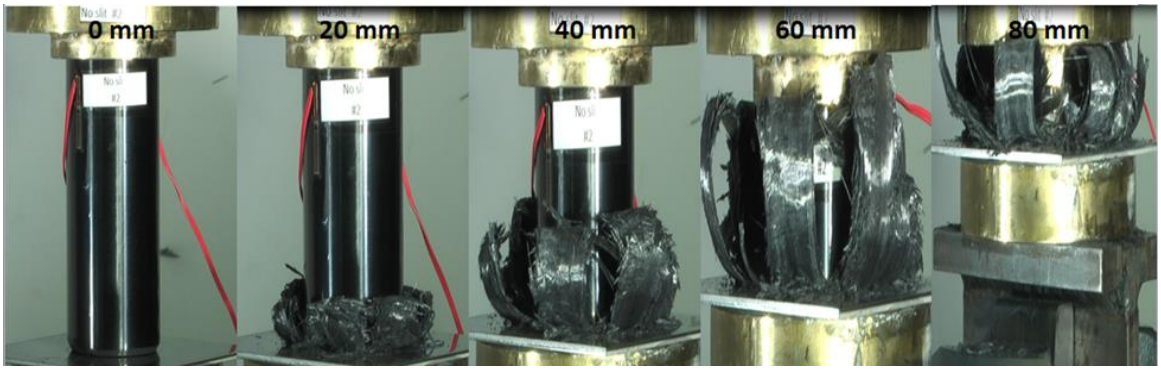

a) Conventional 0˚plies tube

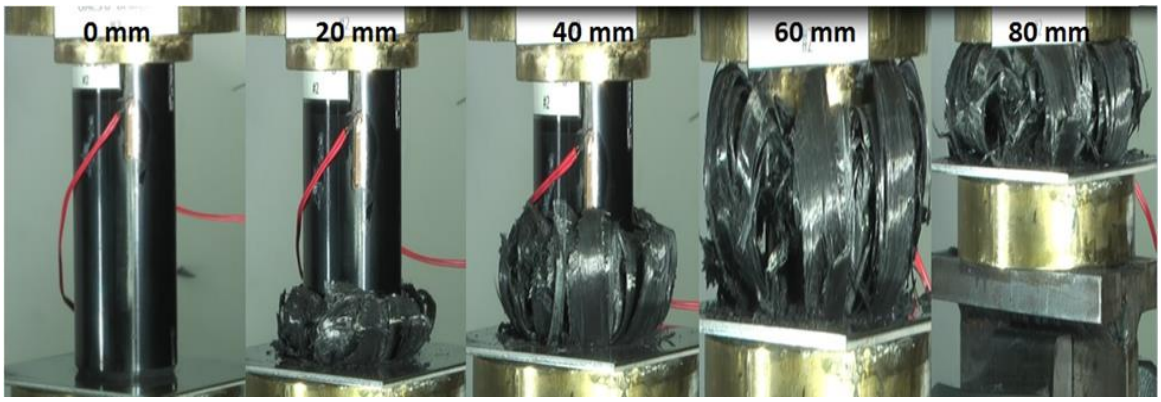

b) Bi-angle 0˚plies UACS tube

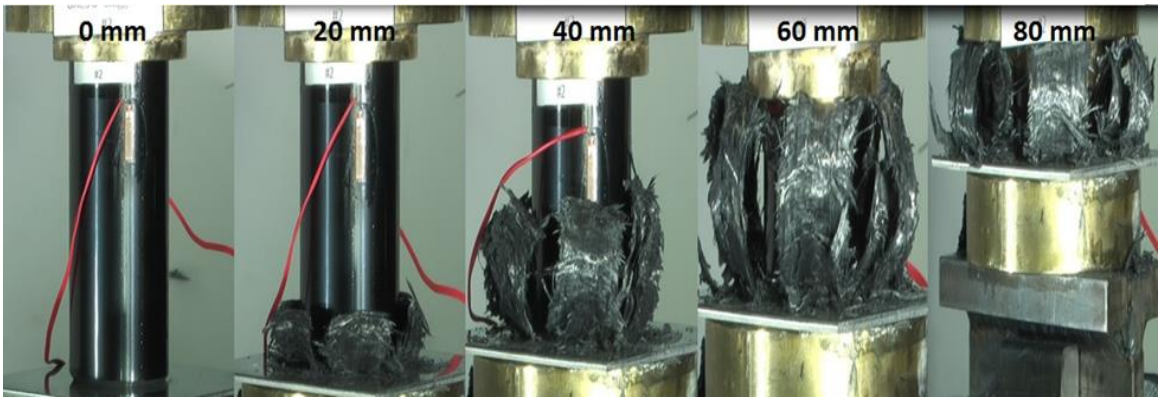

c) Staggered 0˚plies UACS tube

Figure 4-9: Typical crush morphology of a) conventional tube, b) 0˚ plies bi-angle UACS tubes, c) 0˚ plies staggered UACS tubes.

4.3.2 Crashworthiness properties of tubes with UACS 0˚plies

Detailed values of energy absorption and specific energy absorption of various tubes are presented in Fig. 4-10(a) and (b). Standard deviation value is given in round bracket. Three kinds of laminated tubes with conventional 0˚ plies, with bi-angle UACS 0˚ plies, and with staggered UACS 0˚ plies showed slightly different energy absorption capability. The coefficients of variation (the ratio of standard deviation to averaged value) are in the range of 1.2% – 2.4%. Laminated tube with bi-angle UACS 0˚ plies gives the highest energy absorption of 2.87 kJ and specific energy absorption of 71.01 kJ/kg. These values showed an increase of 6.4% and 5% respectively than those of conventional laminated tube. In addition, laminated tube with staggered UACS 0˚ plies gives energy absorption of 2.82 kJ and specific energy absorption of 70.6 kJ/kg. These values are also 4.5% higher than those of conventional laminated tube. These results revealed that although the existence of short fibre UACS 0˚ plies could reduce the compressive strength as reported by [16], it was found that shearing and progressive failure induced by the slits at the interlaminar region had successfully increased the specific energy absorption of tubes with UACS 0˚plies. These results showed a good agreement with previous investigation [17], although the percentage of increment in energy absorbed recorded is not significant. The reason is because specimens with planar section and delamination are much more dominant compared with non-planar section, and energy absorption is attributed to the different failure modes that occurred at cornered or arced section in non-planar specimen [13]. Table 4-1 lists the summary of crashworthiness capability of all kinds tubes investigated in this study.

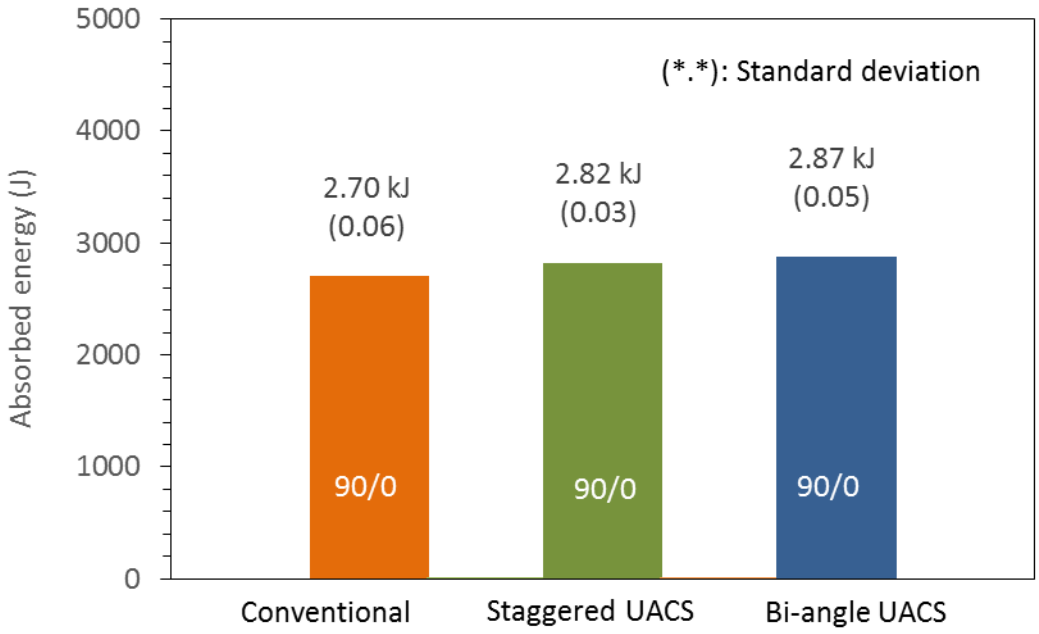

a) Energy absorption

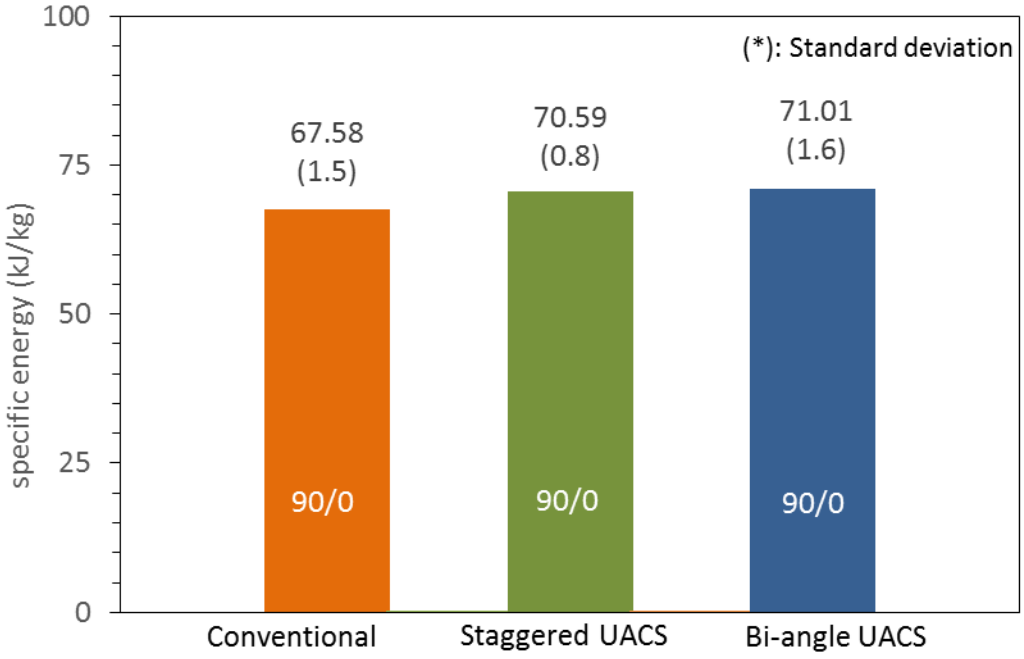

b) Specific energy absorption

Figure 4-10: Comparison of various circular tube. a) total energy absorption, b) specific energy absorption

The average values of maximum peak load are shown in Fig. 4-11. The coefficients of variation are in the range of 2.8% – 6.0%. All UACS tube specimen showed close average peak values to each laminate compared with conventional tube. Large standard deviation at pre-crushing stage among conventional tubes gave facts of unstable collapse during the crushing of specimen. Meanwhile lower deviation between tubes with UACS 0˚plies gave fact that due appearances of slit initiated much more controllable propagation during pre-crushing stage.

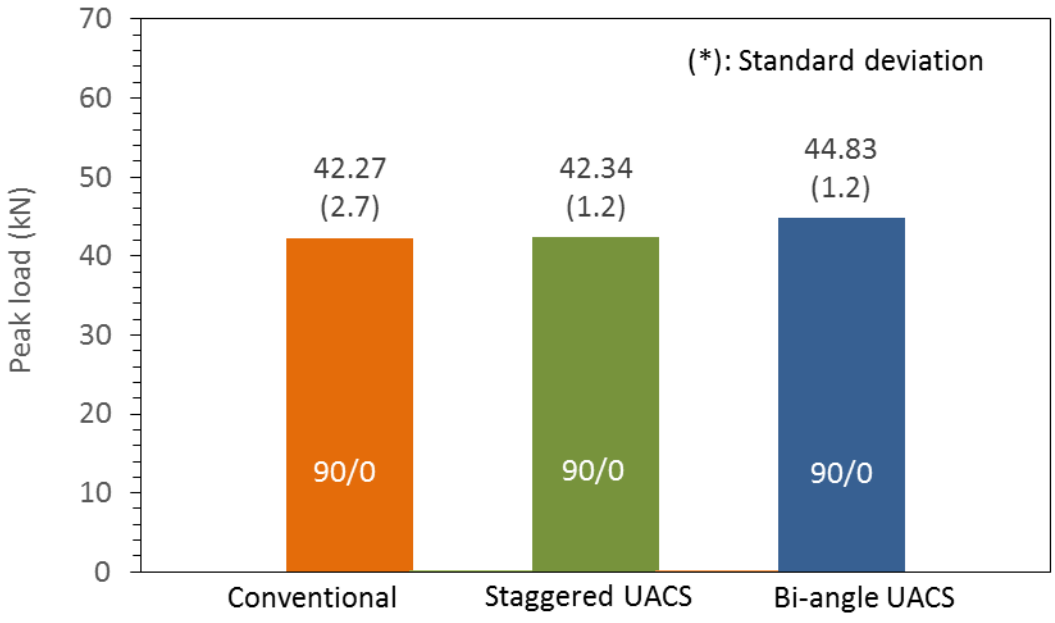

Figure 4-11: Comparison of peak load for various circular tube.

Another important parameter to evaluate energy absorption capability of a material for crashworthy structure is the mean load, which is defined by the ratio of the absorbed energy to the crushed length during the post crush process (after the maximum peak load). Detailed mean loads of various laminate tubes are presented in Fig. 4-12. Two kinds of tubes with UACS 0˚ plies, namely, bi-angle UACS 0˚ plies and staggered UACS 0˚ plies show 35.77 kN and 36.09 kN mean loads, which are 6% and 5% higher respectively than those of conventional laminated tubes.

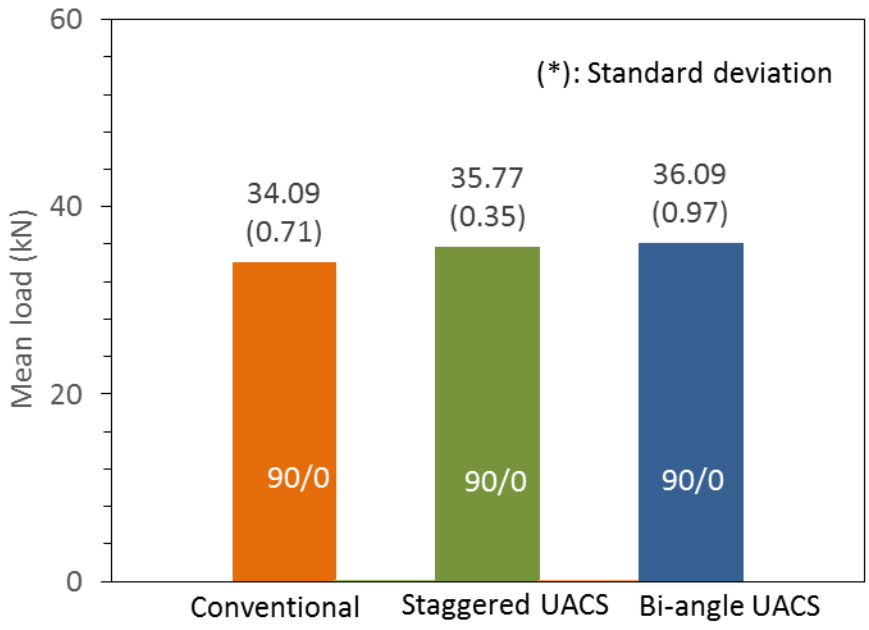

Figure 4-12: Comparison of mean load for various circular tube.

Table 4-1: Summary of energy absorption capabilities for various circular tube.

Circular tube	Total energy absorbed	P_{max}	P_{mean}	weight	SEA	CFE
	(J)	(kN)	(N)	(kg)	kJ/kg	
conventional laminate	2703.17	42.27	34090.9	0.04	67.58	80.65%
UACS 0˚ bi-angle	2874.44	44.84	36094.1	0.04	71.01	80.50%
UACS 0˚ staggered	2823.71	42.34	35768.6	0.04	70.59	84.48%

4.3.3 Failure modes of tubes with UACS 0˚plies

The typical crushing morphology and failure modes of conventional laminated tubes and laminated tubes with UACS 0˚plies are showed in Fig. 4-9. From the photograph images, three kinds of tube specimens absorbed the energy through a process of gradual crushing, with different combination of failure modes. In particular, the tested tube showed two obvious different crushing modes: splaying with axial splitting modes and brittle fracture mode. The splaying mode is characterised by a very long interlaminar crack parallel to fibre where the frond bends inward and outward of the tube, but lamina bundle is not fractured [13]. In present work, the amount of fractured lamina bundle and tearing laminate of conventional tubes were not high, in contrast with the tubes with UACS 0˚ plies.

In order to visualise the damage characteristic at different locations of interface for all kinds of tubes, photomicrograph from vertical-section view and top view of final crushed tube are used to observed failure modes. Fig. 4-13 shows images of final crushed shape and vertical-section view of conventional tube. From the image, it is clear that splaying mode behaviour dominated the crushing failure of conventional tube. As evident from the figure, smooth surface of splaying frond showed that friction effects were minimised and predominant failure was due to splitting. The largest radius of curvature frond with less fibre fracture in Fig. 4-13 (marked 1), and multiple long delamination (marked 2a-b)) were identified, which resulted in decreasing specific energy absorption of the tubes. In addition, less local tearing at the corner of tubes were also observed for conventional tubes as compared to tubes with 0˚ plies UACS.

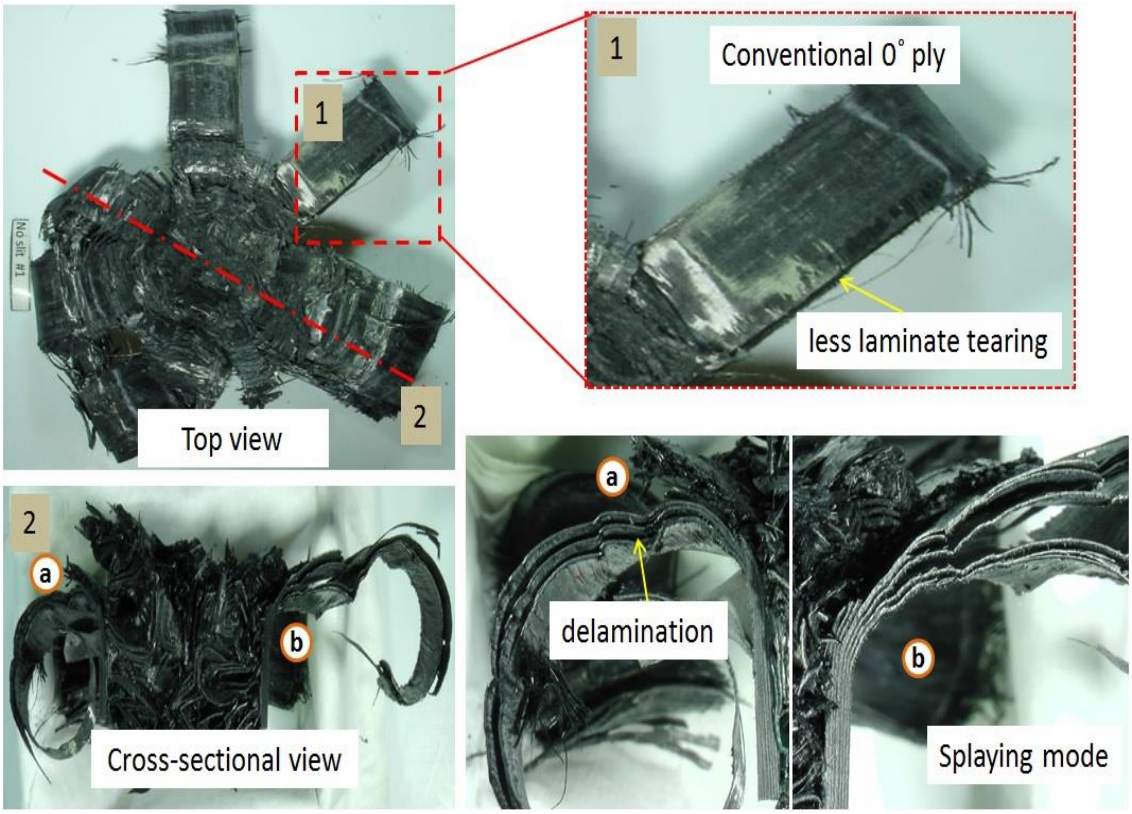

Figure 4-13: Photograph of final crushed shape and cross-sectional view of conventional tube.

The tubes with bi-angle UACS 0˚ plies and staggered UACS 0˚ plies were crushed with the progressive splaying and brittle fracture mode as described in Fig. 4-9(b) and (c). From the images, both showed relatively rough surface with cracks due to shear failure, which showed that friction was predominant for tubes with UACS 0˚ plies. Fig. 4-14 (marked 1) presents the final crushed and vertical-section view (marked b) of the tubes with bi-angle UACS 0˚ plies. In this tube, the fracture on the ply surface of outward frond can be seen containing many laminate tears around the perimeter and with little delamination. Relatively higher energy absorption is associated with laminate tearing and small amounts of accompanied delamination, which provide tubes with bi-angle UACS 0˚ plies with higher specific energy absorption compared with conventional tubes. Fig. 4-14 (marked 2b) showed images where the ply surface was fractured at the location of bi-angle slits, then suppressing the delamination extension. This showed that circumferentially oriented highly aligned discontinuous slits with bi-angle has a major influence on interlaminar crack growth by restricting a mode I crack opening, thus decreasing the lamina bundle length and increasing the energy absorption [3]. Here, large crushing load and energy are required to force the splayed fronds bending into small radius of curvature. Another characteristic of the crush zone in Fig. 4-14 (marked a) is piles of crushed resin and fibres that accumulated in the gap between the external and internal bending frond, known as debris wedge. An increase in size of debris at post crushing for bi-angle 0˚ plies UACS tubes is the key factor in brittle fracture mode as stable mechanism are developing compared with conventional tubes. Therefore, the tube with bi-angle UACS 0˚ plies showed a desirable steady progressive crushing behaviour.

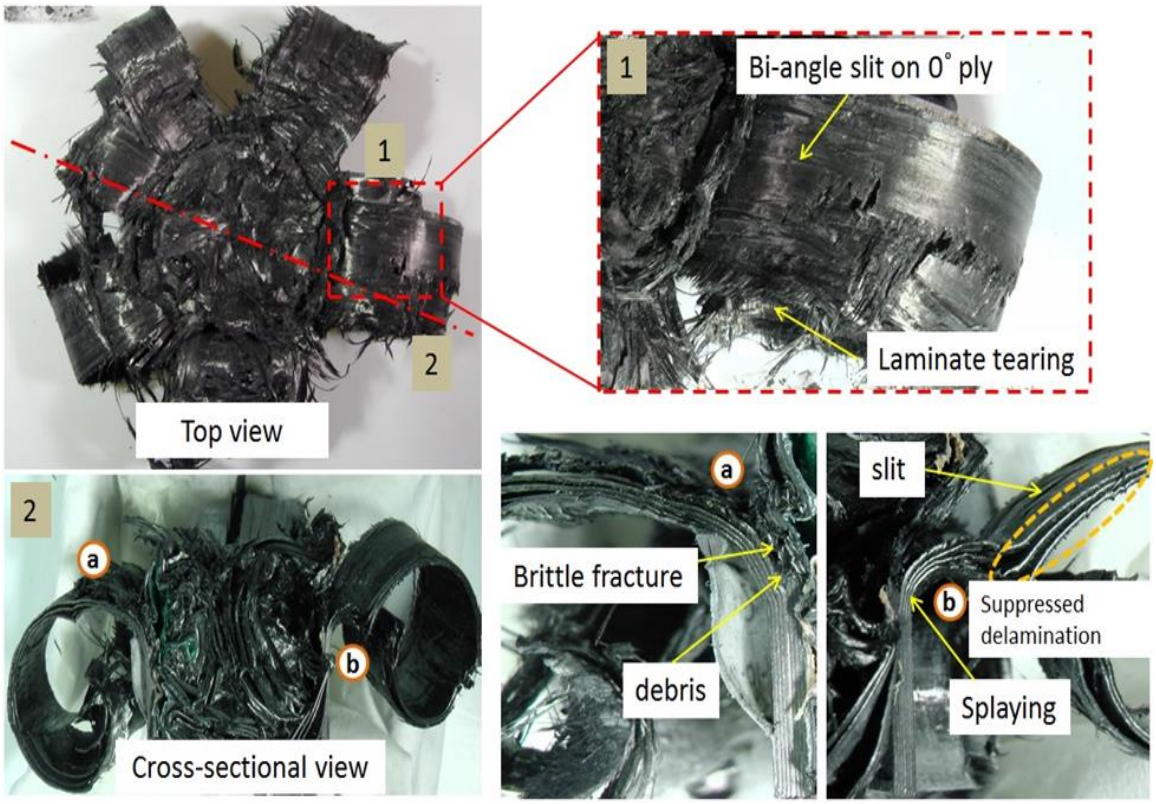

Figure 4-14: Photograph of final crushed shape and vertical-section view of tube with bi-angle UACS 0˚plies.

Likely tubes with bi-angle UACS 0˚ plies and tubes with staggered UACS 0˚ plies have shown failure by brittle fracture modes with much extensive fracture occurring with the combination of splaying and fragmentation modes (see Fig. 4-15). The longitudinal cracks that formed are similar in length to the staggered slit length and are long enough so that fronds are formed as laminas are separated by the cracks. Observation showed that fronds are bent through a small radius curvature such that nearly all the fronds are fractured with the presence of many laminate tears. Most interestingly, from Fig. 4-15 (marked 2b) we found that besides showing splaying and brittle failure mode, the tube with staggered UACS 0˚ plies also showed that some plies were crushed in micro folding modes, which was the same as the metal tubes when loaded in axial compression. These occurred when the stress in the staggered UACS 0˚ plies of the laminated tube is high enough so that the UACS 0˚ ply buckles locally and forms like a hinge to develop small folds. These morphology can be related to the high specific energy absorption of tubes compared with conventional tube as tubes with staggered 0˚ plies may experience significant amount of interlaminar and longitudinal cracking during hinge formation at slit area [14]. Fibre fracture at hinge and slit area that occurred also contributed to the rough surface of delamination frond. One advantage of folding failure mode occurred in tubes with staggered UACS 0˚ plies compared to tubes with bi-angle UACS 0˚ plies and conventional tubes is that the matrix and fibres remain intact to a large extension. These allow tubes to have post crush integrity, which can be seen in load-displacement responses of Fig. 4-8c and are desirable for crashworthy structural application. However, the effect of staggered slit that is perpendicular to fibre reduces the capability of

laminated tube to suppress the extension of delamination. This is the reason why bi-angle slit contributes a much higher energy absorption during crushing stage.

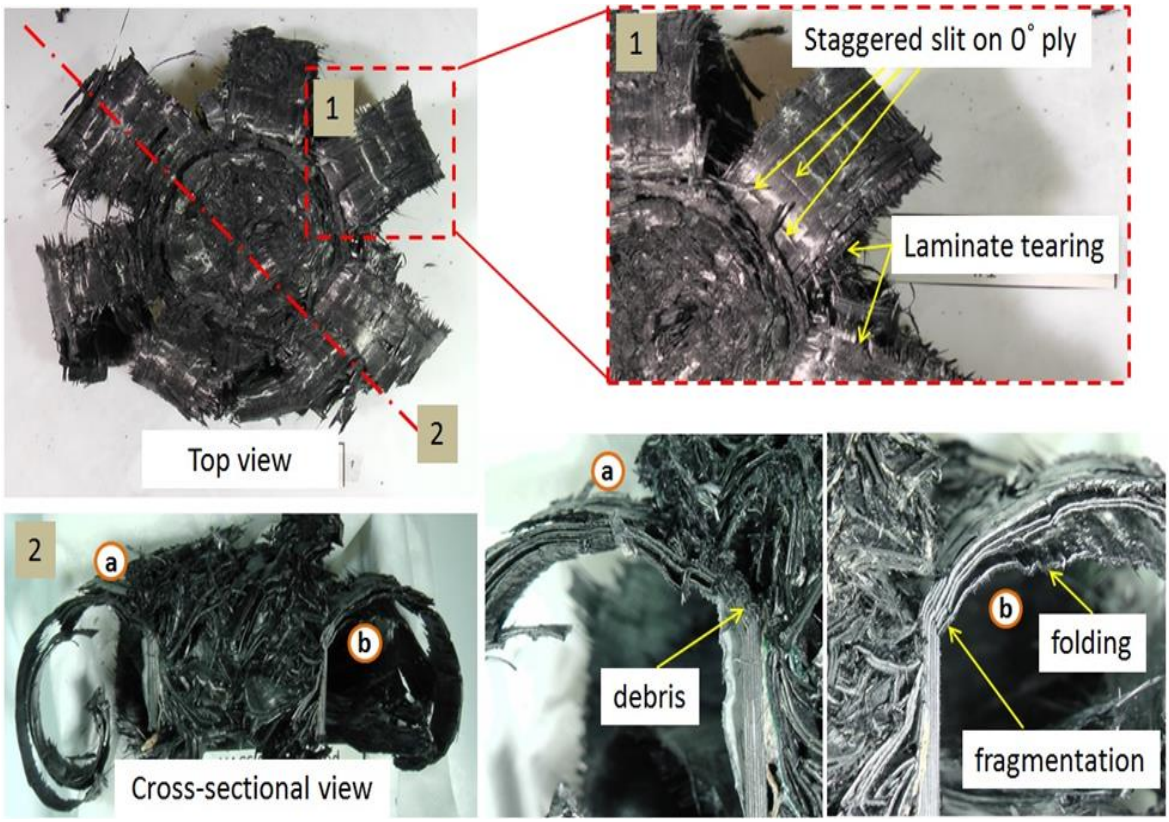

Figure 4-15: Photograph of final crushed shape and vertical-section view of tube with staggered UACS 0˚plies.

4.4 Progressive crushing tests of steel and E-glass/polyester tubes

To further demonstrate the excellent crashworthiness properties, such as steady crushing process and high specific energy absorption, of laminated tubes with UACS 0˚ plies, comparative progressive crushing tests for steel circular tube and E-glass/polyester composite square tube were also carried out and test results of specific energy absorption were compared with those of laminated tubes with UACS 0˚ plies.

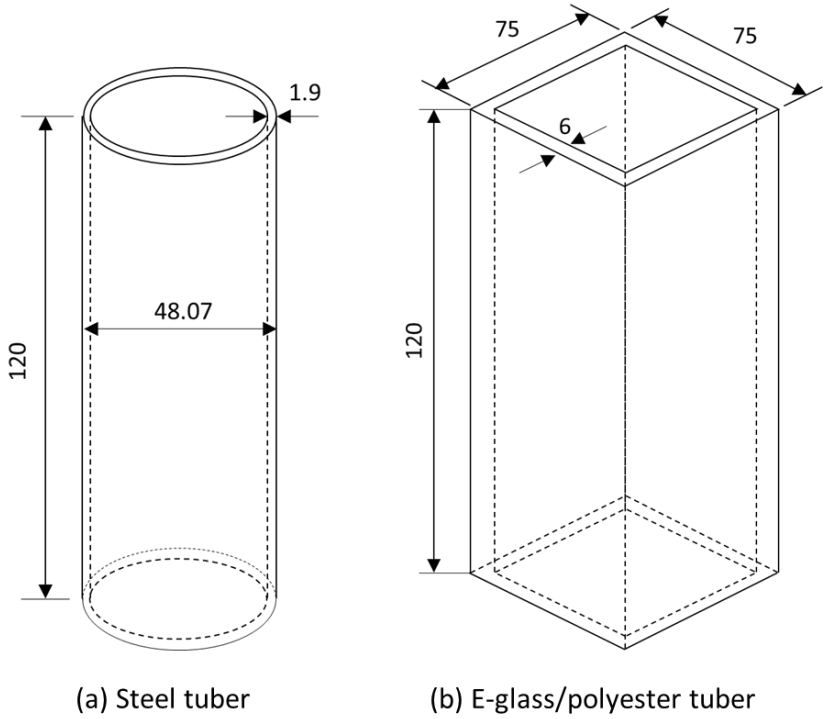

Figure 4-16: Geometries of two kinds of tubes for comparative progressive crushing tests.

The geometries of two kinds of tube are depicted in Fig. 4-16. The geometry of steel circular tube is similar to the circular tube of composite laminated tubes with UACS 0˚ plies as described in Fig. 4-3. The steel circular tube is made by commercially available conventional mild steel and the square tube is made by E-glass fibre reinforced polyester cross-ply composite using pultrusion process. The weight of steel circular tube and

composite square tube are 275.6 g and 334.6 g, respectively. The progressive crushing test for the steel circular tube was conducted using a 200 kN universal testing machine in quasi-static compression mode (about 10 mm/min). The progressive crushing test for E-glass/polyester square tube was conducted using a 100 kN universal testing machine under about 10 mm/min compressive loading rate.

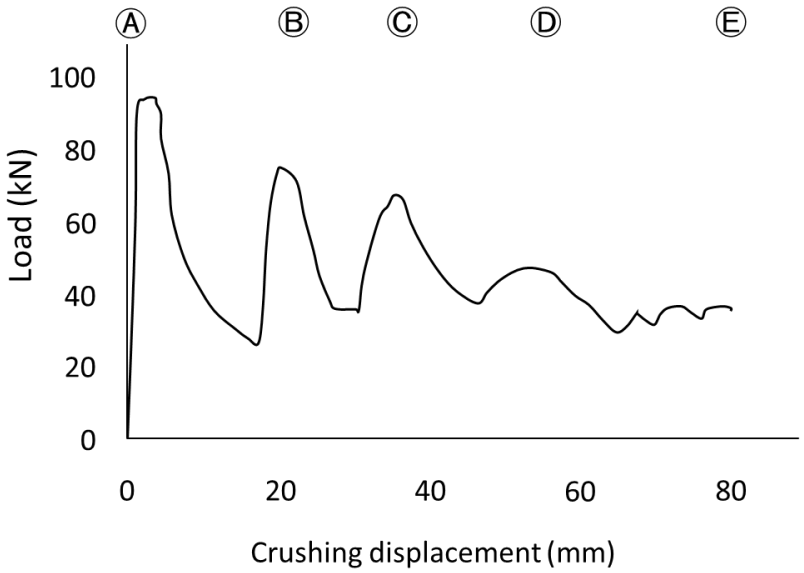

Figure 4-17: Load-displacement curve for steel circular tube.

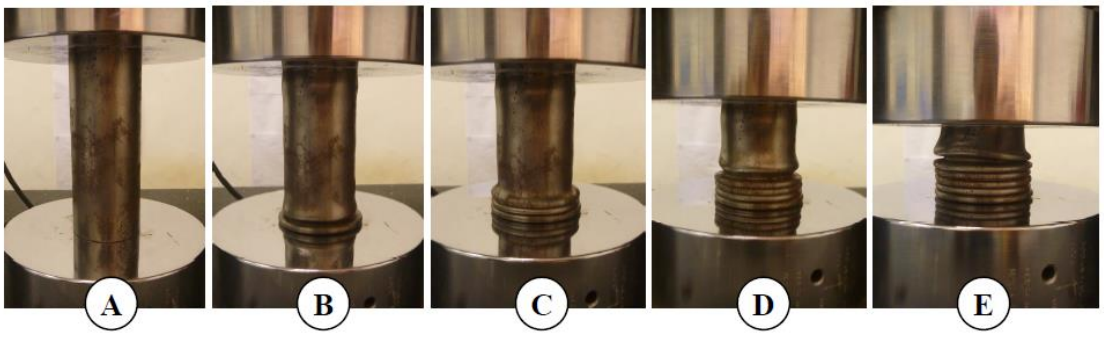

Figure 4-18: Progressive **c**rushing images of steel circular tube.

Test results are presented in Fig. 4-17~Fig. 4-20. The load-displacement curve for steel circular tube is described in Fig. 4-17. The first peak represents the initial buckling of the tube wall, that is, the wall buckles towards outward. Then the tube shortens and further deforms by rolling mode of plastic collapse. This progressive crushing behaviour is quite different from previous circular tube of composite laminates with UACS 0˚ plies. The post crushing behaviour is not as smooth as those of previous circular tube of composite laminates with UACS 0˚ plies. Typical crushing image of the steel circular tube is presented in Fig. 4-18. Five pictures corresponds to five instant times during the crushing test, as marked in Fig. 4-17. This is typical crushing failure mode for metal tubes, which is quite different from fibre reinforced polymer composite tubes. In addition, the specific energy absorption is about 26.1 kJ/kg, much lower than the average value 71.01 kJ/kg of previous circular tubes of composite laminate with bi-angle UACS 0˚ plies. This result demonstrates that tubes of composite laminate with UACS 0˚ plies have much high crashworthiness properties compared to conventional metal and show a great potential for the application to automobile crashworthy structure.

In Fig. 4-19, the load-displacement curve for E-glass/polyester composite square tube is described. As the crushing begins, load quickly rose to the maximum value, then droped off immediately, and stayed relatively constant. Crack initiated from the four corners of the square tube when the load approaches its peak value. The cracks propagated parallel to the tube axis. At the same time, four wall pieces of the tube were split into two continuous fronds that splayed outwards and inwards of the tube. The crushing images are presented in Fig. 4-20. First photograph is the original shape of the tube, following each photograph was taken after each 20 mm crashed displacement. This

progressive crushing process is stable and the fluctuation of load is not significant compared to the steel circular tube. However, the specific energy absorption of the E-glass/polyester composite square tube is about 17.0 kJ/kg, much lower than 71.01 kJ/kg of previous circular tube of composite laminate with bi-angle UACS 0˚ plies. Thus, it is clear that CFRP laminates with UACS plies have much higher crashworthiness properties compared to conventional metal and glass fibre reinforced plastic laminates.

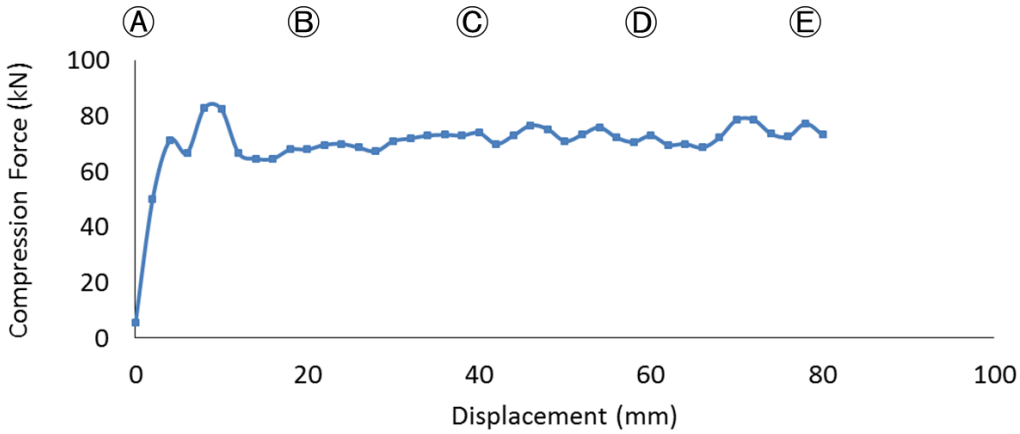

Figure 4-19: Load-displacement curve for E-glass/polyester composite square tube.

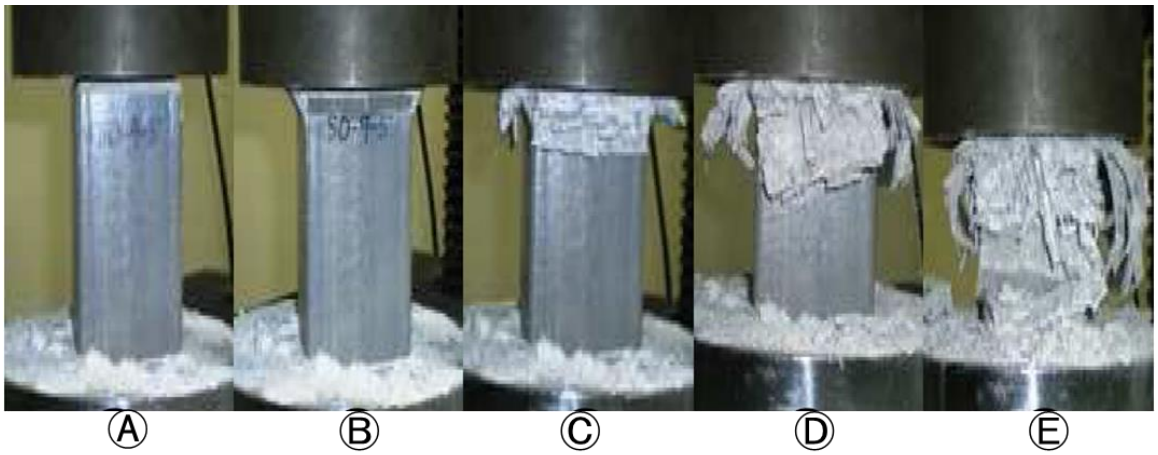

Figure 4-20: Progressive crushing images of E-glass/polyester composite square tube.

4.5 Summary

Based on the reported results of quasi-static progressive crushing tests for various tubes, the observation on the relationship between crushing behaviour and crashworthiness properties of three different kinds of tubes, and the comparative test results, following conclusions are drawn:

1. A novel material by introducing bi-angle UACS 0˚ plies into laminated composite tube instead of the use of continuous fibre has shown an increase in energy absorption capability. Tubes with bi-angle UACS 0˚ plies give the highest energy absorption and specific energy, followed by tubes with staggered 0˚ plies and conventional tube, respectively.
2. In aspect of crushing mode, all kinds of tubes showed significantly different crushing failure modes that attributed to various amounts of energy to be absorbed. The conventional tube without slit was crushed in splaying mode with large radius curvature and less brittle failure. In contrast, both tubes with UACS 0˚ plies failed in a combination of splaying and brittle fracture modes, as a result which gave a stable progressive crushing, thus increasing energy absorption capability.
3. Conventional tubes demonstrated large delamination and bending into large radius of curvature during splaying due to the high bending strength of conventional 0˚ plies with continuous fibres. Large delamination significantly reduced the bending stiffness and critical load of buckling of the laminated tubes, resulting in lower energy absorption capability.
4. Both tubes with UACS 0˚ plies showed controlled and stable crushing process at post crushing stage. Large crushing load and energy are required to force the

splayed fronds bending into small radius of curvature for both tubes. In particular, tubes with bi-angle UACS 0˚ plies demonstrated small delamination because the angled and discontinuous slits in the UACS 0˚ plies reduced the bending strength of the laminate and then suppressed the delamination extension. However, more delamination appeared in tubes with staggered UACS 0˚ plies because of the slits were perpendicular to the fibre direction, which induced large interlaminar shear stress between UACS 0˚ ply and 90˚ continuous fibre ply and was not efficient to suppress the delamination.

5. Energy absorbed because of friction mechanisms in both tubes with UACS 0˚plies is one of the primary modes of energy absorption for composite tubes with UACS 0˚plies.
6. If only the high energy absorption capability is required to be used as energy absorption components, the tube with bi-angle UACS 0˚ plies would be the most suitable. If energy absorption capability and the post crush integrity are required by mainstream structure, the tube with staggered UACS 0˚ plies would be the best candidate.
7. CFRP composite laminated tubes with UACS 0˚ plies have much higher crashworthiness properties compared to conventional metal tube and glass fibre reinforced plastic composite tube and show a great potential for the application to automotive crashworthy structure.

Bibliography

[1] Eshkoor RA, Ude AU, Oshkovr SA, Sulong AB, Zulkifli R, Ariffin AK, Azhari CH. Failure mechanism of woven natural silk/epoxy rectangular composite tubes under axial quasi-static crushing test using trigger mechanism. Int Journal of Impact Engineering 2014;64:53-61.

[2] Hamada H, Coppola JC, Hull D, Maekawa Z, Sato H. Comparison of energy absorption of carbon/epoxy and carbon/peek composite tubes. Composite, 1993; 23(4) :245-252.

[3] Hull D. A unified approach to progressive crushing of fibre-reinforced composite tubes. *Composite Science and Tech*, 1991; 40: 377-421.

[4] Mamalis AG, Robinson M, Manolakos DE, Demosthenous GA, Ioannidis MB, Carruthers J. Review Crashworthy capability of composite material structures. *Composite Structures,* 1997; 37: 109-132.

[5] Jacob GC, Fellers JF, Simunovic S, Starbuck JM. Energy absorption in polymer composites for automotive crashworthiness. Journal of Composite Materials 2002;36(07):813-850.

[6] Yan L, Chouw N. Crashworthiness characteristics of flax fibre reinforced epoxy tubes for energy absorption application. Materials and Design 2013;51:629-640.

[7] Boria S, Scattina A, Belingardi G. Axial Energy absorption of CFRP truncated cones. *Composite structures*, 2015; 130: 18-28

[8] Huang J, Wang X. Numerical and experimental investigations on the axial crushing response of composite tubes. Composite Structures, 2009; 91: 222-228.

[9] Palanivelu P, Paepegem WV, Degrieck J, Ackeren JV, Kakogiannis D, Hemelrijck DV, Wastiels J, Vantomme J. Experimental study on the axial crushing behavior of pultruded composite tubes. Polymer Testing 2010;29:224-234.

[10] Chiu LNS, Falzon BG, Ruan D, Xu S, Thomson RS, Chen B, Yan W. Crush responses of composite cylinder quasi-static and dynamic loading. *Composite Structures*, 2015; 131: 90-98.

[11] Mamalis AG, Manolakos DE, Ioannidis MB, Papapostolou DP. Crashworthy characteristics of axially statiscally compressed thin-walled square CFRP composite tubes: experimental. Composite Structures, 2004; 63: 347-360.

[12] Tao WH, Robertson RE, Thornton PH. Effect of material properties and crush conditions on the crush energy absorption of fiber composite rods. *Composite Science and Technology*, 1993; 47: 405-418.

[13] Corteau MA. Investigating the crashworthiness characteristics of carbon fiber/epoxy tubes. Master thesis, University of Utah, 2011.

[14] Kim JS, Yoon HJ, Shin KB. A study on crushing behaviors of composite circular tubes with different reinforcing fibers. *International Journal of Impact Engineering*, 2011; 38: 198-207.

[15] Taketa I, Sato N, Kitano A, Nishikawa M, Okabe T. Enhancement of strength and uniformity in unidirectionally arrayed chopped strand with angled slits. *Compos Part A*, 2010; 42: 1639-1646.

[16] Li H, Wang WX, Takao Y, Matsubara T. New designs of unidirectionally arrayed chopped strands by introducing discontinuous angled slits into prepreg. *Composite Part A*, 2013; 45: 127-133.

[17] Arifin AA, Wang WX, Matsubara T. Experimental investigation on the compression and crush responses of cross-ply laminates with 0˚plies of unidirectionally arrayed chopped strand. *Composite Part B*, 2016; 98: 182-193.

[18] Yoshiro S, Ogi K. Fracture behavior in CFRP cross-ply laminates with initially cut fibers. *Composite Part A*, 2009; 40: 938-947.

[19] Iarve EV, Kim R. Strength prediction and measurement in model multilayered discontinuous tow reinforced composites. Journal of Composite Materials 2004;38(1):5-18.

[20] Jackson A, David M. Gunnion AJ, Kelly D, Dutton S. Dynamic and quasi-static crush testing of closed carbon-fibre/epoxy elements. 27th International congress of the Aeronautical Sciences, ICAS 2010.

CHAPTER 5

Conclusions and future works

This chapter summarises the main conclusions of this dissertation and suggests the research topics concerning this study in the future.

5.1 Conclusions

UACS composite is one of the latest developments of aligned short fibre composites with highly aligned distributed discontinuous carbon fibres by introducing regular slits into the continuous fibre prepreg before the fabrication of laminates. Previous works showed existing and enhanced UACS composites have superior flowability, but relatively low tensile strength compared with conventional CFRP. In this study, two kinds of existing discontinuous UACS laminates with bi-angle pattern and staggered pattern slits were used to improve the energy absorption performance of conventional CFRP laminate by using UACS 0˚ plies instead of continuous fibre 0˚ plies, making them available for crashworthy structure application that requires complex geometry shape. Compressive strength properties, crashworthiness properties, crushing behaviour characteristics, and plying strategies of UACS laminates are investigated experimentally.

Based on these works, the following conclusions are obtained:

1. The compressive strength of quasi-isotropic UACS laminates with bi-angle slits can be controlled by choosing different angle, which increases the design flexibility of highly aligned short fibre composites. UACS laminates with small angle slits has higher compressive strength than UACS laminates with large angle slits although the fibres in all laminates have the same length. Furthermore, UACS laminates showed comparable progressive crushing properties and implied the possibility of such kind of short fibre composite used in crashworthy structure.
2. Cross-ly laminates with 0˚ plies UACS bi-angle slit and staggered slit enhanced the energy absorption by about 24% and 29%, respectively, compared with conventional

laminate in planar plate specimen. In addition, cross-ply laminated circular tubes with bi-angle UACS 0˚ plies and staggered UACS 0˚ plies also enhanced energy absorption by about 6.5% and 4.5%, respectively, compared with conventional laminated tube for non-planar section tube. Cross-ply laminated tube with bi-angle UACS 0˚ plies appears to have the best crashworthiness properties among all laminates.

3. Laminates with bi-angle UACS 0˚ plies are effective in absorbing energy during crushing process since the stress concentration around slits has successfully changed from a drawback to an advantage by initiating and progressive crushing in a stable and controllable manner. Moreover, ply fracture due to slits had successfully suppressed large delamination extension and made laminate fracture much more extensive, which give higher specific energy absorption.
4. From the comparative crushing test of steel tube and E-glass/polyester tube, it is clarified that CFRP composite tubes have much high specific energy absorption. In particular, laminated tubes with UACS 0˚plies have great potential to replace metal or glass/polymer composite tubes in crashworthy structure.

5.2 Future work

This study investigates the crashworthiness properties of composite laminate with two kinds of UACS 0˚ plies with highly aligned discontinuous slits under quasi-static loading rate. However, crashworthiness properties under dynamic or impact have not been studied due to the limitation of experimental condition. Further experimental research under dynamic or impact load and numerical analysis are necessary for the development of practically useful laminate with UACS 0˚plies in future.

In addition, the fabrication of laminated circular tube with UACS 0˚ plies was investigated in present study, further study on much complicated geometry specimen such as corrugated shape or structure shape with rib is necessary to verify the feasibility of fabricating complex shape structure by laminate with UACS 0˚ plies.

LIST OF FIGURES

LIST OF TABLES

LIST OF PUBLICATIONS

This dissertation is written based on the following publications:

[1] Abdullah Atiq Arifin and Abu Bakar Sulong. Quasi-static Energy absorption of pultruded composite Tubes E-Glass Polyester Under Oblique Loading with different cross-section. *Advanced Materials Research* 2012, Vols. 341-342: 843-847.

[2] Muhammad Izani Sahak1, Ahmad Kamely Mohamad, and Abdullah Atiq Arifin. Experimental study on geometry Energy absorption of Fiber Metal Laminated mild steel under axial compression. *Advanced Materials Research* 2013, Vol. 813: 165-170.

[3] A. A. Arifin, A. Othman. Axial crushes on composite laminated square tubes under compressive loading. *Key Engineering Materials*, 2014, Vols. 594-595: 707-710.

[4] A. A. Arifin, A. Othma. Crush force efficiency of composite square profile under off-axis loading. *Key Engineering Materials*, 2014, Vols. 594-595:711-714.

[5] A. Othman, A. A. Arifin, S. Abdullah1, A. K. Ariffin, N. A. N. Mohamed. Energy absorption of hybrid composite tubes under axial compression. Applied Mechanics and Materials 2014, Vols. 446-447:109-112.

[6] Abdullah Atiq Ariffin, Wen-Xue Wang. Effect of Slit Angle on the Compressive Properties of UACS bi-angle Slits. Proceedings of *7th Kyushu Uni-KAIST symposium on Aerospace Engineering., Kyushu University, Fukuoka,* 10-12 December 2015.

[7] Abdullah Atiq Arifin, Wen-Xue Wang, Terutake Matsubara. Effects of slit angle on the compressive properties of UACS laminates with bi-angle slits. Proceedings of *The 40th Composite Material Symposium.* Kanazawa, Japan, 17-19 Sept. 2015.

[8] Abdullah Atiq Arifin, Wen-Xue Wang, Terutake Matsubara. Experimental investigation on the compression and crush responses of cross-ply laminates with 0˚plies of unidirectionally arrayed chopped strand. *Composites Part B: Engineering*, 2016, 98: 182-193.

ACKNOWLEDGEMENTS

The present study was carried out at Kyushu University from 2013-2016. I would like to express my gratitude to all those who helped me during the research and writing of this dissertation.

My deepest gratitude goes first and foremost to my supervisor, Professor Wen-Xue Wang, not only for accepting me as a doctorate candidate to study at Kyushu University, but also for his constant encouragement and inexhaustible instruction from life details to my work. His wide knowledge and energy have injected tremendous value to the study, and without his consistent and illuminating instruction, it would have been difficult for me to finish my doctorate.

My warmest gratitude should be given to our technical assistant, Mr. Terutake Matsubara, for his insightful advice and generous guidance in technical supports to the experiment on present study and kindly help during the years in Japan. My grateful heart extends to the other members of our laboratory as well, for their cooperation to my study and friendship to my life.

My great gratitude also goes to the committee members of my dissertation for their helpful suggestions and commendations during the reviewing.

My acknowledgement with appreciation is to go to Ministry of Higher Education Malaysia for the financial support and to the Polytechnic Education Department for providing me such an opportunity to study in Japan.

My last gratitude would go to my beloved family my family for understanding and supporting me all through these years. In particular, I thank my wife, Norhaslinda Abdul Rashid, and my sons, Amsyar and Ammar.